Advanced Colloidal Systems for Targeted Chemotherapy

Dissertation

zur

Erlangung des Doktorgrades

der Naturwissenschaften

(Dr.rer.nat.)

dem

Fachbereich Pharmazie der

Philipps-Universität Marburg

vorgelegt von

Muhammad Yasir Ali

aus **Bahawalpur, Pakistan**

Marburg/Lahn **2019**

Erstgutachter: **Prof. Dr. Udo Bakowsky**

Zweitgutachter: **Prof. Dr. Frank Runkel**

Eingereicht am: **25.09.2019**

Tag der mündlichen Prüfung am: **06.11.2019**

Hochschulkennziffer: 1180

Advanced Colloidal Systems for Targeted Chemotherapy

Thesis

Submitted in the fulfilment of the requirements of degree of

Doctor of Natural Sciences (Dr.rer.nat.)

equivalent to

Doctor of Philosophy (Ph.D.)

To

The Faculty of Pharmacy,

University of Marburg.

By

Muhammad Yasir Ali

from Bahawalpur, Pakistan

Marburg/Lahn **2019**

First Supervisor: **Prof. Dr. Udo Bakowsky**

Second Supervisor: **Prof. Dr. Frank Runkel**

Date of Submission: **25.09.2019**

Defense date: **06.11.2019**

Hochschulkennziffer: 1180

EIDESSTATTLICHE ERKLÄRUNG

Ich versichere, dass ich meine Dissertation

"Advanced Colloidal Systems for Targeted Chemotherapy"

selbständig ohne unerlaubte Hilfe angefertigt und mich dabei keiner anderen als der von mir ausdrücklich bezeichneten Quellen bedient habe. Alle vollständig oder sinngemäß übernommenen sind Zitate als solche gekennzeichnet.

Die Dissertation wurde in der jetzigen oder einer ähnlichen Form noch bei keiner anderen Hochschule eingereicht und hat noch keinen sonstigen Prüfungszwecken gedient.

Marburg, den 25.09.2019

....

(Muhammad Yasir Ali)

I declare that this doctoral thesis

"Advanced Colloidal Systems for Targeted Chemotherapy"

has been written entirely by myself except unless stated otherwise by reference or acknowledgement. The research was carried out at the Institut für Pharmazeutische Technologie und Biopharmazie, University of Marburg, at the campus Ketzerbach 63 (old location) and Robert-Koch-Straße. 4 (new location) under the supervision of Professor Udo Bakowsky.

This thesis has not been submitted in any form elsewhere for a higher degree

Marburg, 25th September 2019

....

(**Muhammad Yasir Ali**)

A C K N O W L E D G E M E N T S

Dedication

To my father

TABLE OF CONTENTS

LIST OF FIGURES

LIST OF TABLES

LIST OF ABBREVIATIONS

AFM	Atomic Force Microscopy
Apt	Aptamer
ATR	Attenuated Total Reflection
$CaCl_2$	Calcium Chloride
CLSM	Confocal Laser Scanning Microscopy
Cyn 5	Cyanine 5
DAPI	4′,6-diamidino-2-phenylindole
DCFDA	2′,7′-dichlorofluorescein diacetate
DLS	Dynamic Light Scattering
DMEM	Dulbecco's Modified Eagle Medium
DMSO	Dimethyl Sulfoxide
DNA	Deoxyribonucleic Acid
EDC	1-ethyl-3-(3-dimethylaminopropyl)-carbodiimide
EGFR	Epidermal Growth Factor Receptor
ErbB	Avian Erythroblastosis Oncogene B
FBS	Foetal Bovine Serum
FDA	Food and Drug Administration
FTIR	Fourier Transform Infrared Spectroscopy
H&E	Hematoxylin and Eosin
HER	Human Epidermal Growth Receptor
IMDM	Iscove's Modified Dulbecco's *Media*
KCl	Potassium Chloride

KH$_2$PO$_4$	Potassium Dihydrogen Phosphate
LDV	Laser Doppler Velocimetry
LP	Liposomes
LPS	Sorafenib-Loaded Liposomes
MES	2-(*N*-morpholino) ethanesulfonic acid
MgCl$_2$	Magnesium Chloride
MP	PLGA Microparticles
MPS	Sorafenib-Loaded PLGA Microparticles
MTT	3-(4,5-dimethyl-2-thiazolyl)-2,5-diphenyl-2H-tetrazolium bromide (MTT)
Na$_2$HPO$_4$	Disodium Hydrogen Phosphate
NaCl	Sodium Chloride
NHS	N-Hydroxysuccinimide
PBS	Phosphate Buffer
PDGFR	Platelet Derived Growth Factor Receptor
PLGA	Poly (lactic-co-glycolic acid)
PN	PLGA Nanoparticles
PNS	Sorafenib-Loaded PLGA Nanoparticles
PVA	Poly Vinyl Alcohol
RNA	Ribonucleic Acid
ROS	Reactive Oxygen Species
RPMI	Roswell Park Memorial Institute Medium
SFB	Sorafenib Tosylate

SEM	Scanning Electron Microscopy
TBHP	Tert-butylhydroperoxide
THF	Tetrahydrofuran
Tris	Tris (hydroxymethyl) amino methane
VEGFR	Vascular Endothelial Growth Factor Receptor

Introduction

1.1 BACKGROUND

The word "Chemotherapy" was developed after the observation that the soldiers from World War I and II exposed to nitrogen compounds showed decrease in the levels of leukocytes [1-2]. Therefore, the use of alkylating drugs (cyclophosphamide, chlorambucil and cisplatin) was increased to treat lymphomas [3-4]. Chemotherapy is commonly used as a treatment of cancers with or without surgical [5-8] and radiation therapy [9-12]. Furthermore, one of the major reasons for unsuccessful chemotherapy is the limited accessibility of drugs to the tumor, needing higher doses. The higher doses of chemotherapeutic agents result in generalized toxicity and thus decrease the quality of life. Another problem to face in the arena of chemotherapy is the development of resistance against anti-neoplastic agents due to their non-specific delivery. Therefore, the focus of treatment is changing towards other advance options e.g. targeted therapy and immunotherapy [13-14].

1.2 TARGETED CHEMOTHERAPY

The efforts to combat problems regarding the non-selective chemotherapy have led to targeted drug delivery [15-18]. The development of targeted drug delivery systems has resulted in the effective therapeutic outcomes [19-20]. Microparticles, nanoparticles and liposomes are the pharmaceutical dosage form getting importance in targeting cancers. The targeting of the cancerous cells is possible due to unique small sizes of these formulations [21-23]. Targeting may be achieved either by passive or active targeting.

1.2.1 Passive Targeting

Passive targeting is usually achieved by controlling the sizes, morphology, surface charge and stealthing of the formulations used to deliver chemotherapeutic agent. Tumor tissues, due to rapid growth, are rich in blood vessels and endothelial junctions are loose. Typically, the pore size in normal vessel is 5-10 nm while in case of tumor vessel; this size ranges from 200 nm to several hundred nanometer [24, 25]. This increased pore size is due to multiple factors e.g. increased blood circulation, inflammation, hypoxia etc. Therefore, the formulations of this size range can easily leak through these junctions and exert their pharmacological effects (Figure 1.1). This phenomenon is known as enhanced permeation and retention (EPR) [25-26]. However, particles more or less than this pore size nm are usually not cleared by renal

clearance. Therefore, they may end up in the form of reticuloendothelial system (RES) retention [27-28]. Therefore, there is a need to modify the surfaces of these formulations so that they can bypass RES and show their effects in tumor cells.

1.2.2 Active Targeting

Nano-scale formulations can be modified by different ligands (e.g. aptamer, antibodies, siRNA, peptides etc.) to by-pass the RES [29-30]. These modifying ligands are targeting agents against tumor surfaces, DNA or other molecule. Therefore, surface modified nanoparticles or liposomes will bind to targeted cells (Figure 1.1) and will be then internalized by clathrin-mediated endocytosis, caveolae-mediated endocytosis, combined endocytotic pathways or clathrin/caveolae independent internalization pathways [27-28, 31-32]. These internalized particles, release their content inside cells which inhibit cellular proliferation and metastasis by intracellular supply of particles to specific targets. Beside these, small molecule drug inhibitors (e.g. Sorafenib and Imatinib) are also used to inhibit specific activity in cancers. These are small enough that can be easily absorbed by body as compared to antibodies. They are also non-immunogenic because are chemically synthesized [29, 33]. Thus active targeting therapies have more advantages over passive therapies due to specific delivery of drug to tumor tissues only. The active drug delivery systems by pass RES and thus accumulate in tumor tissues due to EPR. Therefore, the decreased generalized body drug distribution results in less side effects and overall quality of life of the patient is improved.
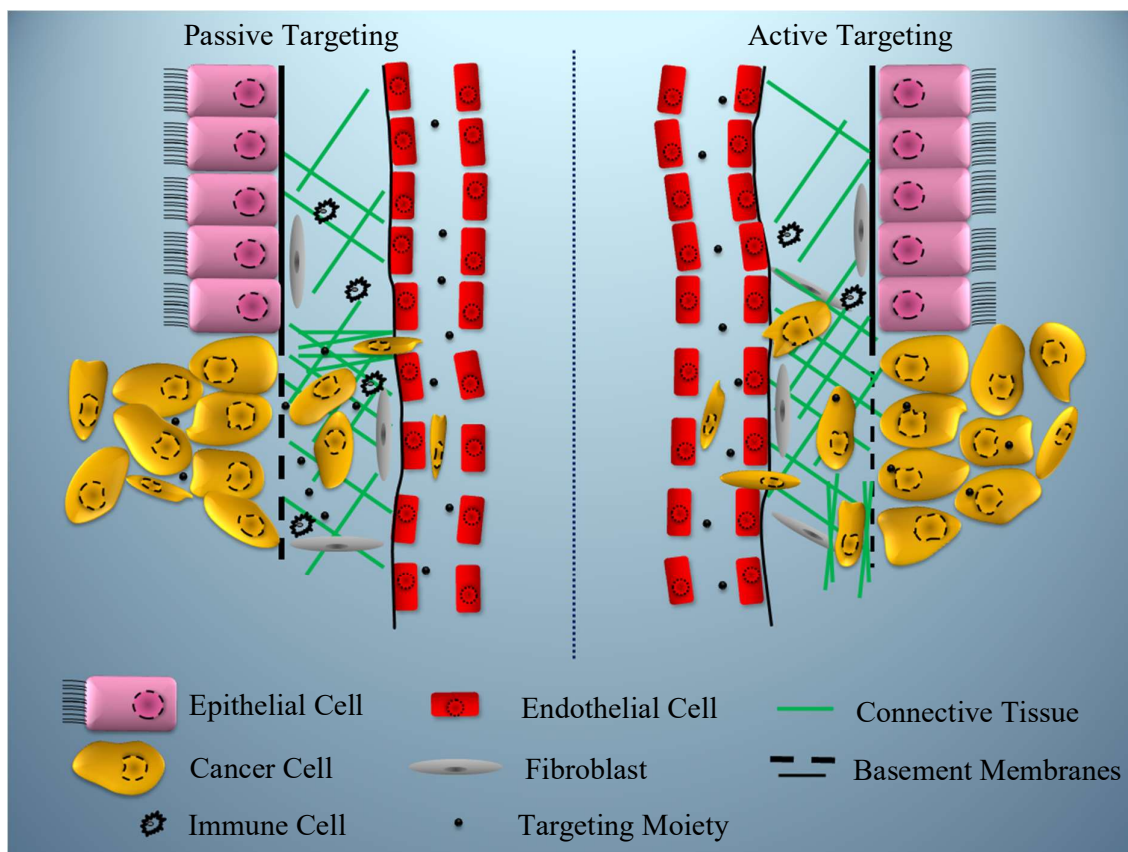
Figure 1.1: Passive and active targeting of cancer tissues [24, 27].

1.3 ADVANCE COLLOIDAL SYSTEMS FOR TARGETED CHEMOTHERAPY

1.3.1 Polymeric Matrices

Nanoparticles are small entities with size ranges from few nano-meters to a few hundreds of nano-meters [34]. On the other hand, microparticles size ranges from a few hundred nano-meters to several micro-meters. Nanoparticles and microparticles are solid matrices of polymers or mixture of polymers which may contain drug or other molecules of interest. The drug molecules can either be entrapped inside or adsorbed on the surfaces of these formulations [35-37]. Their size makes them good candidate for passive drug delivery to cancer cells and make them reside in tissue spaces due to EPR [38]. However, their surfaces can be modified to make them good candidates for active targeting. The surface modification also results in EPR and increase circulation time.

1.3.1.1 Methods of Preparation

The preparation of nanoparticles/microparticles is two step processes. The first step usually is the formation of emulsion and the second step ends up in the formation of nanoparticles/microparticles. The methods of preparation mostly depend upon the starting polymers. A variety of polymers is used for the preparation of these formulations. The most commonly used polymers can be classified as follows [35, 39-41];

Table 1.1: Classification of most commonly used polymers for nanoparticles/microparticles.

Sr. No.	Class	Polymer	Abbreviation
1.	Natural Polymers	Albumin Alignate Chitosan	
2.	Synthetic Homo-polymers	Poly(epsilon-caprolactone) Poly(lactide) Poly(lactide-co-glycolide)	PCL PLA PLGA
3.	Co-polymers	Poly(lactide)-poly(ethylene glycol) Poly(lactide)-poly(ethylene glycol) Poly(epsilon-caprolactone)-poly(ethylene glycol)	PLA-PEG PLGA-PEG PCL-PEG
4.	Colloidal Stabilizers	All Co-polymers Dextran Poly(vinyl alcohol)	 PVA

1.3.1.1.1 Spray Drying

Spray drying is the procedure of conversion of polymeric solution into dried particles, when liquid or dispersion is atomized in the form of spray and subjected to drying. The typical spray drying process encompasses three fundamental steps. The first step involves the atomization of feed. Liquid feed can be sprayed either by solution or by colloidal form. Second step of preparation involves the drying of spray with the help of stream of warm drying gas. The last step of preparation is separation and collection of dried product from the drying air [42]. Inlet temperature, drying gas heat flow and feed rates are the main process controls of the procedure. This technique is mostly used for the preparation of particles intended for pulmonary, nasal and control release oral delivery.

1.3.1.1.2 Solvent Evaporation

Solvent evaporation techniques are performed by agitation of two immiscible liquids (o/w or w/o emulsion). The first step requires emulsification of one liquid phase into another liquid phase. Homogenization is done to get controlled size droplets. During the second step, dispersed phase solvent is evaporated with the help of continuous stirring and thus results in core solvent evaporation forming nanoparticles/microparticles [43]. Finally, washing is done by centrifugation to remove the un-reacted surfactant. The process variables affecting the size are nature of solvents, the type of polymer, concentration of polymers, homogenization speed and rate of evaporation.

1.3.1.1.3 Salting out Method

In this method, polymer is dissolved in organic phase which is miscible with water. One example of such organic solvent is acetone. The aqueous phase consists of surfactant and electrolyte. The most commonly used electrolyte is magnesium chloride hexahydrate. The organic phase is uniformly distributed in the aqueous phase with/without the help of mechanical stirring. The water miscible organic solvent then migrates to aqueous phase changing the amount of organic solvent available for polymer. This results in the formation of precipitates in the form of nanoparticles/microparticles [44]. Finally, washing is done to separate the electrolyte, by centrifugation. The manufacturing parameters are internal/external phase ratio, stirring rate, concentration of polymers and electrolyte [45]. The greatest disadvantage of this method is extensive washing steps.

1.3.1.1.4 Nano-precipitation Method

This method is mostly suitable for hydrophobic drugs. The polymers along with drug are dissolved in organic phase (may be acetone or methanol). This organic phase is drop-wise added to aqueous phase containing surfactant. The diffusion of solvents results in the fabrication of nanoparticles/microparticles [46]. The organic phase then can be evaporated under vacuum conditions. The key parameters in procedure are organic phase injection rate, organic to water phase ratio and aqueous phase agitation rate [47].

1.3.2 Liposomes

Liposomes are artificially prepared lipid bilayer vesicles of size range from nanometers to several micrometers [47]. They can be classified on the bases of number of lipid layers, their size and nature of phospholipids. On the basis of number of bilayers and size, liposomes can be divided into two categories i.e. multilamellar vesicles (MLV) and unilamellar vesicles. Unilamellar vesicles can further be classified into two types i.e. large unilamellar vesicles (LUV) and small unilamellar vesicles (SUV). On the other hand, on the bases of nature of phospholipids there can be either positively charged liposomes (cationic liposomes), negatively charged liposomes (anionic liposomes) or liposomes having no net charge (neutral liposomes). Both hydrophilic drug and hydrophobic drug can be entrapped in liposomes. Moreover, their surfaces can be modified by various strategies to make them suitable for targeted drug delivery and enhanced cellular internalization [48-49].

1.3.2.1 Methods of Preparation

A range of different kinds of lipids are used for the preparation of liposomes. The selection of these lipids usually depends on the size, charge and methods of modification used for active targeting. They are modified with a polyethylene glycol group (PEG) which inhibits the liposomal uptake by RES and therefore result in a longer circulation time. Some of them the most commonly used lipids are listed in Table 1.2.

Table 1.2: Examples of some commonly used lipids for liposomes.

Sr. No.	Name	Abbreviation
1.	1,2-dipalmitoyl-sn-glycero-3-phosphocholine	DPPC
2.	1,2-distearoyl-sn-glycero-3-phosphocholine	DSPC
3.	1,2-distearoyl-sn-glycero-3-phosphoethanolamine	DSPE
4.	1,2-distearoyl-sn-glycero-3-phosphoethanolamine-N-[amino(polyethylene glycol)-2000]	DSPE-PEG(2000) Amine
5.	1,2-distearoyl-sn-glycero-3-phosphoethanolamine-N-[amino(polyethylene glycol)-5000]	DSPE-PEG(5000) Amine
6.	1,2-distearoyl-sn-glycero-3-phosphoethanolamine-N-[cyanur(polyethylene glycol)-2000]	DSPE-PEG(2000) Cyanur
7.	1,2-distearoyl-sn-glycero-3-phosphoethanolamine-N-[maleimide(polyethylene glycol)-5000]	DSPE-PEG(5000) Maleimide
8.	1,2-dipalmitoyl-sn-glycero-3-phosphoethanolamine	DPPE
9.	1,2-dipalmitoyl-sn-glycero-3-phosphoethanolamine-N-[azido(polyethylene glycol)-2000]	DPPE-PEG(2000) Azide
10.	1,2-dioleoyl-sn-glycero-3-phosphoethanolamine	DOPE
11.	1,2-dioleoyl-sn-glycero-3-phosphoethanolamine-N-[amino(polyethylene glycol)-2000]	DOPE-PEG(2000)Amine
12.	1,2-dioleoyl-sn-glycero-3-phosphoethanolamine-N-[carboxy(polyethylene glycol)-2000]	DOPE-PEG(2000)Carboxylic Acid

The preparation of liposomes needs to solubilize all the lipids in the organic phase. This organic phase is then either converted to dry lipid layer which is then hydrated or may directly be incorporated in the aqueous phase. These steps usually end up in the formation of MLV. The formed MLV are then sonicated or extruded from French pressure extruder to get SUV [50].

1.3.2.1.1 Film Hydration Method

The combination of lipids is dissolved in some organic solvent (usually mixture of chloroform and methanol). This step ensures the formation of homogenous lipids mixture.

The organic solvent is evaporated by heating and under vacuum to form uniform layer on some solid surface, usually a round bottom flask. The hydration of this layer results in the formation of MLV [49-50]. The temperature of hydrating medium (water or buffer) should be above phase transition temperature for effective hydration of lipid layer.

1.3.2.1.2 Solvent Spherule Method

The organic and water phases are mixed for nearly one hour under reduced pressure. The outcome of mixing is in the form of o/w emulsion. Thus the formed emulsion is subjected to the removal of organic phase to obtain MLV [49-50].

1.3.2.1.3 Reverse Phase Evaporation Method

This method resembles with the solvent spherule method. However, the vigorous shaking results in the formation of w/o emulsion. The resultant emulsion, when subjected to organic phase evaporation, produces aqueous phase containing distributed large unilamellar vesicles [49, 51].

1.3.2.1.4 Solvent Injection Method

This method is used to prepare SUV. The lipid components of liposomes are dissolved in ethanol. The organic phase is then injected in the aqueous phase, resulting in the fabrication of the formulation. The miscibility of ethanol with water results in decreased concentration of ethanol. Hence, the dissolved phospholipids assemble themselves in the form of SUV. In contrast, the injection of ether dissolved phospholipids cause liposome preparation after evaporation of ether [52-53].

1.3.3 Characterization of formulations for targeted cancer therapies

A number of different formulation related parameters influences efficiency of targeted therapies. These may include size, size distribution, zeta potential and morphological characteristics. Therefore, it is always the first and the most important topic of discussion to characterize these formulations. There is a list of variants for characterization; the most common of them are presented in Table 1.3.

Table 1.3: Techniques for characterization of colloidal used for targeted chemotherapies.

Sr. No.	Technique	Application	References
1.	Atomic Force Microscopy (AFM)	Size and size distribution, shape, structure, aggregates, surface properties	[54-56]
2.	Brunauer, Emmett and Teller (BET)	Surface area, porosity	[56]
3.	Dynamic Light Scattering (DLS)	Hydrodynamic size, size distribution	[57-58]
4.	Differential Scanning Calorimetry (DSC)	Structure and stability	[58-59]
5.	Elemental Analysis	Elemental composition	[56]
6.	Fourier Transform Infrared Spectroscopy (FTIR)	Conformation and structure of conjugate, Surface properties	[55, 58]
7.	Laser Doppler Velocimetry (LDV)	Zeta potential	[56, 60]
8.	Scanning Electron Microscope (SEM)	Shape, size, size distribution	[55, 58]
9.	Transmission Electron microscopy (TEM)	Shape, size, size distribution	[55, 61]
10.	UV-Vis	Concentration, stability	[58, 60]
11.	X-ray Photoelectron Spectroscopy (XPS)	Surface chemistry	[61-62]
12.	X-ray Diffraction (XRD)	Shape, size and structure for crystalline materials	[56, 58]

1.4 APTAMER

Aptamers are small and single stranded DNA or RNA with highly selective targeting ability. In nature they exist in combination with mRNA, influencing protein production. They can bind with different molecules, peptides, proteins or viral particles by hydrogen bonding, electrostatic interactions, and van der Waals forces. They are far superior to antibodies as they are chemically synthesized and molecular weight is between 6 kDa to 30 kDa. They are more stable, have long shelf life, possess less batch to batch variations, have no or low immunogenicity and can be modified at both 5' and 3' ends with any required modification [63-65].

A range of different aptamers have been generated and approved by food and drug administration (FDA). These targets are involved in cell growth, proliferation, migration and metastasis during cancer growth. Therefore, blocking the activities of these targets will block the growth of cancer cells [66-71]. A few examples of aptamers with target molecules are shown in Figure 1.2.
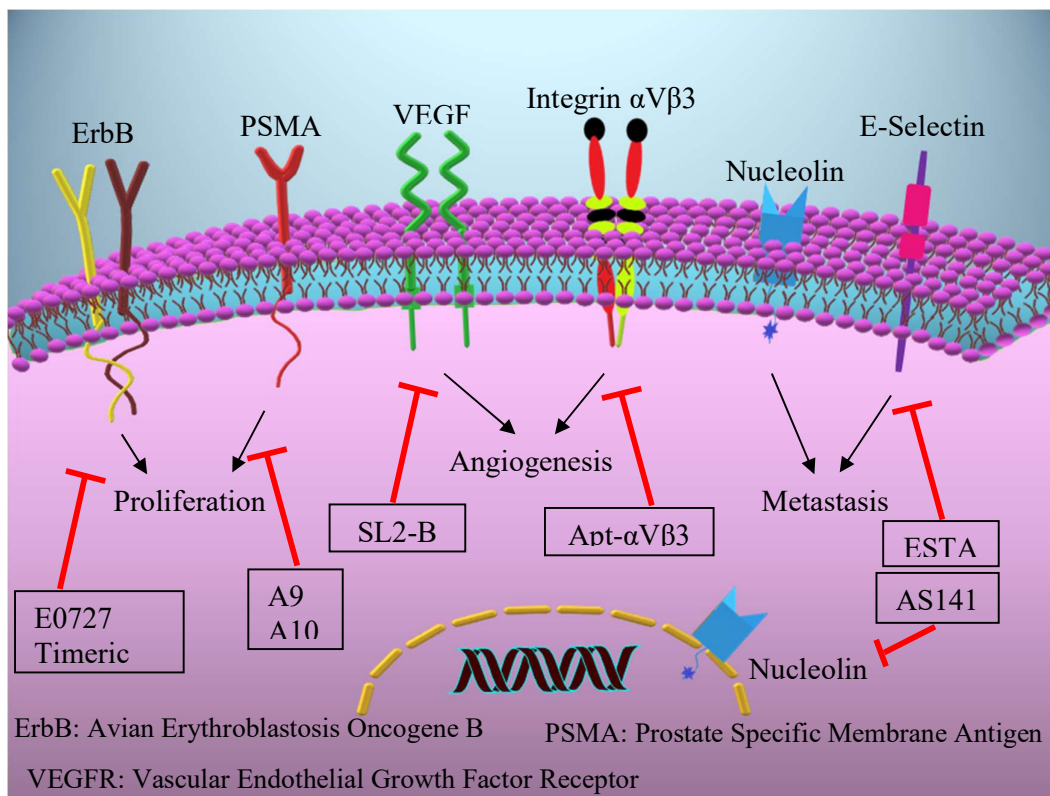
Figure 1.2: Some examples of aptamers (shown in black boxes), their targets and functions performed by targets.

1.5 AIM AND SCOPE

The high expression of different cell surface receptors in cancerous cells as compared to normal cells is well known fact now a days. ErbB3 is one of the receptor tyrosine kinase (RTK) and it is present in much higher concentration in cancerous cells. This receptor is responsible for cell growth, proliferation and metastatic progression [72-77]. Therefore, inhibition of this receptor by a ligand can arrest cell signaling and ultimately the growth of tumors [78-83]. Thus, surface modification of drug-loaded colloidal systems with an anti-ErbB3 aptamer, to achieve specific drug delivery, was the main objective of current study.

Sorafenib was used as chemotherapeutic agent in all advance colloidal systems (nanoparticles, microparticles and liposomes). A set of different *in vitro* and *in vivo* experiments were performed to validate the idea of combining this chemotherapeutic agent and aptamer. Briefly, the key aspects of the study are as follows;

1. Designing of advance colloidal systems (nanoparticles, microparticles and liposomes)
2. Optimizing the formulations according to physiochemical properties
3. Surface modification with anti-ErbB3 aptamer (Figure 1.3)
4. Physico-chemical characterization of final formulations before and after surface modification
5. Confirmation of cytotoxicity and apoptosis body formation by formulations with and without drug and/aptamer
6. Assessing the internalization method of formulations by clathrin and caveolae-mediated endocytosis
7. *In vivo* characterization of selective and most effective formulations
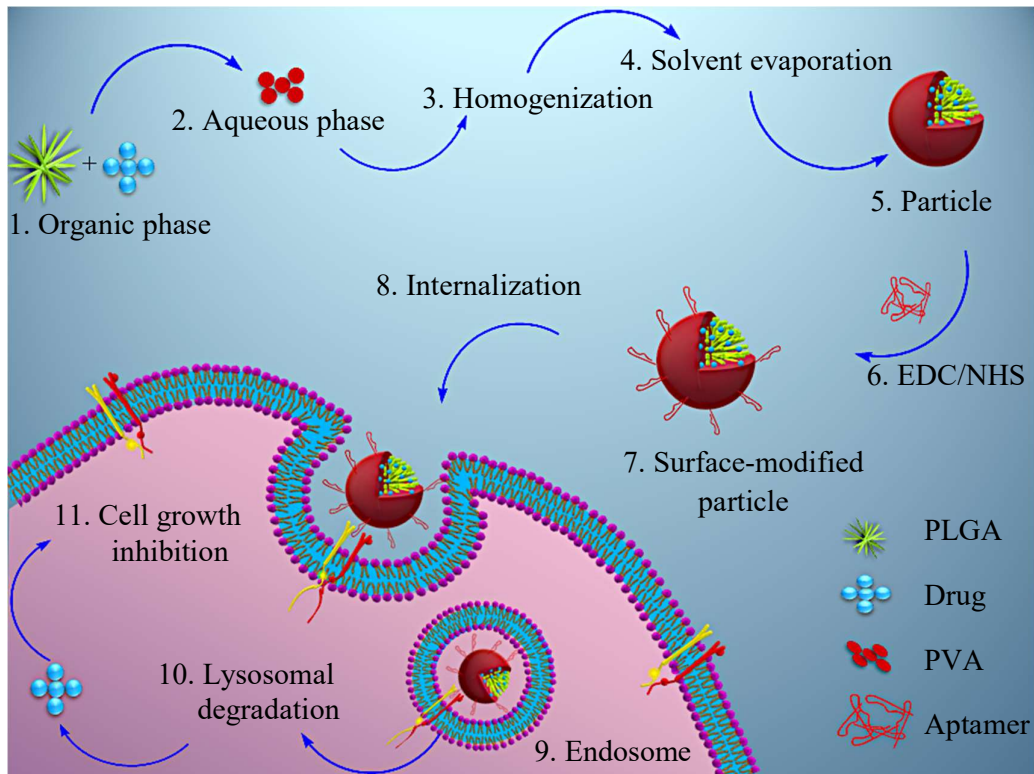
Figure 1.3: Schematic representation of preparation, surface modification, internalization and degradation of PLGA particles.

Materials and Methods

2.1 MATERIALS

2.1.1 Chemicals, Reagents, Equipments and Software

Table 2.1: List of chemicals.

Name	Company
1-ethyl-3-(3-dimethylaminopropyl)-carbodiimide	Sigma Aldrich, Darmstadt, Germany
1,2-dipalmitoyl-sn-glycero-3-phosphocholine	Lipoid GmbH, Ludwigshafen, Germany
1,2-distearoyl-sn-glycero-3-phosphoethanolamine-N-[cyanur(polyethylene glycol)-2000]	Avanti Polar Lipids, Alabam, USA
2-(*N*-morpholino) ethanesulfonic acid	Serva, Heidelberg, Germany
2′,7′-dichlorofluorescein diacetate	Sigma Aldrich, Darmstadt, Germany
3-(4,5-dimethyl-2-thiazolyl)-2,5-diphenyl-2H-tetrazolium bromide	Sigma Aldrich, Darmstadt, Germany
4′,6-diamidino-2-phenylindole	Sigma Aldrich, Darmstadt, Germany
Agar	Sigma Aldrich, Darmstadt, Germany
Agarose	Carl Roth, Karlsruhe, Germany
Calcium Chloride	Carl Roth, Karlsruhe, Germany
Chloroform	Sigma Aldrich, Darmstadt, Germany
Cholesterol	Sigma Aldrich, Darmstadt, Germany
Disodium Hydrogen Phosphate	Carl Roth, Karlsruhe, Germany
Dimethyl Sulfoxide	Acros Organics, Geel, Belgium
Ethanol	Fisher, UK
Ethyl Acetate	Chemsolute, TH. Geyer, Germany
Magnesium Chloride	Carl Roth, Karlsruhe, Germany
Methanol	Sigma Aldrich, Darmstadt, Germany
N-Hydroxysuccinimide	Sigma Aldrich, Darmstadt, Germany
Paraformaldehyde	Carl Roth, Karlsruhe, Germany
Poly(lactic-co-glycolic acid)	Evonic Darmstadt, Germany
Poly Vinyl Alcohol	Kuraray, Hattersheim, Germany
Potassium Chloride	Merck, Darmstadt, Germany
Potassium Dihydrogen Phosphate	Merck, Darmstadt, Germany
Purified Water	Purelab Flex, Elga, UK

Sodium Chloride	Carl Roth, Karlsruhe, Germany
Sorafenib Tosylate	LC Laboratories, USA
Tert-Butylhydroperoxide	Sigma Aldrich, Darmstadt, Germany
Tetrahydrofuran	Carl Roth, Karlsruhe, Germany
Tris (hydroxymethyl) amino methane	Merck, Darmstadt, Germany
Triton™ X-100	Sigma Aldrich, Darmstadt, Germany

Table 2.2: List of cell culture medium and reagents.

Name	Company
Anti-ErbB3 aptamer	Eurogentec, Belgium
Dulbecco's Modified Eagle *Medium*	Capricorn Scientific, Ebsdorfergrund, Germany
FluorSave	Calbiochem Corp, La Jolla, USA
Foetal Bovine Serum	Capricorn Scientific, Ebsdorfergrund, Germany
Iscove's Modified Dulbecco's *Media*	Capricorn Scientific, Ebsdorfergrund, Germany
MDA-MB-231 Cell Line	ATCC, Manassas, USA
Roswell Park Memorial Institute Medium	Capricorn Scientific, Ebsdorfergrund, Germany
SK-OV-3 Cell Line	ATCC, Manassas, USA
Trypsin –EDTA	Sigma-Aldrich, St. Louis, USA

Table 2.3: List of equipments.

Name	Company
AFM Probe; HQ:MSC16/Al BS	Micromasch, Tallinn, Estonia
Atomic Force Microscope; Nanowizard® 1	JPK Instruments AG, Berlin, Germany
Autoclave; DX-45	Systec lab, Linden, Germany
Bath Sonicator; Transonic Digital S	Elma Schmidbauer GmbH, Singen, Germany
Bioshaker; KS4000 IC	IKA Werke, Staufen, Germany

Carbon Tabs	PLANO GmbH, Wetzlar, Germany
CCD-Camera; Gatan Mega Scan 794	Gatan Inc., Pleasanton, USA
Cell Culture Lysis Reagent	Promega GmbH, Mannheim, Germany
Centrifuge; Eppendorf 5418	Eppendorf, Hamburg, Germany
Centrifuge; Beckman J2-21	Beckman Coulter GmbH, Krefeld, Germany
Confocal Laser Scanning Microscope LSM 700	Carl Zeiss Microscopy GmbH, Jena, Germany
Digital Image Acquisition System; DISS 5	Point Electronic GmbH, Halle, Germany
Extruder; Avanti Mini	Avanti Polar Lipids Inc., Alabaster, USA
Fluorescence Microscope; CKX53	Olympus, Hamburg, Germany
Fluostar Optima Plate Reader	BMG Labtech, Offenburg, Deutschland
Freeze Drier; Christ Beta I	Martin Christ Gefriertrocknungsanlagen GmbH, Osterode am Harz, Germany
Laminar Flow Hood; Labgard Class II	NuAire Inc., Plymouth, USA
Magnetic Bar	IKA-Werke, Staufen, Germany
Microscopy Slides	Gerhard Menzel B.V. & Co. KG., Braunschweig, Germany
Multichannel Pipette	Mettler Toledo, Gießen, Deutschland
Multistage Magnetic Stirrer RT10 Power	IKA-Werke, Staufen, Germany
Pipette Tip 100-1000 µl	Sarstedt, Nümbrecht, Germany
Pipette Tip 10-200 µl	Sarstedt, Nümbrecht, Germany
Pipette Tip 1-10 µl	Sarstedt, Nümbrecht, Germany
Rotary Evaporator; Laborota 4000	Heidolph Instruments GmbH & Co. KG., Schwabach, Germany
Scanning Electron Microscope; Hitachi S-510	Hitachi-High Technologies Europe GmbH, Krefeld, Germany
Spectrophotometer; Ultrospec 3000	Pharmacia Biotech AG, Uppsala, Sweden
Sputter Coater; Edwards S150	Edwards, Crawley, UK
Thermometer	IKA-Werke, Staufen, Germany
Ultrasound Bath; Elma Elmasonic P	BANDELIN electronic GmbH & Co. Berlin, Germany
UV Spectrophotometer; UV mini 1240	Shimadzu, Japan
Vacuum Pump; SC 920	KNF Neuberger GmbH, Freiburg, Germany

Water Bath	Kottermann GmbH & Co. KG., Hänigsen, Germany
Weighing Balance; ExplorerEX225D	Ohaus, Parsippany, USA
Zetasizer Nano ZS	Malvern Instruments Ltd, Malvern, UK

Table 2.4: List of self prepared buffers and reagents.

Name	Ingredients	Quantity
Anti-ErbB3 Aptamer	Anti-ErbB3 Aptamer	10 nmol
	PBS pH 7.4 (QS)	1 ml
EDC	EDC	0.08 g
(400 mM)	Purified Water (QS)	1 ml
MES Buffer	MES	9.76 g
	NaCl	2.92 g
	Purified Water (QS)	500 ml
MTT Reagent	MTT	0.20 g
(0.2 %)	Purified Water (QS)	100 ml
NHS	NHS	0.023 g
(200 mM)	Purified Water (QS)	1 ml
Phosphate Buffer	KCl	0.50 g
	NaCl	20.0 g
	KH_2PO_4	0.50 g
	$NaHPO_4.2H_2O$	1.14 g
	Purified Water (QS)	1000 ml
Phosphate Buffer	KCl	0.20 g
(with Ca and Mg)	NaCl	8.00 g
	KH_2PO_4	0.20 g
	$NaHPO_4.2H_2O$	1.14 g
	$MgCl_2.6H_2O$	0.10 g
	$CaCl_2.2H_2O$	0.13 g
	Purified Water (QS)	1000 ml
Poly Vinyl Alcohol	PVA	2.00 g
	Purified Water (QS)	100 ml

TAE Buffer	Tris HCl	4.84 g
	Glacial Acetic Acid	1.14 ml
	EDTA (pH 8.0)	4.00 ml
	Purified Water (QS)	1000 ml
Tris Buffer (0.1 % v/v)	Triton X-100	100 μl
	Purified Water (QS)	100 ml

Table 2.5: List of consumables.

Consumable	Company
0.2 μm PES Syringe Filters	Whatman PLC, Buckinghamshire, UK
1.5 ml Microtubes	Sarstedt, Nümbrecht, Germany
12-well plates; Nunclon Delta	Nunc GmbH & Co. KG., Wiesbaden, Germany
15 ml Falcon Tubes	Sarstedt, Nümbrecht, Germany
18×18 mm cover slips	Gerhard Menzel B.V. & Co. KG., Braunschweig, Germany
24-well plates; Nunclon Delta	Nunc GmbH & Co. KG., Wiesbaden, Germany
3.5 ml Transfer Pipette	Sarstedt, Nümbrecht, Germany
50 ml Falcon Tubes	Sarstedt, Nümbrecht, Germany
96-well plates White	Brand, Wertheim, Germany
96-well plates; Nunclon Delta	Nunc GmbH & Co. KG., Wiesbaden, Germany
Adhesive plate seals	Boehringer Mannheim GmbH, Mannheim, Germany
Disposal Bags	Sarstedt, Nümbrecht, Germany
Paraffin film M	Bemis, Braine L' Alleud, Belgium
Petri Dishes; Tissue Culture grade	Sarstedt, Nümbrecht, Germany
Silicon Wafer	Sigma-Aldrich, St. Louis, USA

Table 2.6: List of software.

Software	Version
ChemDraw	Version 7
Gimp	Version 2.10.6
GraphPad Prism	Version 8.0.1
ImageJ	152 Win
Minitab	Version 17
Microsoft Office	MS 2007
Origin	2016
SketchAnd Calc^{TM}	Free Windows Tool

2.1.2 Polymers and Lipids

2.1.2.1 PLGA

Poly (lactic-co-glycolic acid) abbreviated as PLGA is white amorphous powder and is amongst one of the FDA approved polymer for pharmaceuticals. PLGA 503H (50:50, Lactide:Glycolide) was used for the preparation of nanoparticles and microparticles (Figure 2.1). Its molecular weight is 30,000 g/mol and stored between 2-8 °C. This polymer contains –COOH group at end terminal and thus is suitable candidate for any carboxylic acid reaction [84-85]. PLGA used in current study was obtained from Evonic Darmstadt, Germany. For the preparation of nanoparticles and microparticles freshly weighed PLGA was dissolved in ethyl acetate.
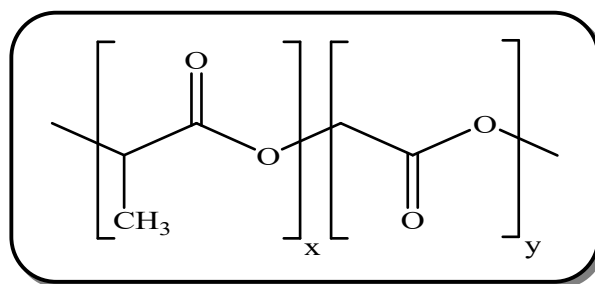
Figure 2.1: Structural formula of PLGA.

2.1.2.2 PVA

Polyvinyl alcohol abbreviated as PVA is an odorless and white to cream-colored granular powder. Its molecular weight is ~31,000 g/mol [84]. It is one the most commonly used stabilizer and viscosity-increasing agent in pharmaceuticals [86]. 2 % stock solution was prepared by heating 2 g of PVA in 100 ml purified water (Purelab Flex, Elga, UK) at 60 °C with constant stirring. The final solution was filtered through 200 nm PES syringe filters Whatman PLC, Buckinghamshire, UK. The stock solution was then stored between 2-8 °C until further use for preparation of PLGA matrices.
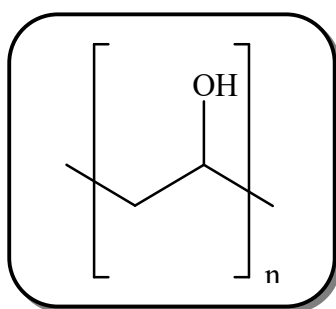
Figure 2.2: Structural formula of PVA.

2.1.2.3 DPPC

Dipalmitoylphosphatidylcholine (1,2-dipalmitoyl-sn-glycero-3-phosphocholine), abbreviated as DPPC is white amorphous powder and is one of the most commonly used fatty acid derivative used in liposomal preparation. Its molecular weight is 734.04 g/mol and phase transition temperature is 41 °C [84]. It is rarely used as auxiliary agent in liposome preparation because of less stability [87]. Hence cholesterol is commonly used along with DPPC to increase stability of liposomes. Cell membrane lipid bilayer is rich in DPPC. However, DPPC used during current study was of chemical origin. 10 mg of this lipid was dissolved in 1 ml chloroform:methanol (2:1) and stored at -20 °C until further use.
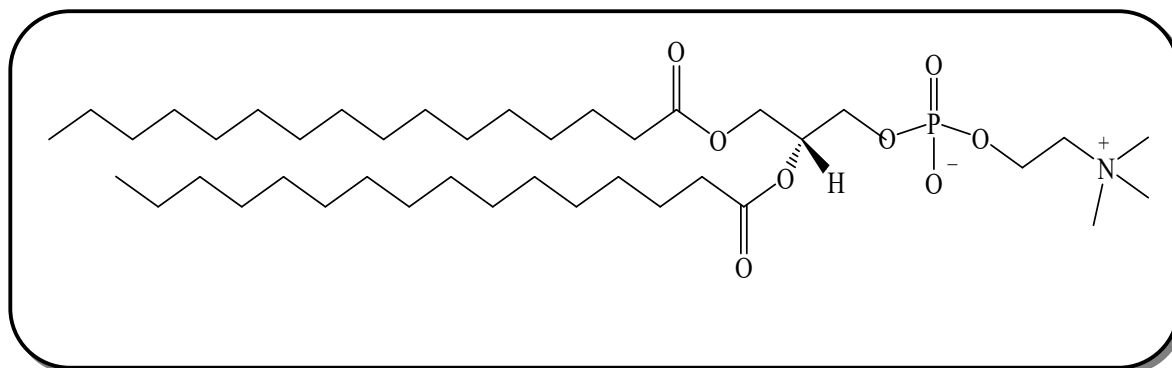
Figure 2.3: Structural formula of DPPC.

2.1.2.4 DSPE-PEG(2000) Cyanur

1,2-distearoyl-sn-glycero-3-phosphoethanolamine-N-[cyanur(polyethylene glycol)-2000] is white to off-white amorphous powder and has molecular weight 2938.44 g/mol (Figure 2.4). This lipid is used for post formulation modification of liposomes. Primary amine linked antibodies or aptamer can be attached on the surface of liposomes in the presence of this lipid [88]. 10 mg of this lipid was dissolved in 1 ml chloroform:methanol (2:1) and stored at -20 ℃ until further use.
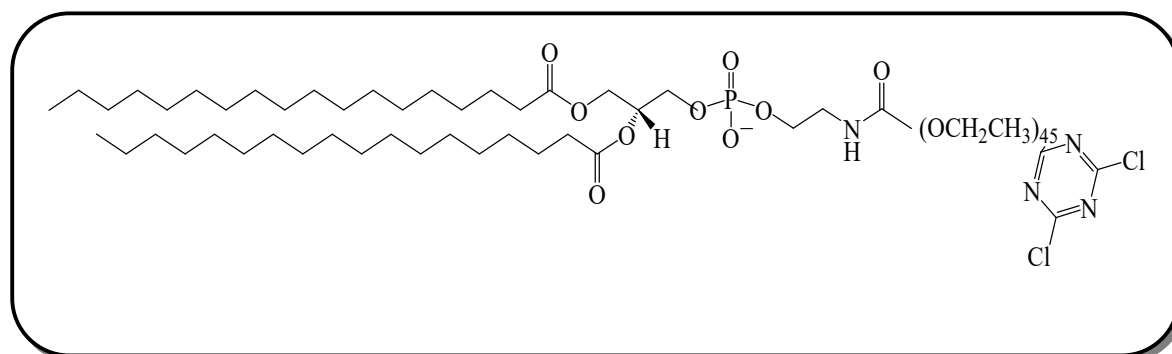
Figure 2.4: Structural formula of DSPE-PEG (2000) cyanur.

2.1.2.5 Cholesterol

Cholest-5-en-3b-ol is white to faintly yellow and almost odorless powder or granule (Figure 2.5). Its molecular weight is 386.67 g/mol [84]. It may be used up to maximum 50 mol % [89] and imparts stability to the liposomes. The stability is due to decrease surface interaction of liposomes with peripheral proteins and cell membrane in the presence of cholesterol and

change in phase transition temperature [90]. 10 mg of cholesterol was dissolved in 1 ml chloroform:methanol (2:1) and stored at -20 °C until further use.
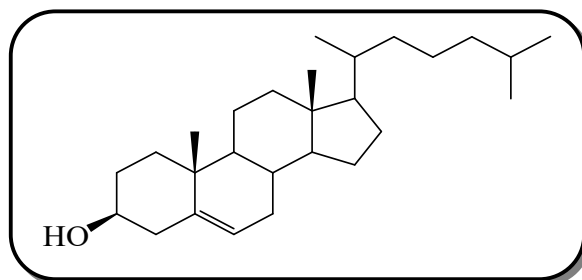
Figure 2.5: Structural formula of cholesterol.

2.1.3 Sorafenib Tosylate

Sorafenib tosylate (SFB) is white crystalline to powder solid with molecular weight 637.03 g/mol (Figure 2.6). Its LogP value is 4.54 with biopharmaceutical classification systems (BCS) class IV making it poorly soluble in water but freely soluble in DMSO [91]. SFB is oral multi-kinase inhibitor, inhibiting VEGFR (vascular endothelial growth factor receptor) and PDGFR (platelet derived growth factor receptor), resulting in inhibition of angiogenesis and vasculogenesis [91-93].
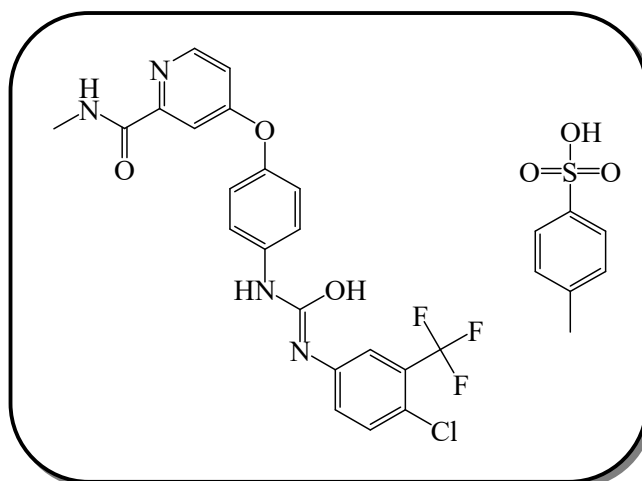
Figure 2.6: Structural formula of sorafenib tosylate.

2.1.9.1 Anti-ErbB3-Aptamer

Anti-ErbB3 RNA aptamer, (Apt) with 5' cyanine 5 (Cyn 5) and 3' C6 amino modifier spacer group(5′-CAGCGAAAGUUGCGUAUGGGUCACAUCGCAG-3′) was used for targeted

chemotherapy. Fluorescent dye was intentionally attached to Apt to visualize formulations in cell culture studies. The primary amine of C6 spacer group (Figure 2.7) also provided space for attachment of aptamer on the surfaces of formulations. 3' end modification was done to save aptamer from attack of nucleases [94-95]. The mother solution of Apt was prepared in PBS (pH 7.4) at concentration of 10 nM/ml and stored at -20 °C until further use.
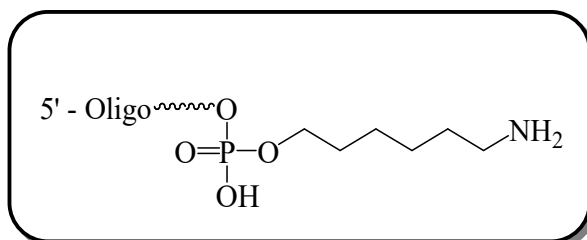
Figure 2.7: 3' C6 Amino modifier group.

2.1.10 Cell Line and Cell Culture

ErbB3 positive human breast cancer cell line MDA-MB-231 was purchased from ATCC Manassas, USA. Cells were grown in RPMI:DMEM (50:50) (Capricorn Scientific, Ebsdorfergrund, Germany) supplemented with 10 % fetal bovine serum (Sigma Aldrich). Cells were cultivated in humid conditions at 37 °C and 7% CO_2.

2.2 METHODS

2.2.1 Preparation of Formulations

2.2.1.1 Preparation of Nanoparticles and Microparticles

Preparation of PLGA nanoparticles (PN) was performed by o/w emulsion solvent evaporation method [43]. Briefly, 50 mg of PLGA was dissolved in 5 ml of ethyl acetate (organic phase). The organic phase was added drop wise to a 5 ml solution of 2 % of PVA in purified water (Purelab Flex 4, Elga Labwater, High Wycombe, UK). The resultant emulsion was then homogenized using Ultra-turrax homogenizer (IKA-T25, IKA Werke, Staufen, Germany) with 18 G dispersing stainless steel element at a constant speed of 14,500 rcf for 10 min. Water was added to facilitate organic solvent evaporation (see Graphical Abstract). SFB-loaded PLGA nanoparticles (PNS) were prepared by the same method, except that SFB was dissolved in THF:EtOH (4:1) and was mixed with PLGA solution in ethyl acetate. On the other hand, the preparation of microparticles (MP)/ SFB-loaded microparticles (MPS) was also done with the same procedure except using 0.25 % solution of PVA and homogenization was done at 3.2 rcf for 25 sec (Figure 2.8). The prepared nano/microparticles were washed

three times with purified water followed by centrifugation for 10 min for each washing step. Finally, particles were re-suspended in purified water.
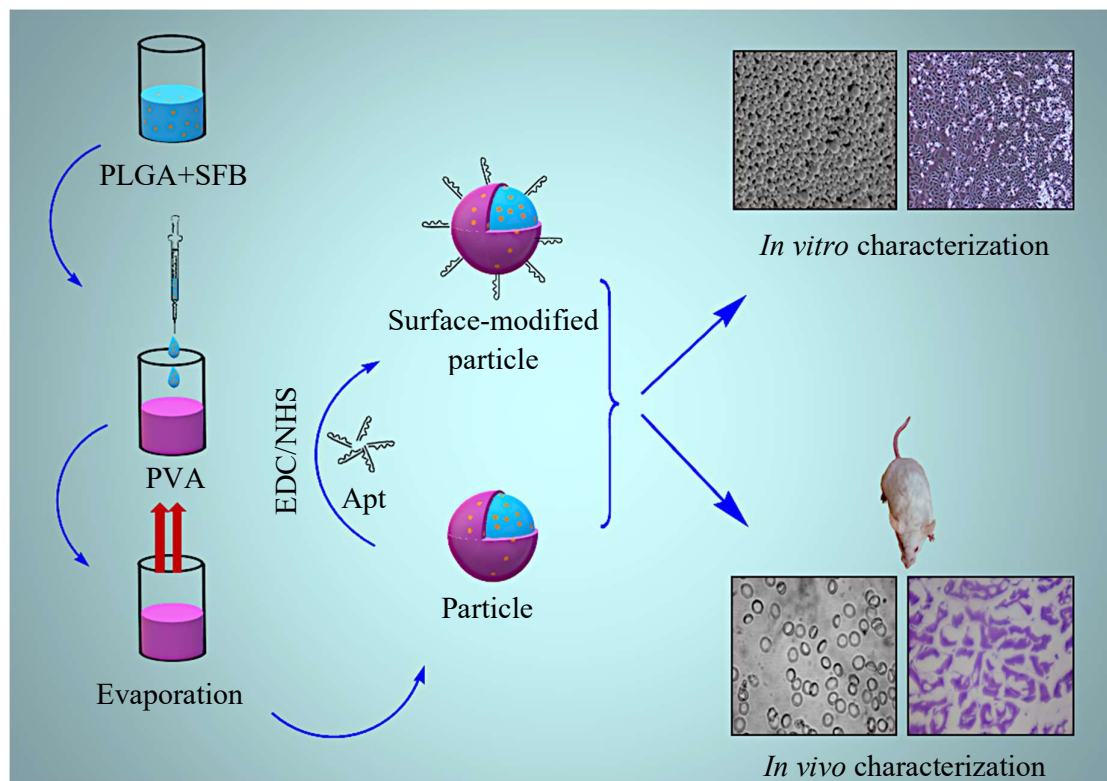
Figure 2.8: Preparation of nano/microparticles and in *vitro* and *in vivo* characterization.

2.2.1.2 Preparation of Liposomes

Liposomes (LP) were prepared by film hydration method. Briefly, DPPC:Cholesterol:DSPE-PEG (2000) cyanur (80:10:10) stock solutions were taken in 5 ml round bottom flask. Using rotary evaporator (Laborota 4000, Heidolph Instruments GmbH & Co. KG., Schwabach, Germany) equipped with vacuum pump, organic solvents were removed. This resulted in the formation of dried lipid layer. The film was hydrated with 1 ml of 100 mM sodium borate buffer (pH 8.8) making final concentration of lipids 5 mg/ml and sonicated in bath sonicator (Transonic Digital S, Elma Schmidbauer GmbH, Singen, Germany) for 20 min. The colloidal system of liposomes was then extruded 25 times through 200 nm polycarbonate membrane filters at 45 °C (Whatman, Buckinghamshire, UK) using an extruder (Avanti Mini, Avanti Polar Lipids Inc., Alabaster, USA). SFB-loaded liposomes (LPS) were prepared in similar fashion, except, drug solution in THF:EtOH (4:1) was added in organic phase (Figure 2.9).
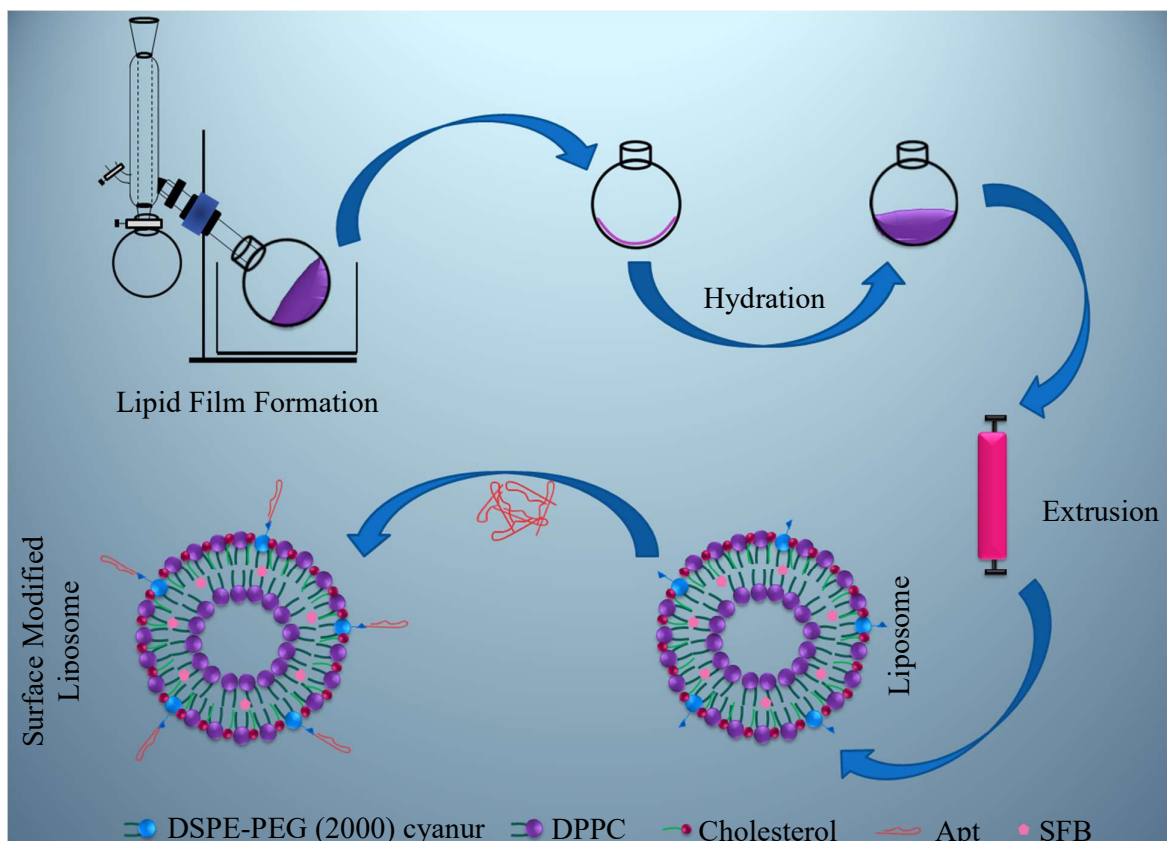
Figure 2.9: Preparation of liposomes by film hydration method.

2.2.2 Encapsulation Efficiencies

PNS and MPS were centrifuged (Eppendorf centrifuge 5418, Eppendorf, Germany) at 14,500 and 10,000 rcf, respectively, for 10 min at room temperature. On the other hand, LPS were centrifuged at 6,000 rcf for 1 h at 4 °C. The supernatant was removed and the pellet was dissolved in DMSO to extract the drug from the respective formulations. Samples were analyzed by UV spectrophotometry (UV mini 1240, Shimadzu, Japan) at 265 nm. A calibration curve was recorded with known concentrations of the drug. The solvent background was recorded from particles without drug and encapsulation efficiency was calculated using the following equation:

$$EE(\%) = \frac{Amount\ of\ drug\ in\ formulation}{Amount\ of\ drug\ loaded} * 100$$

2.2.3 *In Vitro* Release Profile

The release profile of SFB was evaluated in PBS (pH 7.4) with 1 % v/v Tween 80. 1 ml of nano/microparticle suspension was washed thrice with PBS, followed by centrifugation at 14,500 or 10,000 rcf, respectively, for 10 min. The pellets were re-suspended in 1 ml PBS with 1 v/v % Tween 80 and placed in an orbital shaker, KS4000 IC (IKA Werke, Staufen, Germany) at 150 rpm and 37 ± 0.5 °C. The samples were removed after designated time intervals, after centrifugation, the pellets were re-suspended in 1 ml PBS/1 % Tween 80 and returned to the shaker. After defined time intervals, pellets were dissolved in 1 ml DMSO and analyzed by UV spectrophotometer (UV mini 1240, Shimadzu, Japan) at 265 nm. The vehicle background was then subtracted by measuring the pellet of PLGA nano/microparticles, without SFB, prepared under the same condition.

2.2.4 Surface Modification

Surface modification of nano/microparticles was carried out using EDC and NHS coupling reaction with a primary amine at the 3'prime end of Apt. Particles were washed three times with purified water followed by centrifugation and finally re-suspended in MES buffer (pH 5.5). They were then treated with 400 mM EDC and 200 mM NHS for 30 min for surface activation. The particles were incubated with Apt at a particle:Apt ratio of 1:12. This resulted in the reaction of the primary amine of Apt with EDC/NHS activated nano/microparticles. After 2 h of incubation, washing was done with purified water and nano/microparticles were re-suspended in purified water (Figure 2.10). The modified particles were stored at 4 °C until further use.

On the other hand, for the modification of liposomes, Apt was added to prepared liposomes at equimolar DSPE-PEG (2000) cyanur: Apt ratios [88]. The reaction mixture was allowed to react for 24 h (Figure 2.11). The un-conjugated Apt was separated by dialysis (MWCO 6000) in PBS (pH 7.4). The modified liposomes were stored at 4 °C until further use.
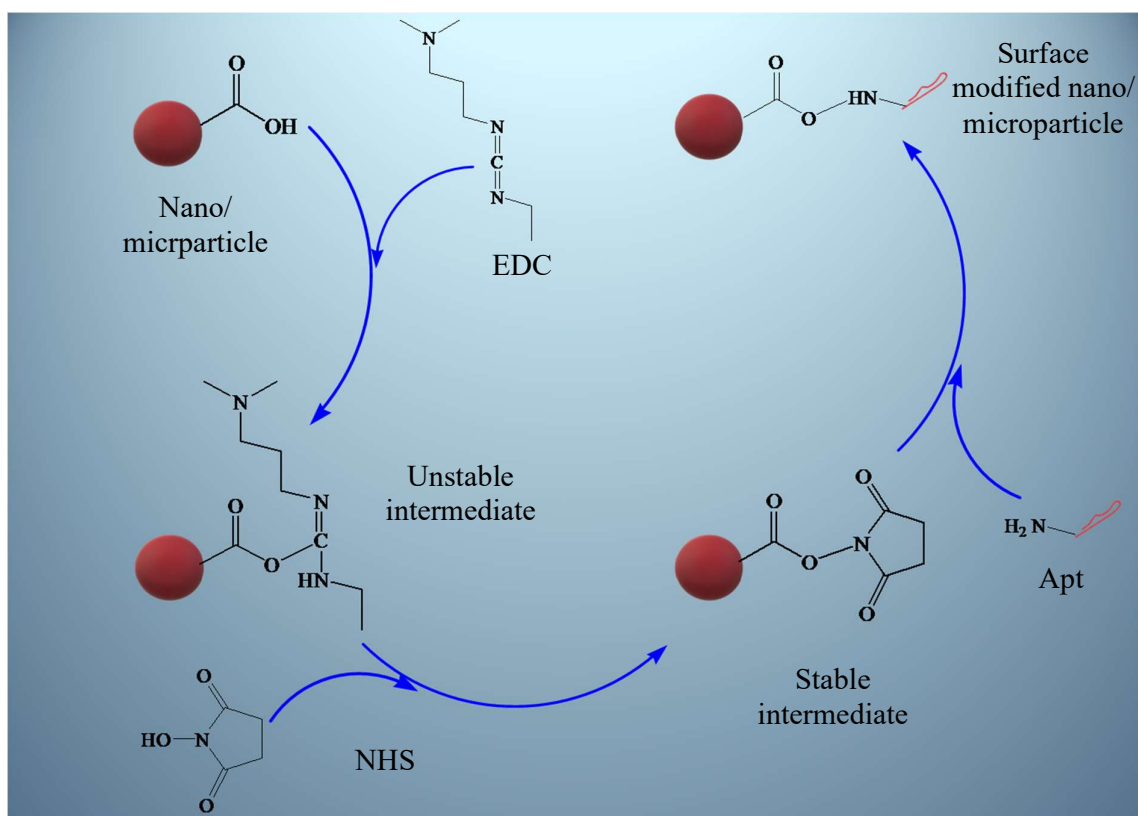
Figure 2.10: Surface modification of nano/microparticles.
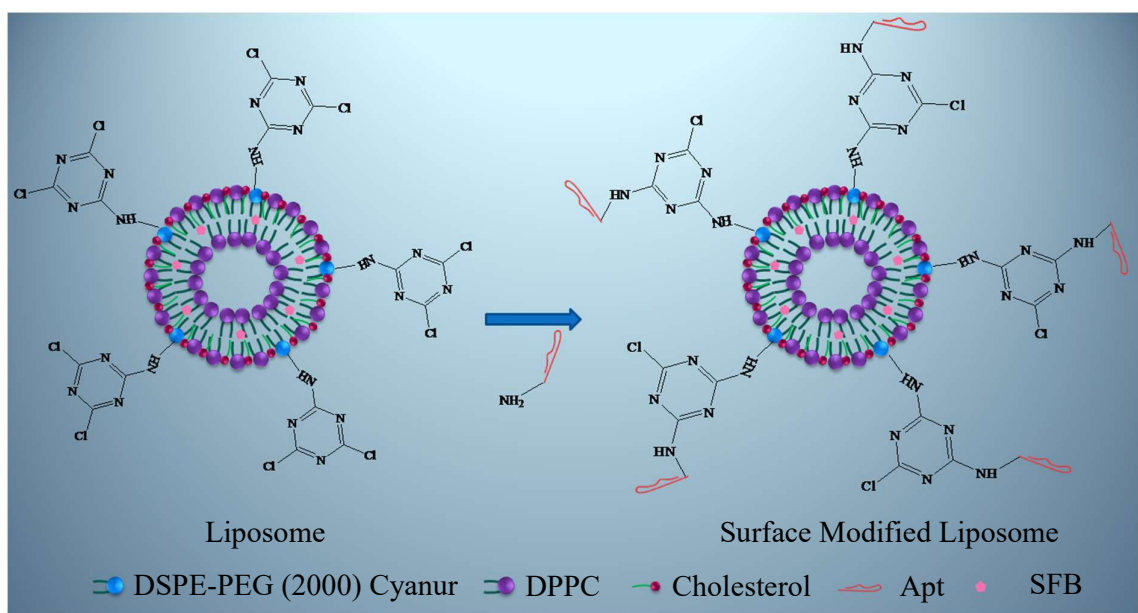
Figure 2.11: Surface modification of liposomes.

2.2.5 *In Vitro* Characterization

2.2.5.1 Physicochemical Characterization

2.2.5.1.1 Aptamer Coupling

Fluorescence of Cyn 5 labeled Apt was quantified in all colloidal systems to assess the binding of Apt. For this, freshly prepared surface-modified particles were washed and fluorescence of the supernatant and the pellet was quantified using a Fluostar Optima plate reader (BMG Labtech, Offenburg, Germany) at λ_{ex} 630 nm and λ_{em} 670 nm as follows;

$$Fluorescence\ (\%) = \frac{Fluorescence\ of\ Formulation}{Fluorescnce\ of\ Aptamer} * 100$$

2.2.5.1.2 FTIR Spectroscopy

The assessment of coupling of Apt with PLGA matrices by Fourier transform infrared spectroscopy (FTIR) was done by single reflection diamond ATR module FTIR (Alpha-P, Bruker Instruments, Massachusetts, USA). Freeze dried particles were loaded onto ATR platinum diamond crystal. Back correction was done in the absence of any sample. The average of 21 scans at spectral resolution of 2 cm^{-1} was taken automatically to obtain each spectrum. The spectrum was collected at a range between 4,000 cm^{-1} and 400 cm^{-1} and was expressed as % transmittance.

2.2.5.1.3 Elemental Analysis

PLGA and PVA molecules lack nitrogen in their atomic structure. However, the Apt contains nitrogen as a part of nucleotide bases. This fact was used to analyze the presence or absence of Apt in formulations by elemental analysis. Freeze dried samples were taken in aluminum crucibles, weighed and loaded into the elemental analyzer combustion chamber (VarioMicro Cube, Elementar Analysensyteme, GmbH, Langenselbold, Germany). Percentage of carbon, hydrogen and nitrogen was obtained and averages of three independent formulations were considered.

2.2.5.1.4 Particle Size and Zeta Potential

The size distribution of the formulations was measured by dynamic light scattering (DLS) using Zetasizer Nano ZS (Malvern Instruments, Malvern, UK). Samples were diluted with purified water in a ratio of 1:50 and were analyzed. Before the measurement, the sample

temperature was equilibrated to 25 °C. All the measurements were done independently in triplicates and the sub runs were adjusted by the instrument automatically. Size distribution was evaluated by intensity distribution and PDI was also calculated by Zetasizer Nano ZS software. Zeta potential was assessed by laser doppler velocimetry (LDV) using the same instrument at conductivity of < 100 µS/cm. All the results were represented as mean ± standard deviation of three individual experiments.

2.2.5.2 Morphological Characterization

2.2.5.2.1 Atomic Force Microscopy (AFM)

To study the morphology of the nanoparticles and liposomes, samples were diluted (1:100) with purified water and were analyzed using atomic force microscopy (Nano Wizard, JPK Instruments, Berlin, Germany). Samples were pipette onto silicon wafers. After 10 min, the liquid was aspirated and was let dry for 5 min. After drying, samples were analyzed by aluminium coated silicon nitride cantilever (HQ: NSC14AL/BS, Mikromasch, Tallinn, Estonia) at a frequency of 148 kHz and a force constant of 5 N/m. Scan speed was adjusted between 0.5 and 1.5 Hz. The surface roughness was measured automatically by JPK data processing software and was mentioned in the form of root mean square average (RMS Rq) values [96-98].

2.2.5.2.2 Scanning Electron Microscopy (SEM)

Hitachi S-510 scanning electron microscope (Hitachi-High Technologies Europe GmbH, Krefeld, Germany) was used for the analysis of the morphology of microparticles. Briefly, 20 µl samples were applied onto specimen stubs with conductive carbon tabs (PLANO Leit-Tabs; Ø 9 mm) and left to dry under a laminar airflow hood (Labgard Class II, NuAire Inc, Plymouth, USA). The samples were then sputtered with gold at 13.3 Pa Argon using an Edwards S150 sputter coater (Edwards Vacuum, Crawley, UK) and were examined using SEM at an accelerating voltage of 5 kV and focal distance 12 mm under 5.3×10^{-4} Pa vacuum [99]. The signals were processed digitally by DISS 5 digital image acquisition system (Point Electronic GmbH, Halle, Germany).

2.2.5.3 Cell Culture Studies

2.2.5.3.1 2D Cell Viability and IC$_{50}$

Cell viability and IC$_{50}$ values were evaluatedusing3-(4,5-dimethylthiazol-2-yl)-2,5-diphenyltetrazolium bromide (MTT) assay. 10,000 MDA-MB-231 cells/well (0.35 cm^2) were seeded in a 96-well plate and were incubated for 24 h. The cells were then treated with different concentrations of SFB-loaded formulations. After 5 h of incubation, the medium was removed and replaced with fresh medium and incubated further. After 12 h, the medium was removed and replaced with 2 mg/ml MTT reagent containing medium and incubated for 4 h. The resultant formazan crystals were dissolved using DMSO and absorbance was measured in a FluoStar Optima plate reader at 570 nm. The experiment was repeated three times and the percentage cell viability was calculated. IC$_{50}$ values were calculated by the concentration of nano/microparticles showing 50 % of the cell survival.

2.2.5.3.2 3D Cell Viability Assay

MDA-MB-231 cells were grown on 0.5 % agarose coated 96 well plates at concentration of 1,500 cells per well. After 72 h, culture was washed three times with PBS (pH 7.4). Formed *3D* cell cultures were treated with different liposomal formulations for 24 h. The untreated cultures were used as control. The morphology and size of *3D* cell cultures were then visualized under an inverted microscope (CKX53, Olympus, Tokyo, Japan) and percent change in area of *3D* culture was calculated by following equation;

$$3D\ Culture\ Area\ (\%) = \frac{Area\ at\ time\ t_{\mathrm{x}}}{Area\ at\ time\ t_{\mathrm{o}}} * 100$$

Whereas, t_{o} is zero time of experiment and t_{x} is time when area was measured.

2.2.5.3.3 Internalization Pathway

MDA-MB-231 cells were seeded into 96 well plates in a similar manner as for the viability experiments. After 24 h, the cells were incubated with either filipin III (6 µg/ml) or chlorpromazine (6 µg/ml) for 2 h. Cells were then treated with different formulations. After 4 h of incubation, the medium was removed and replaced with fresh medium. The cells were subsequently incubated for 12 h and the cell viability was determined by MTT assay as described above.

2.2.5.3.4 Apoptosis Assay

MDA-MB-231 cells were cultured on sterile cover slips in 24 well plates at a seeding density of 50,000 cells per well (1.8 cm^2) for 24 h. Cells were washed thrice with cold PBS buffer (pH 7.4). 500 µl of different formulations were added to the wells. After 12 h, cells were washed again with PBS and fixed using 4 % paraformaldehyde for 15 min. Cells were counterstained using DAPI (0.1 µg/ml) solution for 20 min. Washing was performed with PBS and cells were examined using a fluorescence microscope (CKX53, Olympus, Tokyo, Japan).

2.2.5.3.5 Reactive Oxygen Species Assessment

Determination of ROS production was done using 2',7'-dichlorodihydrofluorescein diacetate (carboxy-H$_2$DCFDA) conversion into 2',7'-dichlorofluorescein (DCF) as previously reported [100]. Briefly, MDA-MB-231 cells grown in 96 well plates for 24 h were washed (PBS buffer; pH 7.4) and incubated with phenol red-free medium containing 25 µM of carboxy-H$_2$DCFDA for 45 min. The cells were subsequently washed twice with PBS. Cells were then treated with nano/microparticles containing 1.0 µM and 1.5 µM of SFB. After 1 h, cells were washed again with PBS and lysed using lysis reagent (Promega, Mannheim, Germany). The fluorescence was observed at λ_{ex} 485 nm/ λ_{em} 520 nm using a FluoStar Optima plate reader.

2.2.5.3.6 Metastatic Progression

Inhibition of cell migration and metastasis was evaluated by wound healing assay. MDA-MB-231 cells were seeded in 24 well plate. After 24 h, cells were treated with nano/microparticles containing 5 µM SFB for 2 h in serum-free medium. A scratch was made with a 200 µl pipette tip. Cells were then washed twice with ice-cold PBS (pH 7.4) and fresh medium was added. Wound closure was observed using an inverted microscope (CKX53, Olympus, Tokyo, Japan) at different time intervals. Cell migration and percentage wound healing were also calculated using SketchAndCalcTM® along with Gimp2.10.10® application software measuring the distance between wound closures.

2.2.5.3.7 Cellular Uptake

For cellular uptake studies, MDA-MB-231 cells were cultured on sterile cover slips in 12-well plates at a seeding density of 90,000 cells per well (3.5 cm^2). After 24 h, the supernatant was removed and washed three times with PBS (pH 7.4). Cells were incubated for either 30

min or 2 h with different formulations. After washing with PBS cells were fixed with 4% paraformaldehyde for 20 min. Cell nucleus was then counterstained with DAPI (0.1 µg/ml) for 15 min in the dark. Cells were washed and the cover slips were mounted on to glass slides and with FluorSave (Calbiochem Corp, La Jolla, USA). Uptake analysis was performed using a confocal laser scanning microscope (LSM700, Carl Zeiss, Jena, Germany).

2.2.5.4 Chorioallantoic Membrane (CAM) Assay

Specific pathogen free fertilized eggs were purchased from Mastkukenbruterei Bromann (Rheda Wiendenbruck, Germany). The eggs were disinfected with 70 % ethanol and incubated in an egg hatching incubator, equipped with an automatic rotator at a temperature of 37 °C with a relative humidity of 60 %. On the egg development day 4, hole of 30 mm diameter was made into eggshell using a pneumatic egg punch (Schuett Biotech, Germany), to expose the CAM surface. The exposed part of the egg was then covered with a small petri dish and placed back into the incubator. On the egg development day (EDD) 11, 50 µl of different formulations were injected into the mesoderm of CAM, with the help of glass cannulas. The eggs were further incubated for 24 h and 1 cm of the CAM was dissected and placed on clear glass slide after washing with 0.9 % NaCl. Uptake analysis was performed using a confocal laser scanning microscope (LSM700, Carl Zeiss, Jena, Germany).

2.2.5.5 Hemocompatibility Studies

2.2.5.5.1 Ex vivo Hemolysis Assay

To determine the compatibility of the formulations with blood, human erythrocytes were isolated from fresh blood as described previously [101]. Briefly, erythrocytes were obtained by centrifugation of fresh blood in tubes containing EDTA. The pellet was washed three times with PBS buffer (pH 7.4) and diluted to1:50 with PBS. The erythrocytes were incubated together with the formulations in v-bottom microtitre plates (1 h, 37°C) and placed in an orbital shaker. The plates were centrifuged and the absorbance of the collected supernatant was determined at 540 nm in a FluoStar Optima plate reader. As controls, saline (NaCl 0.9 %), 1% Triton X-100 and blood were used.

2.2.6 *In Vivo* Characterization

2.2.6.1 Acute Toxicity Assessment

Female BALB/c (8–10 weeks old) mice weighing 31.1 ± 2.6 g, were divided into 6 groups (n = 3) and with free access of food and water (*ad libitum*). Experimental protocols were approved by the GC University animal experiment and ethical committee and were performed in collaboration with the in-house facility of My Pets clinic for clinical investigations. The animals were kept at 40 % humidity and a temperature of 22 ± 2 °C. The dose of the microparticles was equivalent to the 10 mg/kg dose of SFB. The first group was treated with MP, second with MP-Apt, third with MPS and fourth with MPS-Apt. One group was administered with the aptamer. Normalsalinetreated group was considered as control. The particle suspension was injected in the peritoneal cavity using a 26 G syringe needle in two equally divided doses on day 1and day 3. The mice were kept under observation for 7 days for alteration in body weight and visual observations for mortality, skin, sleek of fur, urine color, feces, salivation, respiration, eyes and sleep pattern and day-by-day signs of illness. Onthe 7th day, complete blood analysis was done and mice were euthanized for tissue histology studies. The vital organs (heart, liver, kidneys and lungs) were removed, carefully washed with normal saline and weighed. The comparison was made with weights of control and visceral index was calculated by the following equation;

$$\text{Visceral Index} = \frac{\text{Organ Weight}}{\text{Body Weight}} \times 100$$

2.2.6.2 Blood Biochemistry

Blood was drawn by intra-cardiac injection before euthanizing the mice. The effect of administration of microparticles on the biochemical markers of the blood was observed on the 7th day. These markers include complete blood count (CBC), liver function test (LFT), renal function test (RFT) and total plasma protein.

2.2.6.3 RBC Aggregation Test

To determine the compatibility of the formulations with blood, mice erythrocytes were incubated with different formulations. Briefly, red blood cells were obtained by centrifugation of fresh blood in tubes containing EDTA and then the pellet was washed three times with PBS (pH 7.4). The dilution with PBS (pH 7.4) was done at 1:10

(microparticle:PBS) ratio. The erythrocytes were incubated with the formulations for 30 min at 37 °C. Centrifugation was done at 500 rcf and the pellet washed with PBS. The cell suspension was directly observed under a light microscope.

2.2.6.4 Histopathology

Heart, liver, kidney and lungs were removed after euthanizing the mice and washed with PBS (pH 7.4). These organs were visually inspected for lesions and any abnormality. The organs were placed in 4 % formalin solution for 24 h. Dehydration with gradient ethanol and fixation in paraffin wax blocks was done. Sections of 1 μm were cut carefully with a rotary microtome (Hunan Kaida Scientific Instruments, China) and were transferred to a glass slide. Staining was done with H & E stains and tissues were observed under a microscope (Olympus BX51M, Tokyo, Japan) for any sign of toxicity [102].

2.2.7 Statistical Analysis

All experiments were performed in triplicates and the values were presented as mean ± standard deviation unless otherwise stated. One way ANOVA was performed to identify statistically significant differences between the groups. The probability values < 0.05 were considered significant. Statistical differences were denoted as "*" $p < 0.05$, "**"$p < 0.01$ and "***" $p < 0.001$.

Results and Discussion

3.1 POLYMERIC MATRICES

3.1.1 Preparation of Nanoparticles and Microparticles

Different sized PLGA base colloidal systems were prepared to evaluate the idea of combing drug and aptamer in single formulation. The concentration of PLGA and PVA used for the preparation of nano/microparticles by solvent evaporation was optimized in preliminary experiments. Several solvents were screened and we found that the particle size was at its lowest using ethyl acetate with drug solution in THF:EtOH (4:1). Homogenization along with constant stirring and addition of water facilitated the evaporation of organic phase. The formed nano/microparticles were then washed and used for further studies discussed in following sections.

3.1.2 Characterization

3.1.2.1 Physico-chemical Characterization

3.1.2.1.1 Encapsulation Efficiency and In Vitro Release Profile

A challenging issue regarding the preparation of nano/microparticles is encapsulation of drug. Encapsulation efficiency of SFB in nanoparticles and microparticles was 85.7 ± 2.11 % and 74.64 ± 5.43 %, respectively. Once incorporated, the amount of SFB released from PNS was calculated in percentage and data is shown in Figure 3.1A. It is evident from the results that more than 50 % drug was released from PNS within the first 24 h. The remaining SFB was released subsequently (91.31 ± 8.12 % until 96 h). The initial burst release was due to the presence of SFB on the surface of the nanoparticles. The subsequent release was due to drug entrapment inside nanoscale formulations. This second release phase could be due to the diffusion from the pores of non-degraded PLGA matrix as reported previously [103-105]. On the other hand, it is clear from Figure 3.1B that nearly 70 % SFB was released from MPS with in the first 24 h. This represented the initial burst release of drug from the surfaces of microparticles. This second phase of release represented the combination of diffusion and erosion process of PLGA polymeric chains in microparticles [106-110].

(A)

(B)
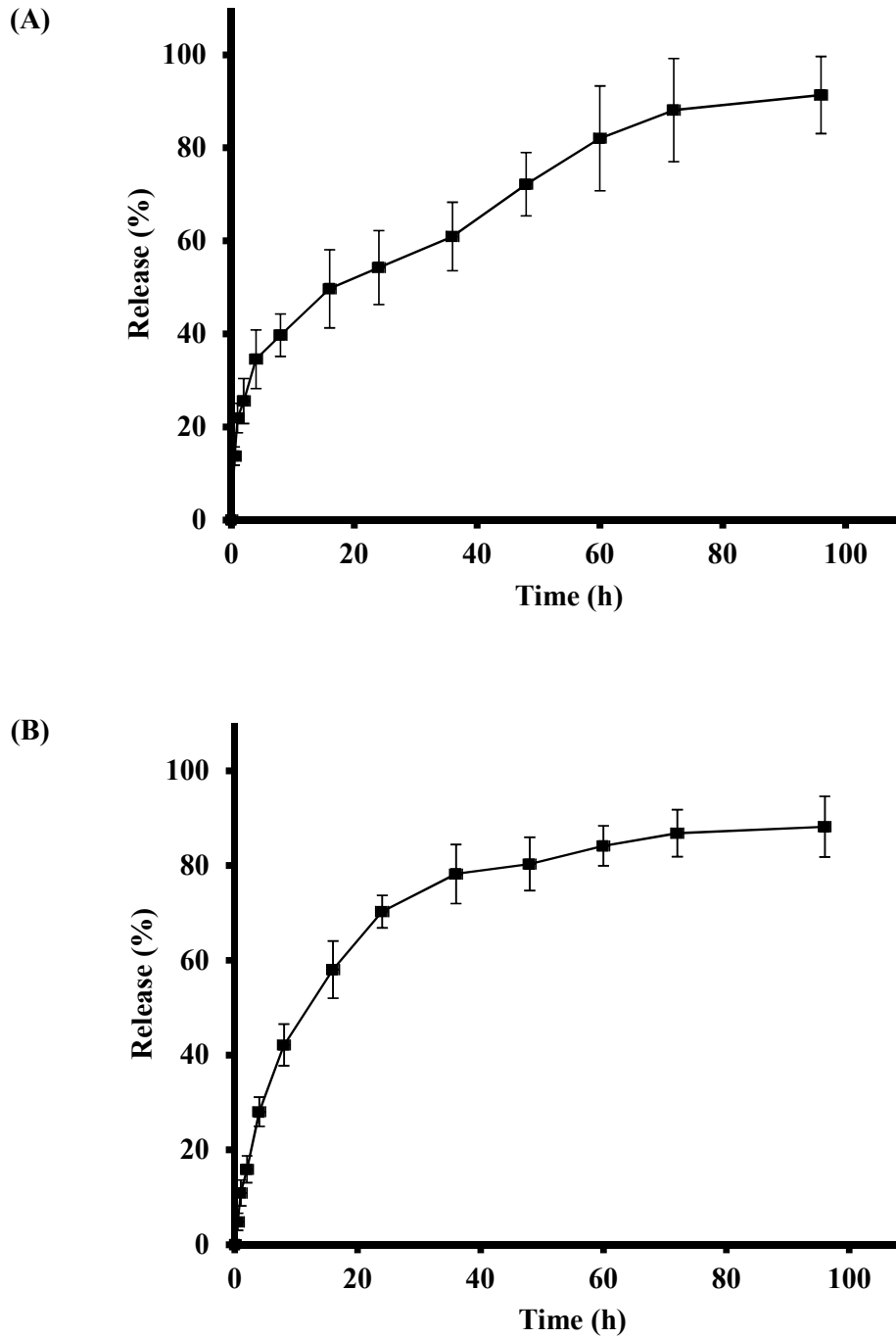
Figure 3.1: Release profile of sorafenib tosylate from (A) SFB-loaded nanoparticles and (B) SFB-loaded microparticles.

3.1.2.1.2 Aptamer Coupling

Binding of Apt on the surface of nano/microparticles was evaluated by fluorescence analysis of Cyn 5 (Figure 3.2). Fluorescence quantification at λ_{ex} 630 nm and λ_{em} 670 nm confirmed the attachment of Cyn 5 labeled Apt to the nanoparticle surface. The results showed that 73.91 ± 4.01 and 70.65 ± 5.01 percent of Apt was bound on the surface of PN and PNS respectively (Figure 3.3A). On the other hand, in the case of microparticles, results showed that 68.36 ± 2.69 and 60.75 ± 1.02 % of Apt was present on the surface of MP and MPS respectively (Figure 3.3B).
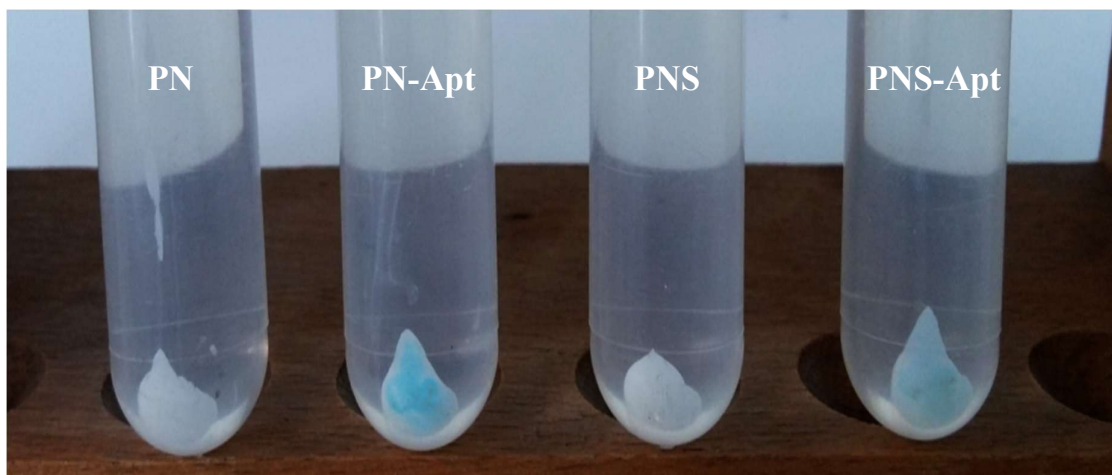
Figure 3.2: Nanoparticle pellets during surface modification and purification.
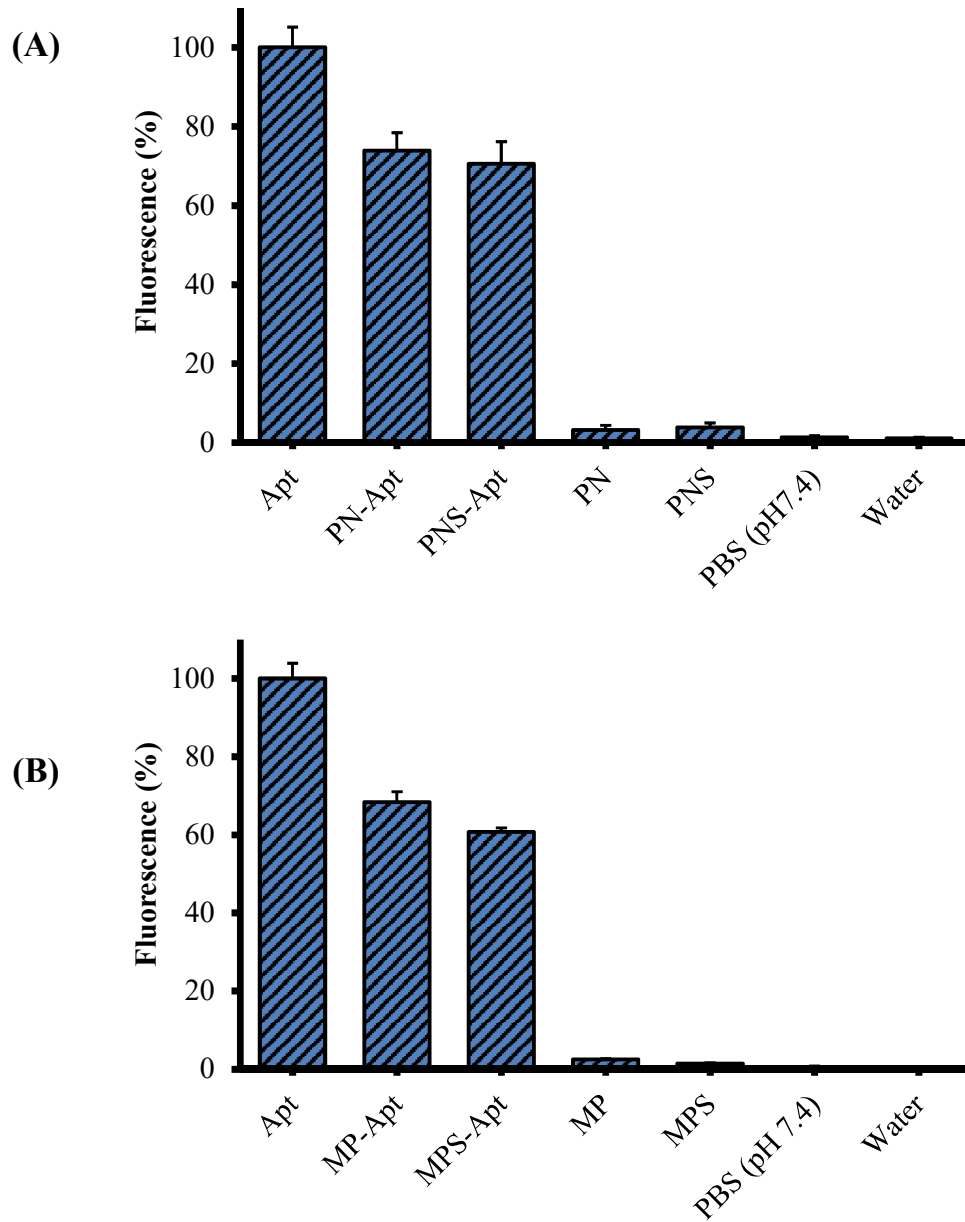
Figure3.3: Fluorescence analysis of cyanine 5-Apt at $\lambda_{ex}/\lambda_{em}$ 630/670 nm; (A) Fluorescence of surface-modified nanoparticles (PN-Apt), surface-modified SFB-loaded nanoparticles (PNS-Apt), nanoparticles (PN) and SFB-loaded nanoparticles (PNS); (B) Fluorescence of surface-modified microparticles (MP-Apt), surface-modified SFB-loaded microparticles (MPS-Apt), microparticles (MP) and SFB-loaded microparticles (MPS). The fluorescence of Cyn 5 of pure Apt was considered as a reference.

3.1.2.1.3 FTIR Spectroscopy

FITR was used to confirm the presence of SFB and Apt in nano/microparticle formulations. PN and MP showed a characteristic peak of carboxylic acid (from PLGA) at 1751 cm^{-1} and 1750 cm^{-1}, respectively. The alkene stretching due to SFB was present between 1503 cm^{-1} and 1501 cm^{-1}. On the other hand, in the spectra of PN-Apt, PNS-Apt, MP-Apt and MPS-Apt conjugated acid stretching between 1703 cm^{-1} and 1700 cm^{-1} along with imine peaks between 1650 cm^{-1} and 1648 cm^{-1} were observed. These results showed the presence of SFB in formulations. Moreover, peaks of imine showed the coupling of Apt with PLGA in formulations (PN-Apt, PNS-Apt, MP-Apt and MPS-Apt). This confirms the successful EDC/NHS surface coupling reaction.

3.1.2.1.4 Elemental Analysis

Nucleotide bases of Apt contain nitrogen. Therefore, the assessment of presence of Apt can also be done by elemental analysis, by which percentages of carbon, hydrogen and nitrogen were calculated. PNS showed 0.25 ± 0.06 % nitrogen due to presence of SFB as compared to 0 % in case of PN. On the other hand, PN-Apt and PNS-Apt showed 1.16 ± 0.45 % and 0.51 ± 0.25 % nitrogen content (with respect to carbon and hydrogen percentages), respectively. This confirmed the results obtained from the FTIR analysis.
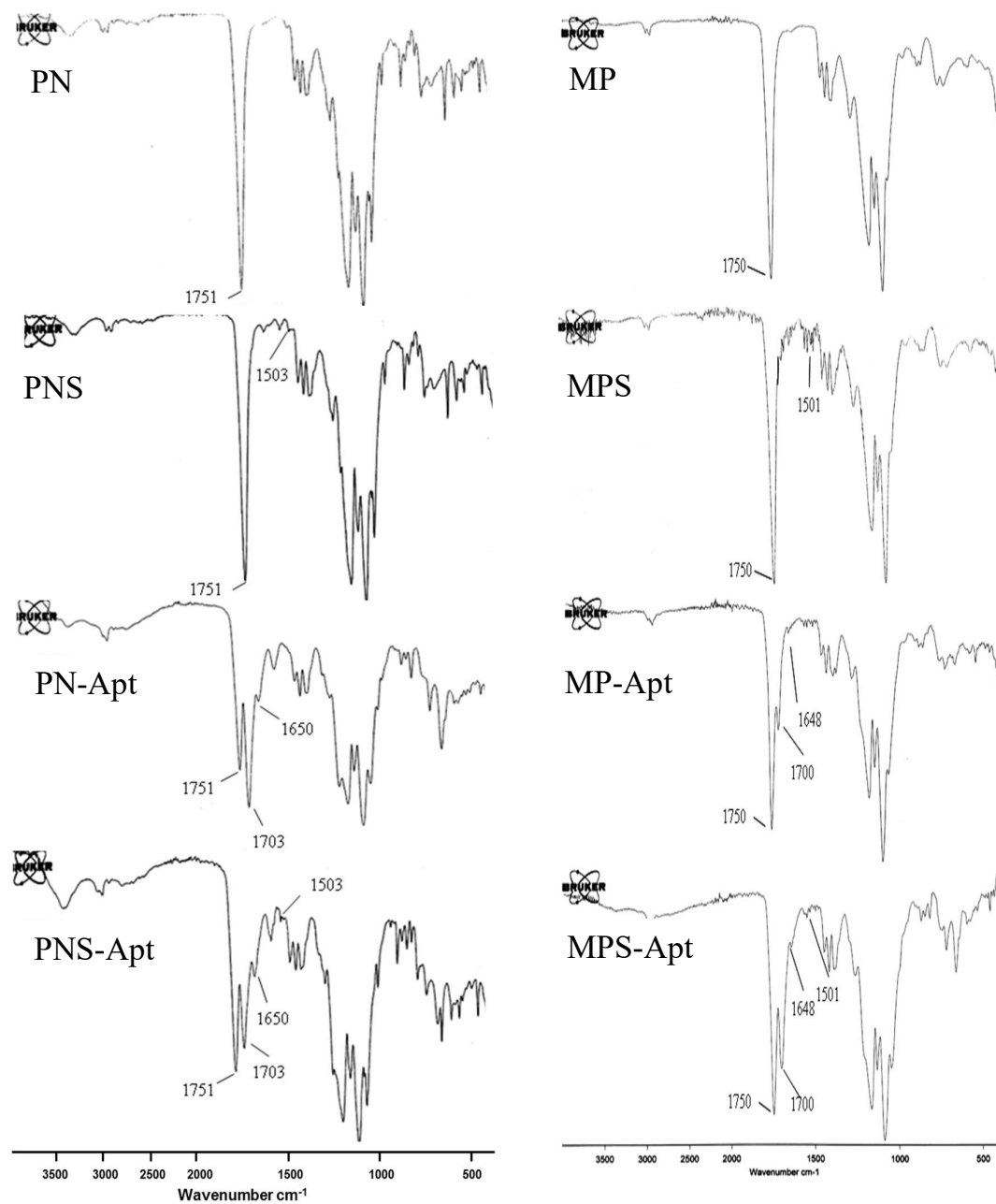
Figure 3.4: FTIR spectrogram of nanoparticles (PN), SFB-loaded nanoparticles (PNS), surface-modified nanoparticles (PN-Apt), surface-modified SFB-loaded nanoparticles (PNS-Apt), microparticles (MP), SFB-loaded microparticles (MPS), surface-modified microparticles (MP-Apt) and surface-modified SFB-loaded microparticles (MPS-Apt).

3.1.2.1.5 Particle Size and Zeta Potential

Dynamic ligh scattering (DLS) and laser doppler velocimetry (LDV) were used to measure particle size and zeta potential. The particle diameter (hydrodynamic diameter as a function of intensity) measured by DLS showed an increase with the addition of drug and aptamer (Table 3.1). On the other hand, the zeta potential measured was negative in all cases with a maximum of -25.29 ± 1.90 for MP-Apt. Hydrodynamic diameter and zeta potential are influenced by pH and ionic concentrations. Therefore, the presence of SFB changed the diameter and zeta potential of formulations [111-113]. On the other hand, the amide bond formed between the carboxylic group of PLGA and the amine of aptamer resulted in the attachment of aptamer onto the surface of particles (as shown by FTIR results). This is evident from the change in diameter and zeta potential.

Table 3.1: Size and zeta potential of nanoparticles, microparticles and liposomes.

Formulations	Size ± SD (nm)	Zeta Potential ± SD (mV)	PDI
PN	179.69 ± 5.90	-16.20 ± 0.71	0.19 ± 0.02
PN-Apt	204.91 ± 12.53	-18.81 ± 1.81	0.24 ± 0.03
PNS	185.12 ± 10.34	-14.04 ± 0.57	0.21 ± 0.05
PNS-Apt	222.29 ± 9.91	-16.75± 2.55	0.22 ± 0.07
MP	692.32 ± 41.38	-21.48± 0.62	0.30 ± 0.01
MP-Apt	800.07 ± 78.48	-25.29± 1.90	0.32 ± 0.03
MPS	913.54 ± 45.33	-19.31± 2.20	0.31 ± 0.02
MPS-Apt	1042.62 ± 52.60	-24.09± 1.47	0.34 ± 0.04
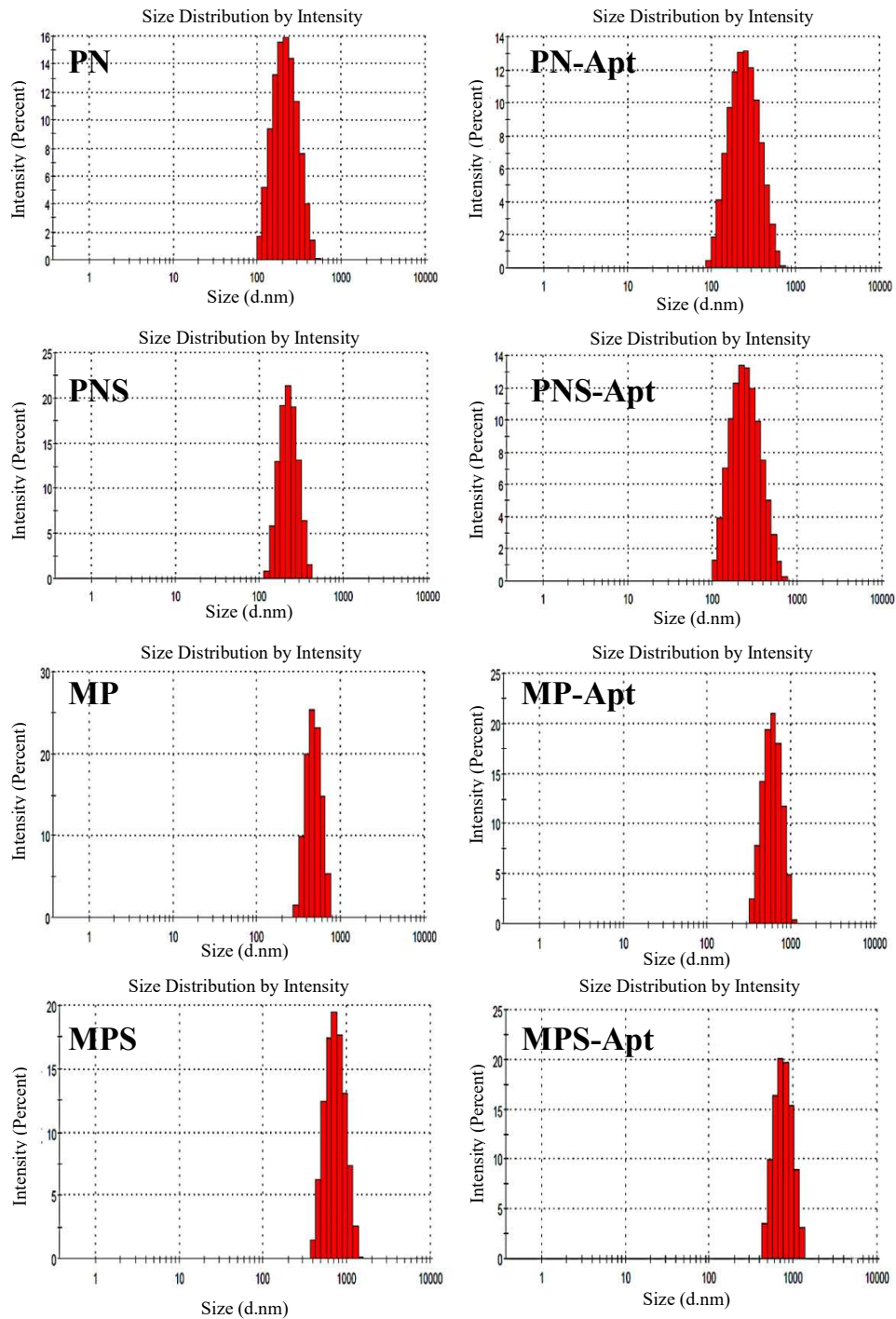
Figure 3.5: Size histogram from dynamic light scattering of nanoparticles (PN), surface-modified nanoparticles (PN-Apt), SFB-loaded nanoparticles (PNS), surface-modified SFB-loaded nanoparticles (PNS-Apt),microparticles (MP), surface-modified microparticles (MP-Apt), SFB-loaded microparticles (MPS) and surface-modified SFB-loaded microparticles (MPS-Apt).

3.1.2.2 Morphological Characterization

Atomic force and scanning electron microscopies were used to assess the morphology and surface roughness of nanoparticles and microparticles.

3.1.2.2.1 Atomic Force Microscopy (AFM)

Morphological characterization of nanoparticles was done using an atomic force microscope (AFM). AFM analysis revealed spherical shaped particles among all formulations (Figure 3.6). The coupling of Apt resulted in an increase in the diameter and size distribution of the modified particles. Surface roughness (by RMS; Rq) of the nanoparticles was also calculated with 38.0 ± 14.8 nm, 54.8 ± 7.1 nm, 47.7 ± 10.9 nm and 64.0 ± 6.0 nm in case of PN, PN-Apt, PNS and PNS-Apt. This increase in Rq value represented surface modification in case of PN-Apt. More the surface roughness more will be the wettability of the nanoparticles and thus will affect nanoparticle-cell interaction [97-98, 114-115].

3.1.2.2.2 Scanning Electron Microscopy (SEM)

Morphological characterization of microparticles was done by scanning electron microscopy. Samples were dried under laminar airflow hood (Labgard Class II, NuAire Inc, Plymouth, USA) on conductive carbon tabs. This resulted in the settlement of microparticles while at the same time maintaining their structure. SEM analysis revealed a smooth surface with a diverse range of sizes was seen in the micrographs (Figure 3.7). The sizes were between 0.5 to 0.7 μm, which were smaller than that measured by DLS. This was due to the presence of an electrical double layer on the surface of microparticles when measured in suspension form by DLS, whereas for SEM, the particles are measured in vacuum.
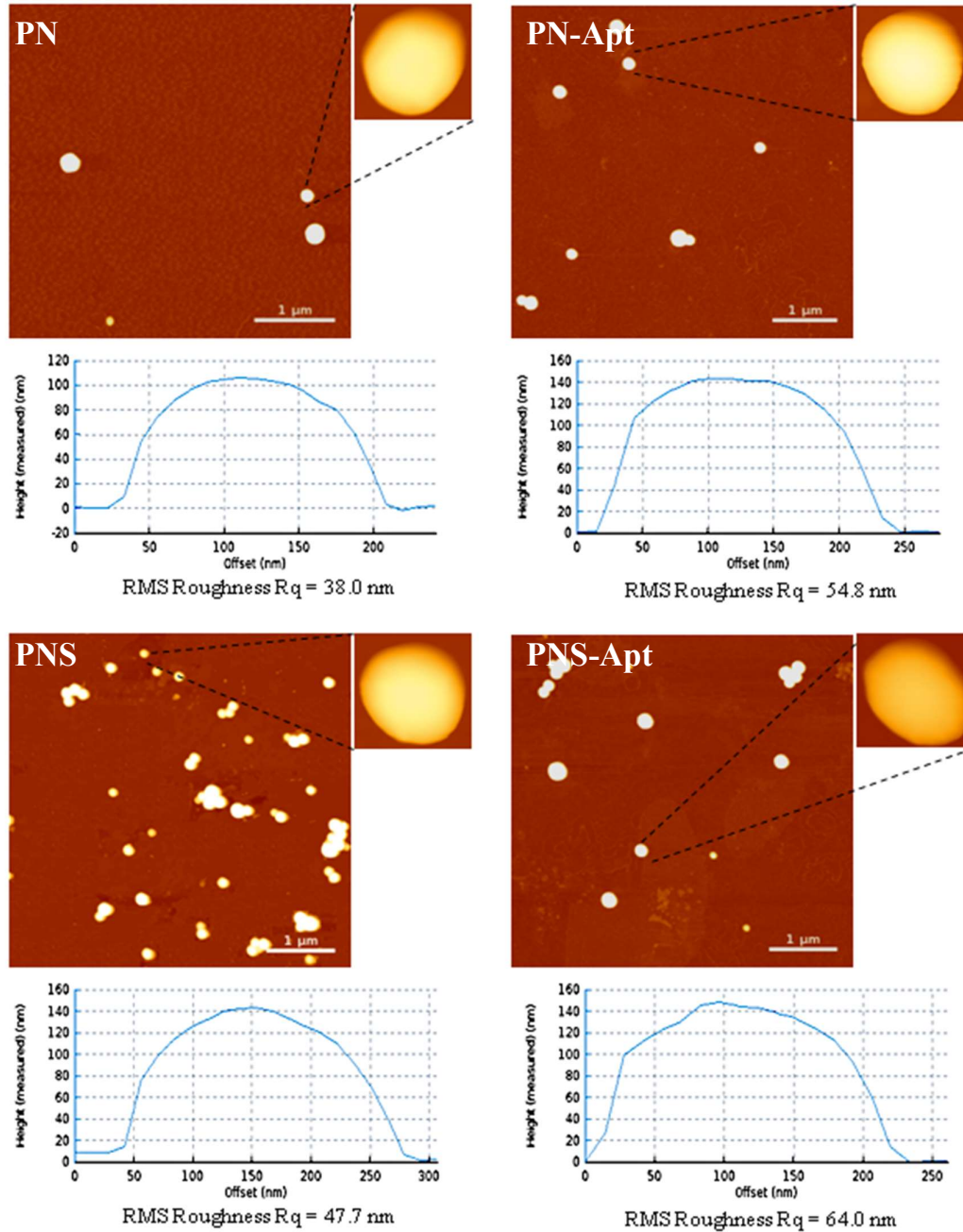
Figure 3.6: AFM images (height) of nanoparticles with surface roughness Rq of nanoparticles (PN), surface-modified nanoparticles (PN-Apt), SFB-loaded nanoparticles (PNS) and surface-modified SFB-loaded nanoparticles (PNS-Apt).
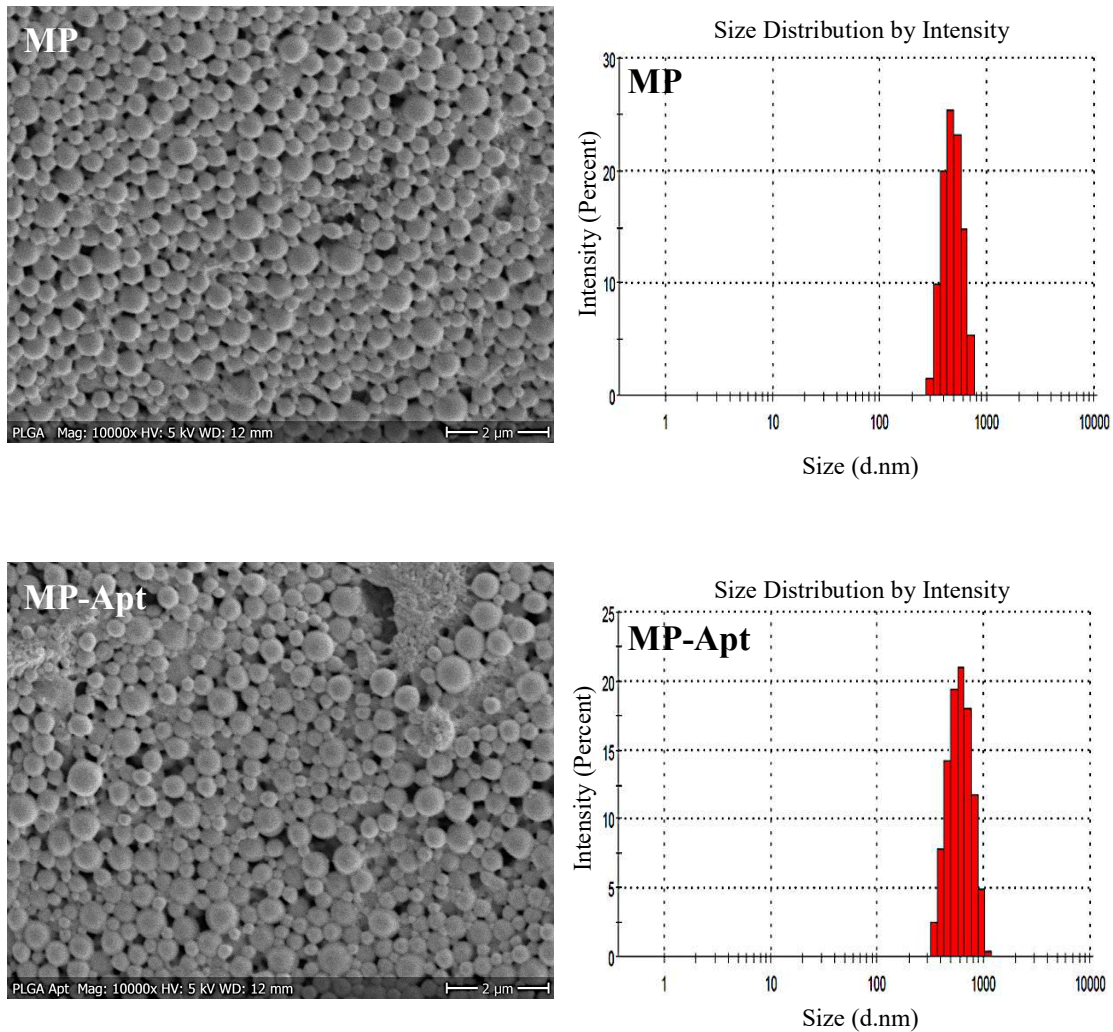
Figure 3.7: SEM micrographs of microparticles (MP) and surface-modified microparticles (MP-Apt). Images on the right side depict the size histogram (dynamic light scattering) of the nanoparticles.

3.1.3 *In Vitro* Evaluation

3.1.3.1 Cell Culture Studies

3.1.3.1.1 Cell Proliferation and IC$_{50}$

MTT assay was performed to assess the cell viability. Cell viability was dose-dependent, increasing with decreasing the nano/microparticle concentration. Maximum viability for PNS-Apt and MPS-Apt was achieved with 0.19 μM SFB. IC$_{50}$ values were 1.75 μM and 1.0 μM for PNS-Apt and MPS-Apt, respectively. In case of formulations without SFB, an

equivalent nano/microparticle amount was considered.PN/MP showed a cell viability of more than 80 % as shown in Figure 3.8 and Figure 3.9. This depicted the safety of formulations, in the absence of Apt or SFB. The presence of Apt along with SFB decreased cell viability significantly ($p < 0.001$). This decrease indicated the interaction between anti-ErbB3-Apt modified particles and cells on one hand and anti-proliferation effect of SFB itself on the other hand [116-117]. Therefore, this combination of anti-ErbB3-Apt and drug exhibited a synergistic effect thereby addressing the problem of resistance towards SFB [118-121].

Figure 3.8: Cell viability assay of nanoparticles (PN), surface-modified nanoparticles (PN-Apt), SFB-loaded nanoparticles (PNS) and surface-modified SFB-loaded nanoparticles (PNS-Apt). Statistical differences were denoted as "*" $p < 0.05$, "**" $p < 0.01$ and "***" $p < 0.001$.

Figure 3.9: Cell viability assay of microparticles (MP), surface-modified microparticles (MP-Apt), SFB-loaded microparticles (MPS) and surface-modified SFB-loaded microparticles (MPS-Apt). Statistical differences were denoted as "**" $p < 0.01$ and "***" $p < 0.001$.

3.1.3.1.2 Internalization Pathway

To examine the mechanism of nanoparticle internalization into MDA-MD-231 cells, different endocytosis pathways were used. Chlorpromazine and Filipin III were used to suppress the clathrin and the caveolae mediated endocytosis, respectively. It was evident from the results that cells, pre-treated with chlorpromazine, showed increased cell viability as compared to control group and Filipin III group (Figure 3.10). Chlorpromazine blocks clathrin dependent internalization pathway of receptor tyrosine kinase [85-87]. The presence of chlorpromazine resulted in the blockade of nanoparticle internalization. This was evident from the increased cell viability in chlorpromazine treated cells. On the other hand, Filipin III blocks caveolae mediated endocytosis. A decreased cell viability in its presence further endorsed that the clathrin dependent pathway as a possible mechanism of nanoparticle internalization [122-124].

Figure 3.10: Pathway analysis of nanoparticles (PN), surface-modified nanoparticles (PN-Apt), SFB-loaded nanoparticles (PNS) and surface-modified SFB-loaded nanoparticles (PNS-Apt). Each formulation was equivalent to 1.5 µM SFB concentration in nanoparticles.

3.1.3.1.3 Apoptosis Assay

The mechanism of killing of the cells was evaluated by DAPI staining. DAPI is a nuclear stain, which binds to double-stranded DNA and can detect the chromatin or nuclear condensation and helps localize the formation of apoptotic bodies, which result ultimately in the death of cells. Cell shrinkage, loss of cell membrane, blebbing and chromatin degradation along with nuclear condensations can be observed using this assay [121, 125-126]. More the apoptosis denser DAPI staining will be there in the cells.

The untreated cells did not show any sign of apoptotic body formation. On the other hand,cells treated with different formulations showed significant apoptotic body bodies formation. PN/MP showed some cells with nuclear condensation. The cells treated with nano/microparticles in the presence of SFB showed nuclear condensation. However, the in the presence of Apt chromatin degradation was observed. The nuclear blebbing was also prominent due to the presence of SFB and Apt (Figure 3.11 and Figure 3.12). The presence of

denser DAPI stained cells showed enhanced apoptosis. Therefore, the formation of apoptotic bodies was potentiated in the presence of both SFB and Apt, revealing the synergism amongst them. Similar results were reported previously, showing enhanced cell death in the presence of anti-ErbB3 aptamer and chemotherapeutic agent [120, 127-129]. These results were also in good coordination with cell proliferation assay showing decreased toxicity in absence of SFB and/or Apt.
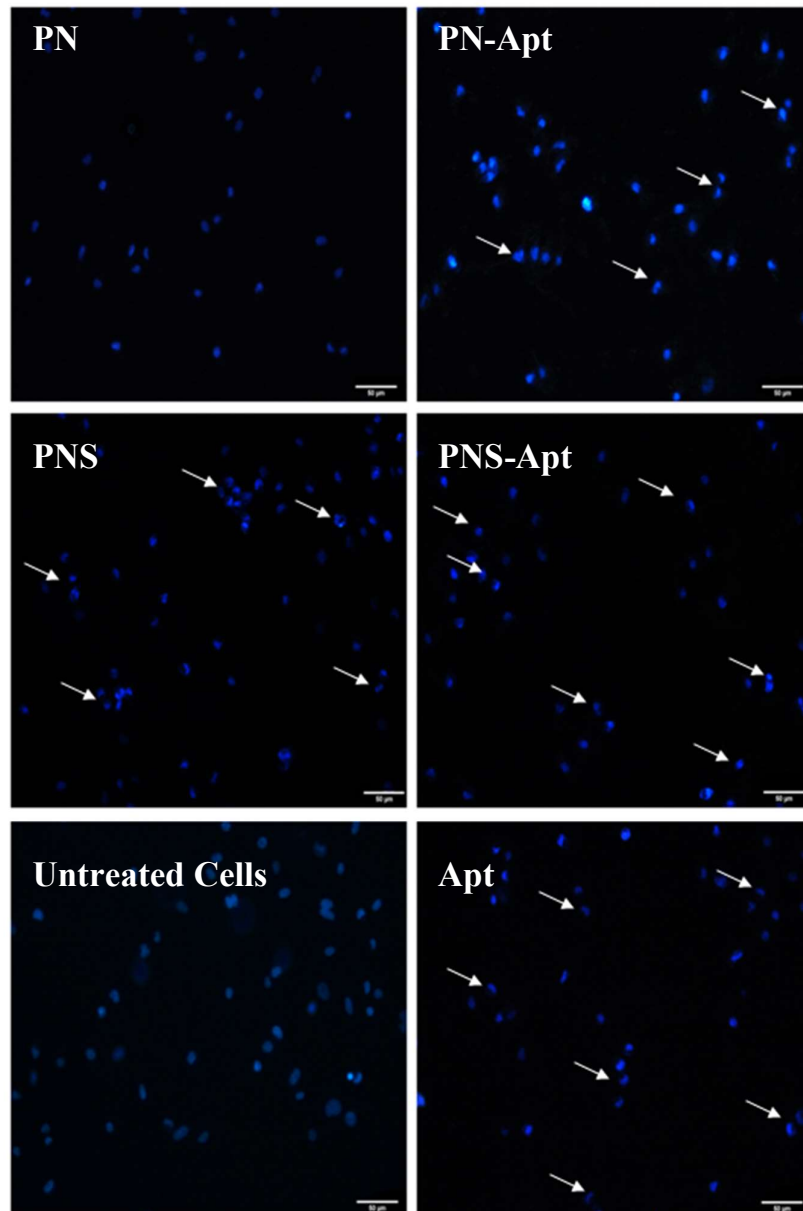
Figure 3.11: Apoptosis assay showing nuclear condensation and chromatin fragmentation of nanoparticles (PN), surface-modified nanoparticles (PN-Apt), SFB-loaded nanoparticles (PNS) and surface-modified SFB-loaded nanoparticles (PNS-Apt).
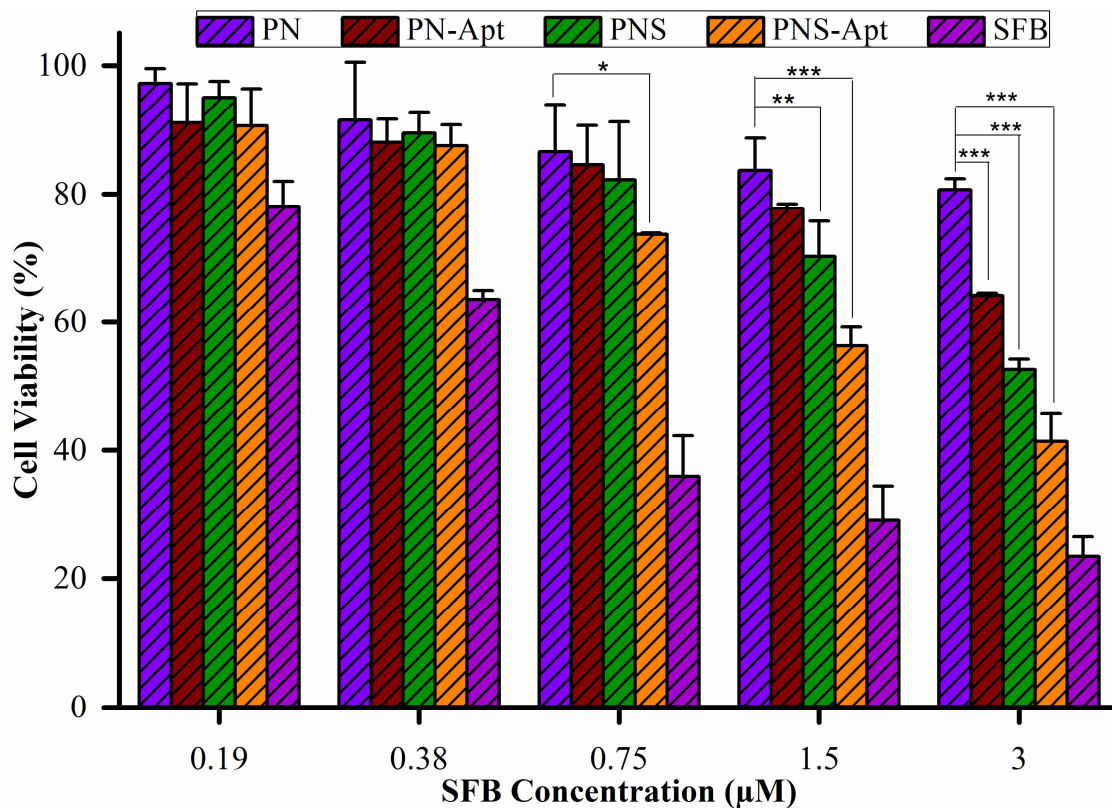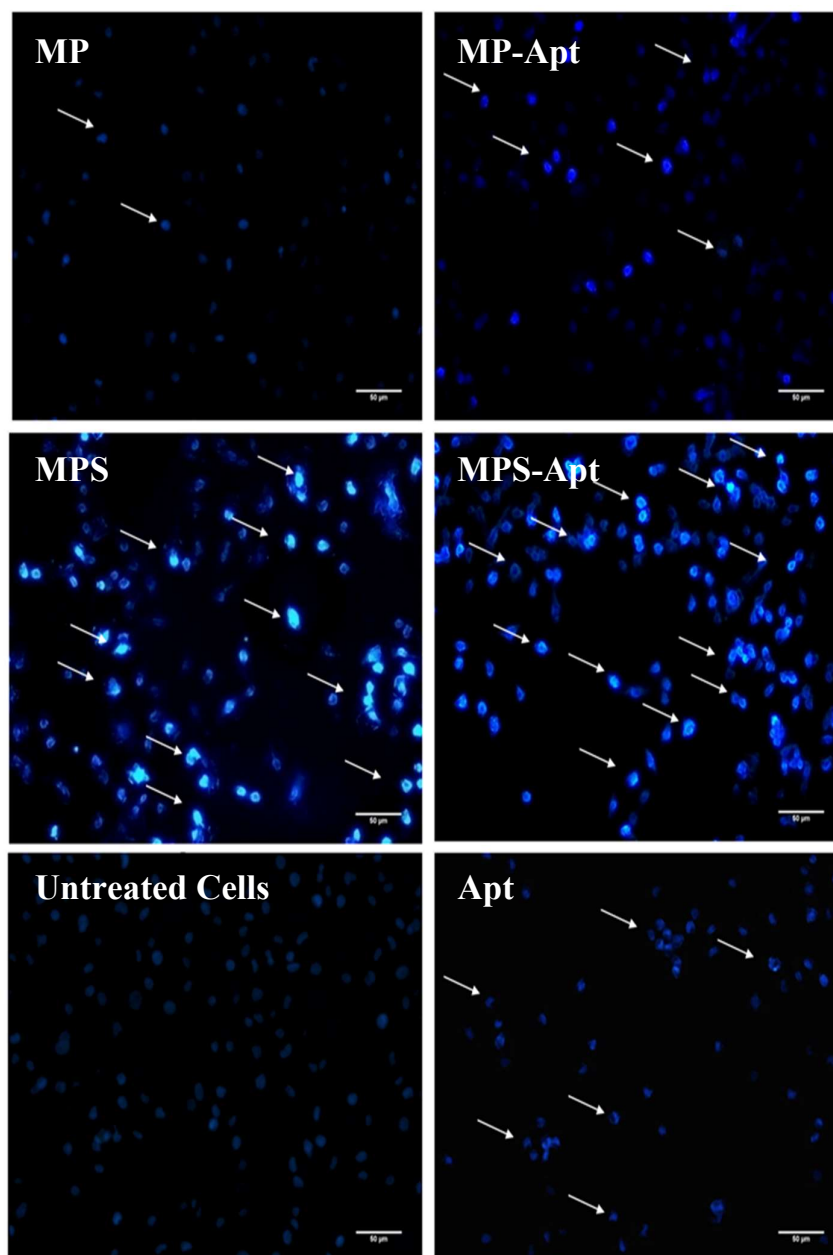
Figure 3.12: Apoptosis assay showing nuclear condensation and chromatin fragmentation of microparticles (MP), surface-modified microparticles (MP-Apt), SFB-loaded microparticles (MPS) and surface-modified SFB-loaded microparticles (MPS-Apt).

3.1.3.1.4 Reactive Oxygen Species Assessment

Reactive oxygen species (ROS) can convert carboxy-H_2DCFDA into DCF. The results showed dose-dependent ROS production in the presence of both drug only and drug-aptamer formulations (Figure 3.13). It was obvious that due to presence of SFB increased level of ROS production was present. However, in the presence of both the SFB and aptamer, ROS were significantly higher ($p < 0.01$ or $p < 0.001$) as compared to the blank formulation (NP/MP). However, the aptamer alone did not significantly induce ROS production. On the other hand, in case of SFB only treated cells, a decrease in level of ROS production was obvious.

The release of the SFB inside cells caused the production of ROS due to the production NADPH oxidase in mitochondria. This is the proposed mechanism of ROS production in the presence of SFB [130]. The presence of anti-ErbB3 Apt caused an increased production of ROS in combination with SFB as compared to only SFB containing formulations. However, in the presence of only Apt, low amounts of ROS were produced. Therefore, synergism was observed between SFB and Apt in the production of ROS. This synergism was also in good correlation with cell proliferation and apoptosis assays i.e. presence of Apt potentiates the effect of SFB. Nevertheless, this production of ROS controls cell growth and differentiation process, increase in production will cause apoptosis of cells, leading to death [131-133]. This fact was confirmed by increasing the incubation time of cells with colloidal systems, which reduced the production of DCF. The visual inspection of cells with long incubation time showed killing of cells and thus less cells per well were present. Therefore, it was postulated that, ROS were responsible for cell death in cell viability assay and Apt potentiated killing by SFB also in synergistic way.
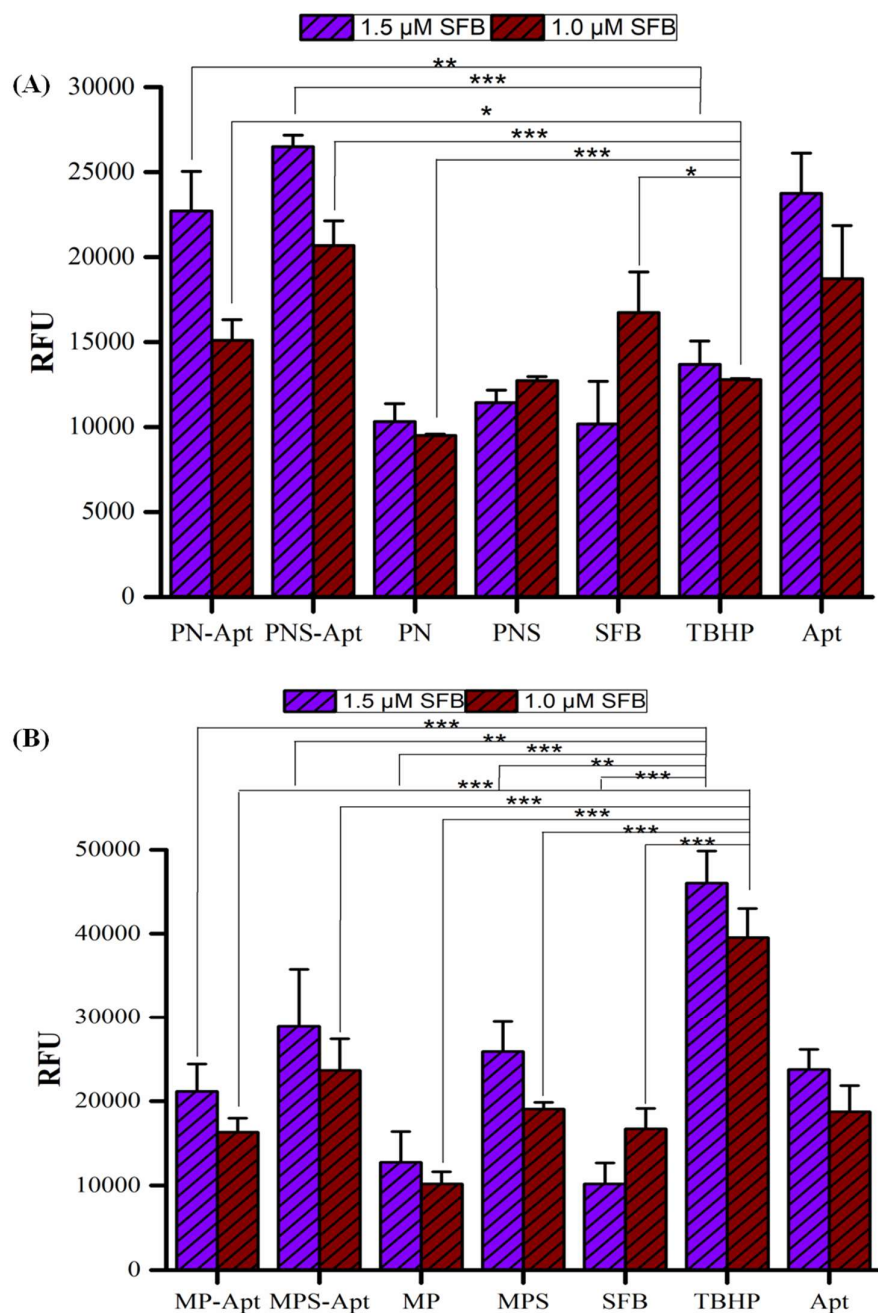
Figure 3.13: ROS assay measuring the production of 2',7'-dichlorofluorescein (DCF); A) nanoparticles (PN), surface-modified nanoparticles (PN-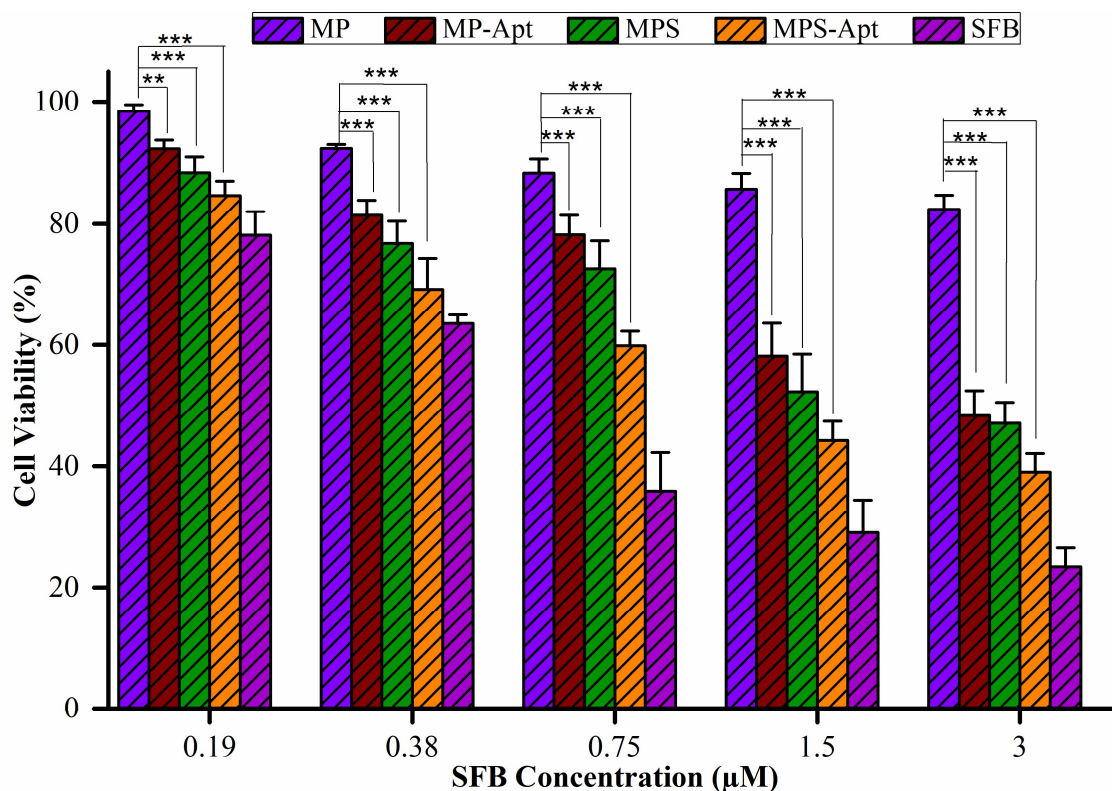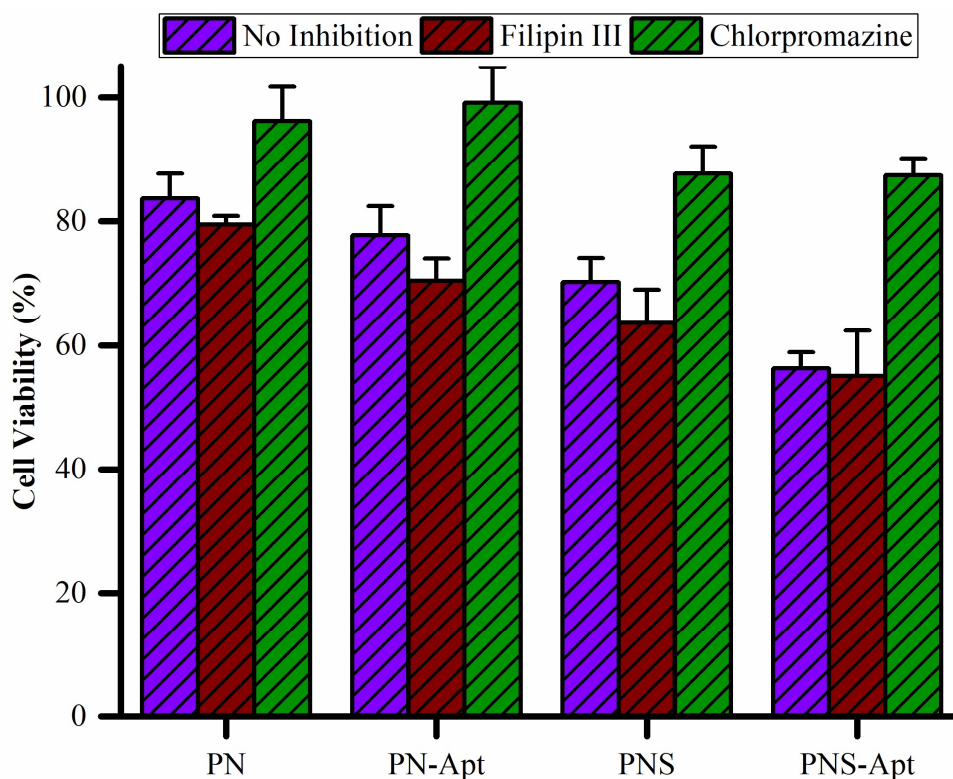Apt), SFB-loaded nanoparticle (PNS) and surface-modified SFB-loaded nanoparticles (PNS-Apt); B) microparticles (MP), surface-modified microparticles (MP-Apt), SFB-loaded microparticles (MPS) and surface-modified SFB-loaded microparticle (MPS-Apt). Tert-butylhydroperoxide (TBHP) was used as a positive control. Statistical differences are denoted as "$*$" $p < 0.05$, "$**$" $p < 0.01$ and "$***$" $p < 0.001$.

3.1.3.1.5 Metastatic Progression

Cell progression, migration and inhibition of apoptosis are all associated with the progression of cancer. ErbB3 is one of the responsible receptor involved in these progressions [134-136]. On the other hand, SFB has also been reported to inhibit metastasis [137-138]. Therefore, we performed a wound healing assay to assess the inhibition of metastasis. Presence of Apt and SFB blocked progression and wound healing significantly as compared to untreated cells up to 24 h ($p < 0.001$). The percentage of wound healing for nanoparticles treated cells was in decreasing order i.e. untreated cells>PN>PN-Apt>PNS>PNS-Apt (100 %, 98 %, 95 %, 91 % and 89 % respectively). In similar fashion wound healing for microparticles treated cells was in decreasing order from untreated cells>MP>MP-Apt>MPS>MPS-Apt (100 %, 96 %, 92 %, 90 %, and 88 % respectively). However, after 36 h more than 95 % area was covered by the cells in all treatment cases. Nevertheless, SFB and Apt blocked wound healing but in the presence of only one of these or in the absence of both, cell migration rate was higher. From these findings, it was clear that presence of Apt and SFB have a synergistic effect in blocking metastatic progression.
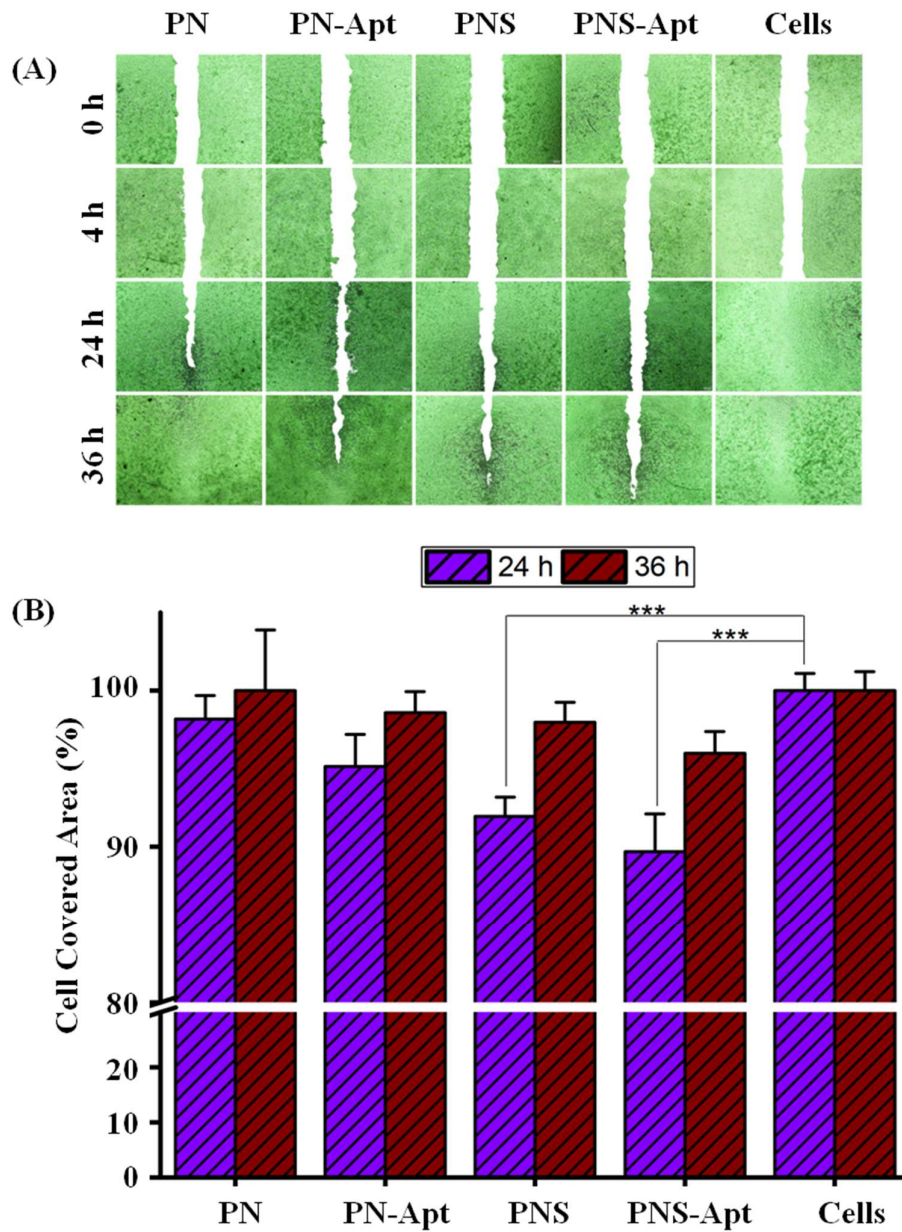
Figure 3.14: Effect of formulations on cell migration; scratch was applied using 200 µl pipette tip; A) wound healing by scratch test; B) time-dependent wound healing under the influence of nanoparticles (PN), surface-modified nanoparticles (PN-Apt), SFB-loaded PLGA nanoparticles (PNS-Apt) and surface-modified SFB-loaded nanoparticles (PNS-Apt). Statistical differences are denoted as "∗∗∗" $p < 0.001$.
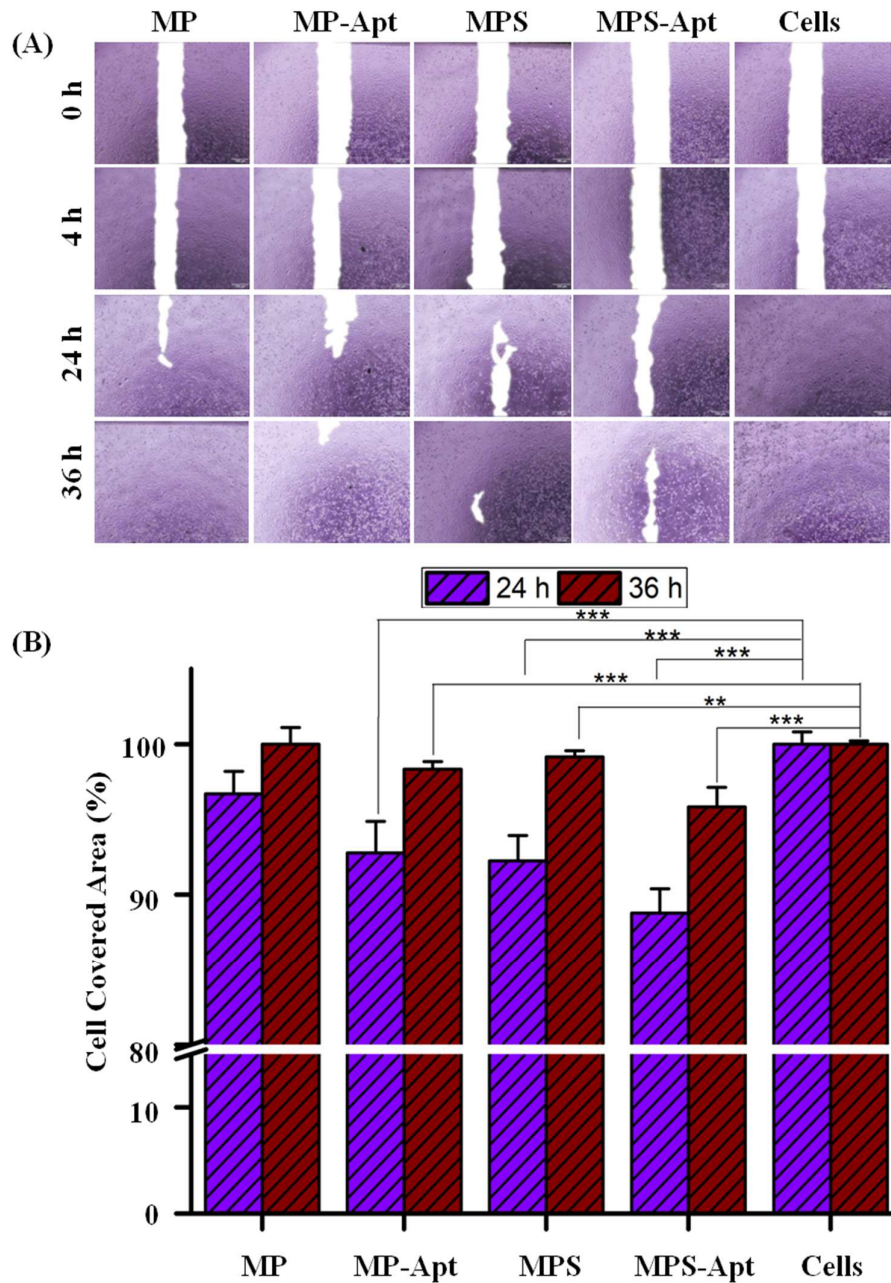
**Figure 3.15:** Effect of formulations on cell migration; scratch was applied using 200 µl pipette tip; A) wound healing by scratch test; B) time-dependent wound healing under the influence of microparticles (MP), surface-modified microparticles (MP-Apt), SFB-loaded microparticles (MPS) and surface-modified SFB-loaded microparticle (MPS-Apt). Statistical differences are denoted as "∗∗" $p < 0.01$ and "∗∗∗" $p < 0.001$.

3.1.3.1.6 Cellular Uptake

Cyanine 5 was attached to the 5' end of Apt as a fluorophore. Detection of its fluorescence was used to visualize the uptake of the nano/microparticles. Cells were treated for different formulations of nanoparticles and microparticles for different time duration. After 30 min of the treatment, most of the particles accumulated near the cell membrane. On the other hand, upon incubation with the particles for 2 h, fluorescence was observed mostly near the nucleus. This was also confirmed by z-stack images as shown in Figure 3.16-3.18. The intensity plot for co-localization shows the intensity of DAPI (cell nucleus) on the x-axis and Cyn 5 (aptamer) on the y-axis. Co-localization coefficient was measured by ZEN software (Carl Zeiss). This ranges from 0 to 1, where 0indicates no co-localization and 1 indicates 100 percent co-localization.

Clathrin dependent internalization and endocytosis was found to be responsible for the transfer of nanoparticles from cell membrane to nucleus. ErbB3 receptors are also internalized by this mechanism [139-141]. Time dependent locations of PLGA matrices were due to this mechanism of transport. Increased cellular toxicity was observed due to binding of the particles with these receptors [142]. The z-stack images showed the presence of Cyn 5 labeled aptamer in nuclear region. Co-localizations were differential, showing co-localization coefficients less than 0.4 in case of 30 min incubation time with nanoparticles. This represented the location of nanoparticles in cytoplasm away from DAPI channel (nucleus). However, for 2 h treatment time, co-localization coefficient was above 0.7 in every treatment case, representing nearly the same location of DAPI and Cyn 5, suggesting that the nano/microparticles were closer to the nucleus. Based on these findings, Apt modified PLGA colloidal systems may be used as a carrier for targeted drug delivery to the cytoplasm of cells rich in ErbB3 receptors. The surface modification of different formulations resulted in uptake of these formulations, regardless of size. Therefore, the surface modification of particles with aptamer can be used for the targeted drug delivery. The presence of a drug together with aptamer would result in specific effects to arrest the growth or even destroy the cells.
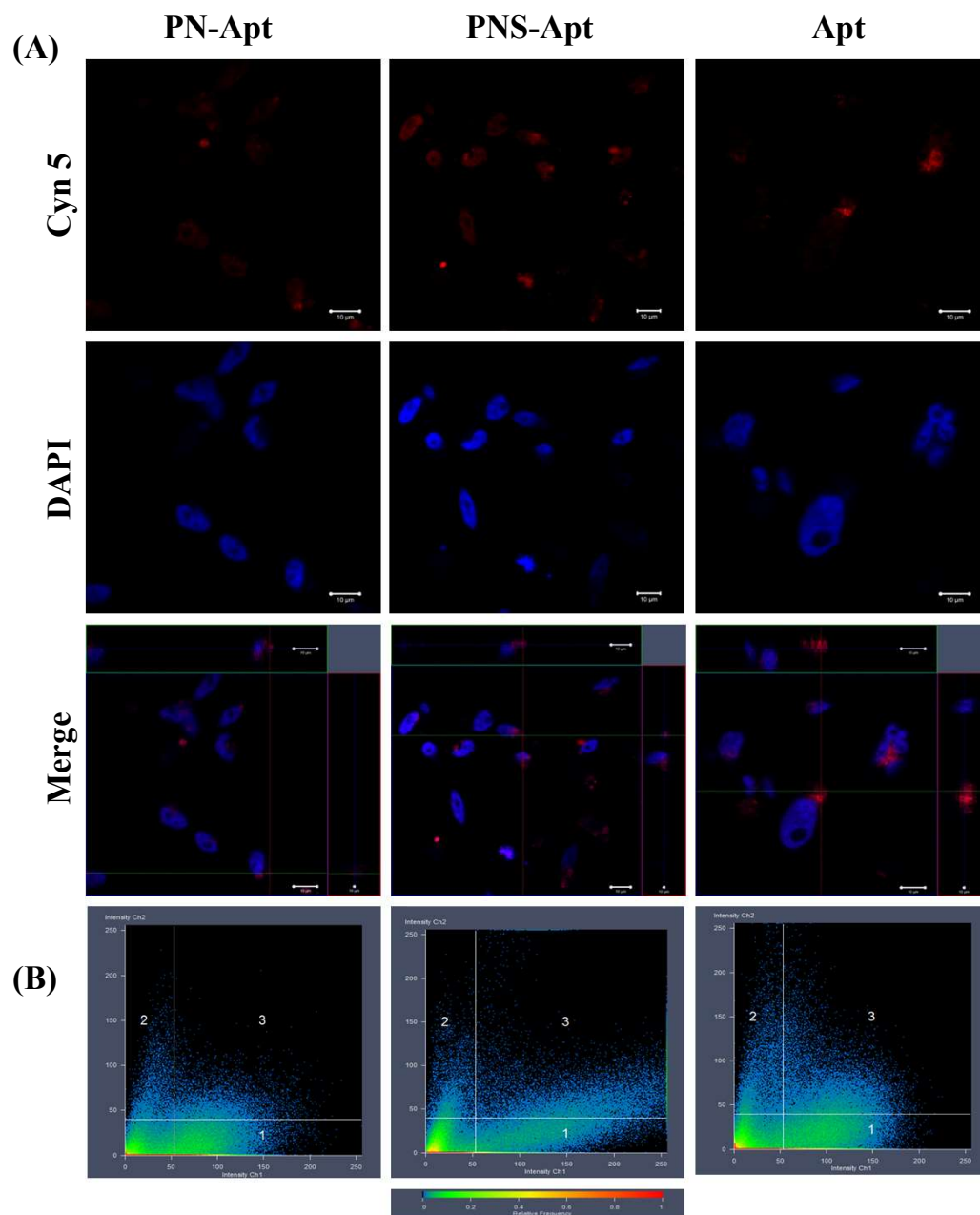
Figure 3.16: Cellular uptake of Cyn 5 labeled nanoparticles after 30 min in MDA-MB-231 cells; A) cellular uptake, merge images are represented in the form of z-stack to visualize the presence of aptamer functionalized nanoparticles near nucleus; B) co-localization of surface-modified nanoparticles (PN-Apt), surface-modified SFB-loaded nanoparticles (PNS-Apt) and aptamer (Apt) treated cells.
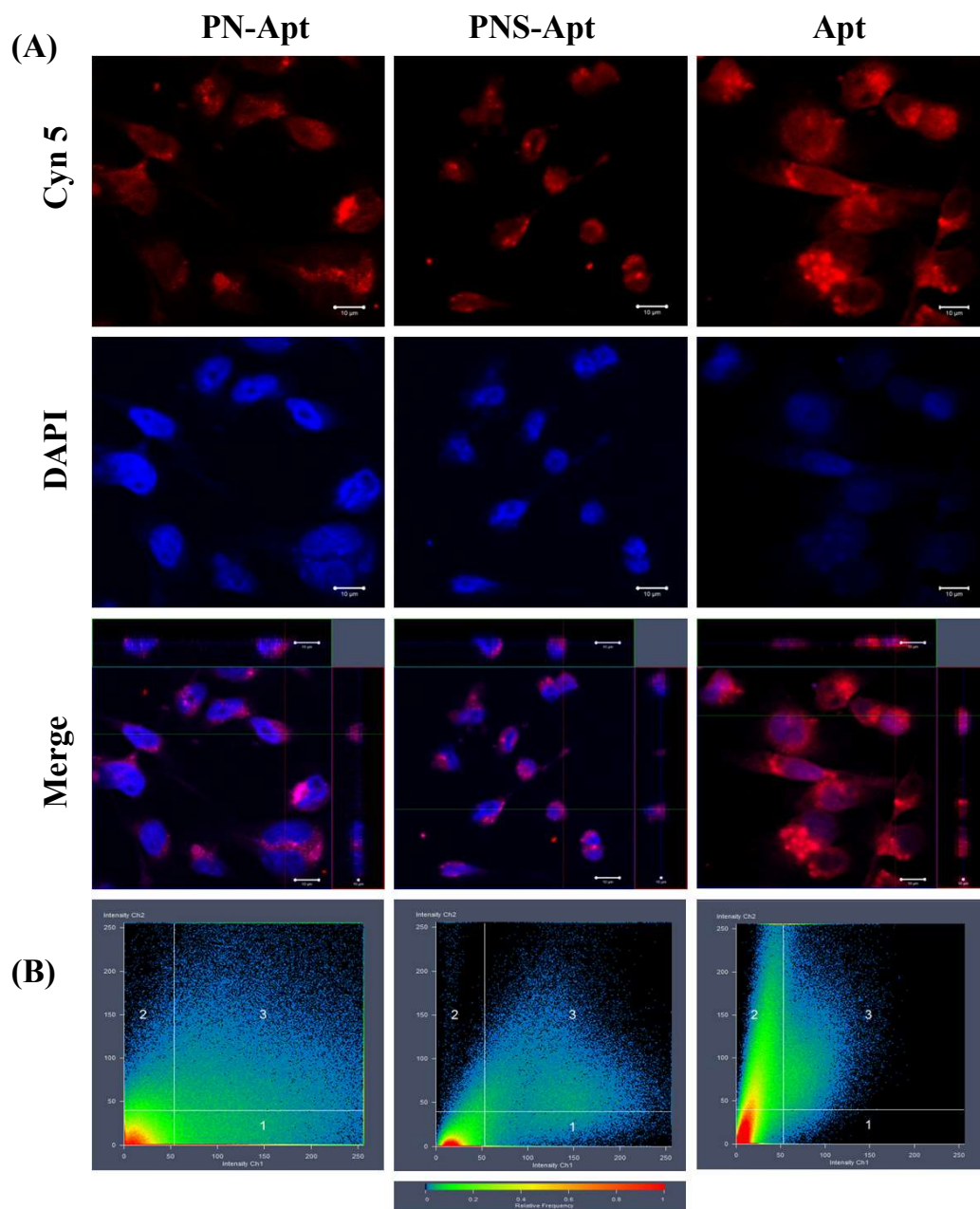
Figure 3.17: Cellular uptake of Cyn 5 labeled nanoparticles after 2 h in MDA-MB-231 cells; A) cellular uptake; merge images are represented in the form of z-stack to visualize the presence of aptamer functionalized nanoparticles near nucleus; B) co-localization of surface-modified nanoparticles (PN-Apt), surface-modified SFB-loaded nanoparticles (PNS-Apt) and aptamer (Apt) treated cells.
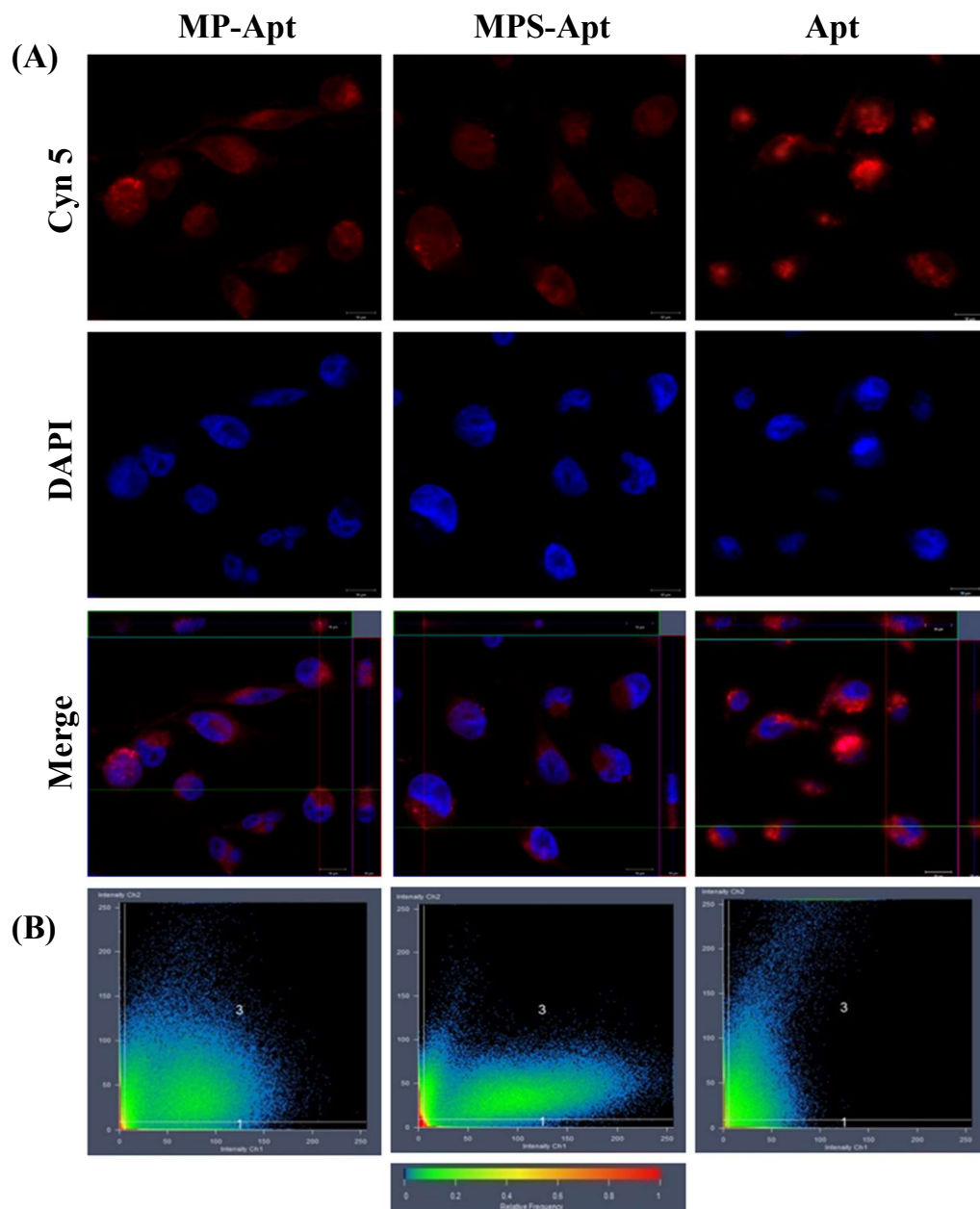
Figure 3.18: Cellular uptake of Cyn 5 labeled microparticles after 2 h in MDA-MB-231 cells; A) cellular uptake; merge images are represented in the form of z-stack to visualize the presence of aptamer functionalized microparticles near nucleus; B) co-localization of surface-modified microparticles (MP-Apt), surface-modified SFB-loaded microparticles (MPS-Apt) and aptamer (Apt) treated cells.

3.1.3.2 Hemocompatibility Studies

3.1.3.2.1 Ex vivo Hemolysis Assay

Compatibility of formulations with erythrocytes was evaluated by hemolysis assay. This assay determines the release of hemoglobin from erythrocytes after exposure to nanoparticles. Percentage of oxyhemoglobin formed after the reaction of released hemoglobin with atmospheric oxygen can be determined spectroscopically. Hemolytic potential among all formulations was less than 15 % indicating a good hemocompatibility profile (Figure 3.19). Maximum hemolysis of 13.01 ± 2.15 % was observed in case of pure drug. From the results, it can be concluded that the presence of Apt and SFB did not affect the normal physiology of erythrocytes, thereby rendering the formulations suitable for i.v. administration.
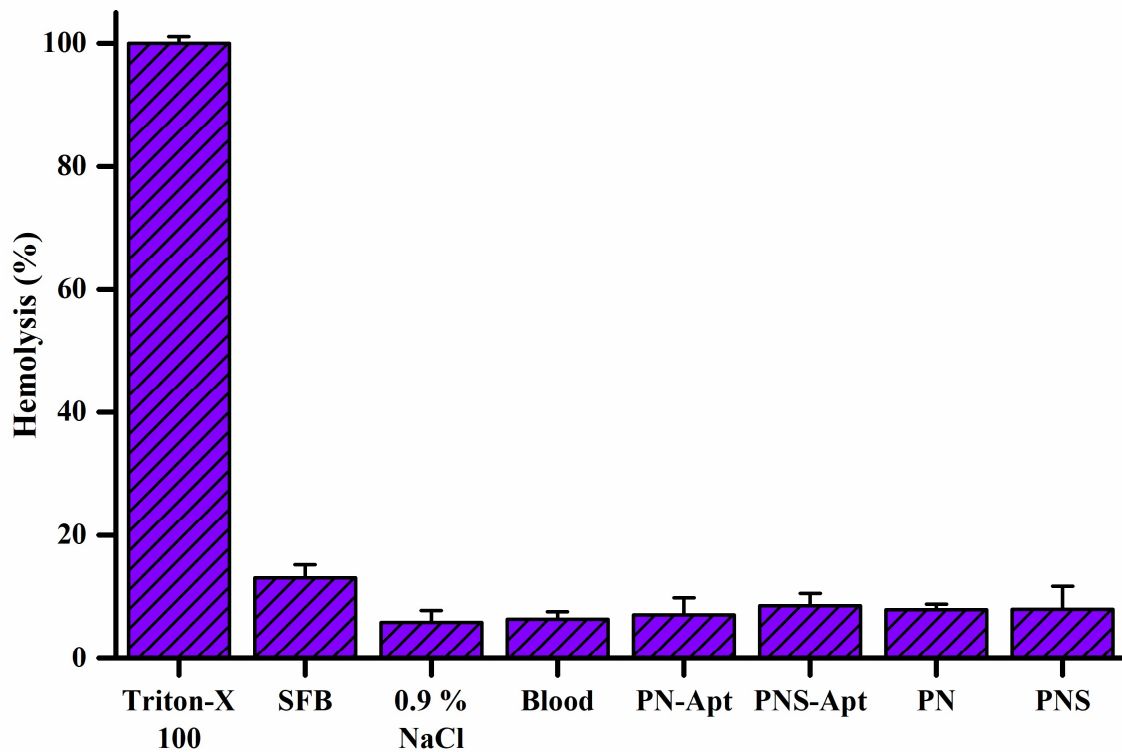
Figure 3.19: Hemolysis assay of nanoparticles (PN), surface-modified nanoparticles (PN-Apt), SFB-loaded nanoparticles (PNS) and surface-modified SFB-loaded nanoparticles (PNS-Apt). 1% Triton-X 100, 0.9 % NaCl and blood were used as controls.

3.1.4 *In Vivo* Evaluation

3.1.4.1 Acute Toxicity

Female BALB/c mice were injected (intra-peritoneal) with different formulations of microparticles; aptamer and normal saline were used as controls. Mice were observed for 7days after injection for any abnormal behavior, skin, sleek of fur, urine color, feces, salivation, respiration, eyes and sleep patterns. All the mice survived and showed no physical or behavioral changes. A record of body weight was performed to calculate percentage change on day 7. All these parameters remained unchanged in all cases, except for MPS treated group. The body weight on day 7 in MPS treated group decreased by 3.30 %. In all other groups, there was an increase in the body weight from nearly 3 to 8 % confirming the safety of the formulations (Table 3.2A). The second assessment was the effect of formulations on body viscera. The presence of SFB and Apt produced pronounced effect on the visceral index (Table 3.2B). There was little increase in visceral indices of heart and liver in case of the aptamer, MP-Apt and MPS-Apt groups.

The effect of microparticles on the blood profiles of the mice was also investigated (Table 3.2C). There were major differences in the values of total leukocyte count ($p < 0.001$). Hemoglobin concentrations also changed, but only slightly with significantly lower levels in case of MPS-Apt ($p < 0.001$) and MPS ($p < 0.001$). However, in the case of the aptamer change was less significant ($p < 0.05$) indicating a less pronounced effect on hemoglobin. These results showed that the formulations altered the normal physiological values of mice used in the study. As reported previously, the presence of anti-ErbB3 agents (aptamer in our case) altered the immune response and was responsible for decreased TLC levels, causing a decrease in the inflammatory response [143-144]. This surface functionalized therapy can be safe for i.v administration because all the changes were within accepted limits.

Table 3.2A: Body weight changes in mice in different treatment groups.

Treatments	Body Wt. Start (gm ± SD)	Body Wt. End (gm ± SD)	Change (%)
MP	34.13 ± 1.54	35.07 ± 1.77	2.66
MP-Apt	30.43 ± 1.18	32.43 ± 2.59	6.17
MPS	32.30 ± 4.90	31.27 ± 4.82	-3.30
MPS-Apt	27.01 ± 1.27	30.57 ± 3.00	8.51
Apt	28.54 ± 2.82	30.10 ± 3.64	5.17
Control	33.47 ± 2.49	34.60 ± 1.61	3.28

Table3.2B: Body Viscera Index of mice after treatment with formulations.

Treatments	Weight (%) ± SD			
	Heart	Liver	Kidney	Lungs
MP	0.49 ± 0.04	4.94 ± 0.27	0.72 ± 0.06	0.78 ± 0.04
MP-Apt	0.61 ± 0.02	6.41 ± 0.57	0.80 ± 0.01	0.79 ± 0.05
MPS	0.49 ± 0.04	6.21 ± 0.33	0.71 ± 0.05	1.14 ± 0.06
MPS-Apt	0.63 ± 0.02	7.09 ± 0.03	0.77 ± 0.01	0.97 ± 0.02
Apt	0.64 ± 0.05	5.87 ± 0.46	0.73 ± 0.03	0.70 ± 0.03
Control	0.55 ± 0.023	4.38 ± 0.15	0.74 ± 0.03	0.74 ± 0.03

Table3.2C: Complete blood count of mice after treatment with formulations.

Treatments	Hemoglobin (g/dl)	TLC (*10^9/l)	RBC (*10^{12}/l)	HCT (PCV) (%)	MCV(fl)	MCH (pg)	MCHC (%)	Platelets (*10^9/l)
MP	12.20 ± 0.10	9.60 ± 0.50	6.99 ± 0.03	43.60 ± 0.53	54.27 ± 0.38	15.27 ± 0.06	28.33 ± 0.58	652.00 ± 2.08
MP-Apt	11.27 ± 0.15	7.27 ± 0.12	5.55 ±0.04	42.00 ± 0.10	62.23 ± 0.12	17.50 ± 0.10	28.23 ± 0.06	1015.33 ± 5.51
MPS	11.27 ± 0.21	7.20 ± 0.10	5.60 ± 0.03	39.91 ± 0.10	49.60 ± 0.10	14.67 ± 0.06	29.73 ± 0.06	910.67 ± 0.58
MPS-Apt	11.90 ± 0.10	5.70 ± 0.10	5.98 ± 0.03	42.50 ± 0.20	63.60 ± 4.59	16.80 ± 0.26	28.33 ± 0.21	1167.00 ± 5.69
Apt	12.33 ± 0.21	6.53 ± 0.06	6.99 ± 0.01	43.13 ± 0.32	62.27 ± 0.15	17.93 ± 0.06	28.80 ± 0.10	959.00 ± 9.85
Control	12.83 ± 0.31	9.67 ± 0.85	6.07 ± 0.29	44.23 ± 0.61	49.93 ± 1.17	13.90 ± 0.53	26.07 ±0.85	1274.00 ± 20.66

Total leukocyte count (TLC)
Red blood cells (RBC)
Hematocrit (HCT)
Mean corpuscular volume (MCV)
Mean corpuscular hemoglobin (MCH)
Mean corpuscular hemoglobin (MCHC)

3.1.4.2 Blood Biochemistry

The effects of different formulation on the blood clinical markers i.e. liver function test and kidney function test were investigated (Figure 3.20 and Figure 3.21). Nearly in all the treatment groups, alanine aminotransferase (ALT) and aspartate aminotransferase (AST) increased significantly ($p < 0.001$). Exceptions were in case of MP (ALT) and MP-Apt (AST), where no profound change was observed. However, a profound decrease in levels of alkaline phosphatise (ALP) was found in all treatment groups, except MP-Apt. These elevated levels after treatment were representative of cardiac problems and non-alcoholic fatty liver. Moreover, AST to ALT ratio was more than 3 which was indicative of liver inflammation, fatty liver and cardiac injury. These results were in accordance with the results of body visceral indices. A decrease in total serum proteins and a slight increase in bilirubin also predicted liver malfunctioning, usually associated with fatty liver [145-146]. Kidney function tests (Figure 3.22) included uric acid, creatinineand blood urea nitrogen (BUN). The values changed significantly ($p < 0.01$ or $p < 0.001$) in all cases, except MP-Apt in the case of uric acid. The concentrations of these markers indicated the poor kidney function or malfunctioning of the liver [146]. Liver and heart muscles are usually rich in ErbB3 receptors. Therefore, the attachment of aptamer on the surface of microparticles mediated their delivery to the organs rich in ErbB3 receptors, resulting in a change in the normal physiology of these organs.
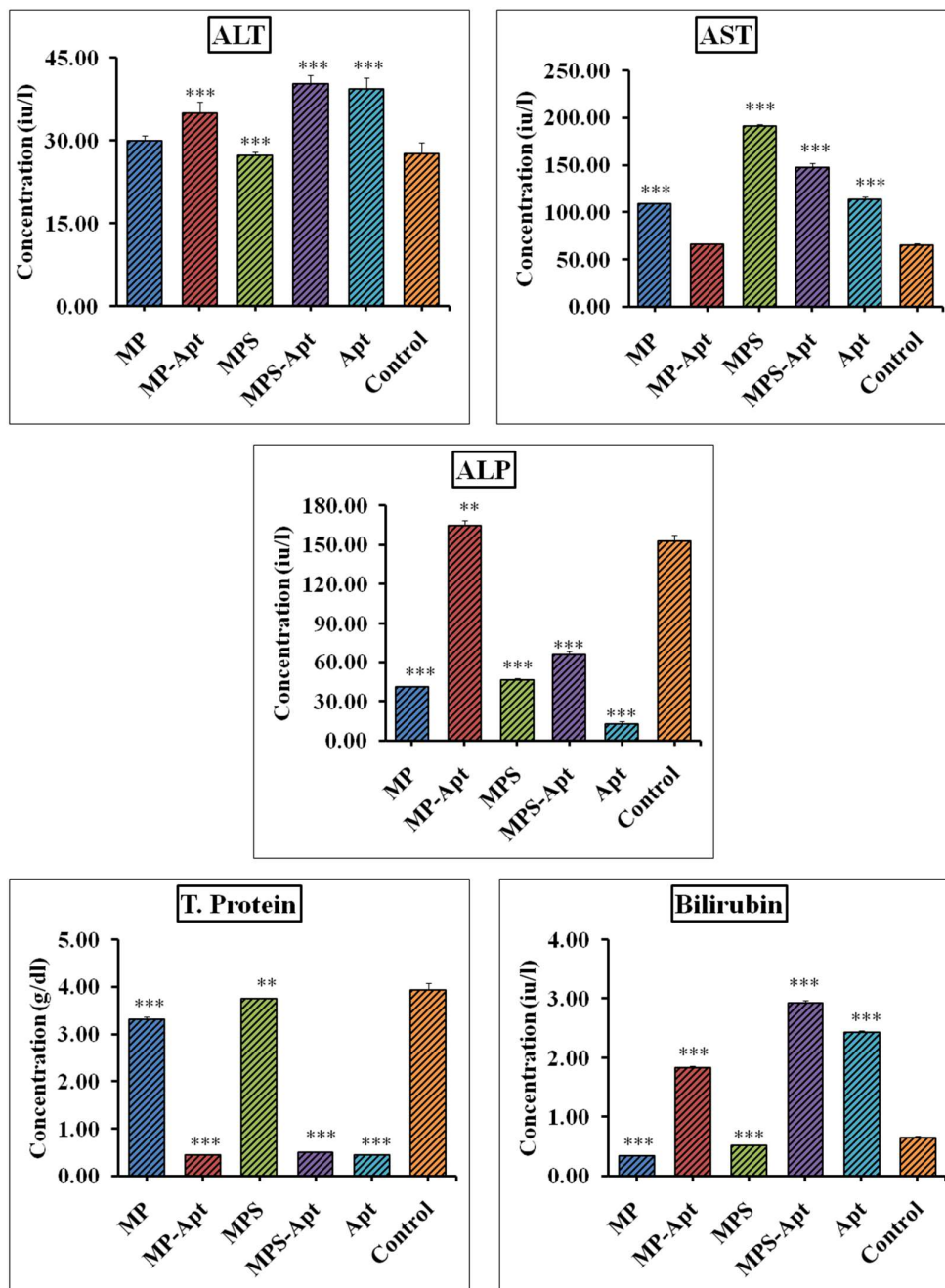
Figure 3.20: Liver function test of microparticles (MP), surface-modified microparticles (MP-Apt), SFB-loaded microparticles (MPS) and surface-modified SFB-loaded microparticles (MPS-Apt). Statistical differences are denoted as "∗∗" $p < 0.01$ and "∗∗∗" $p < 0.001$ and were calculated using controls in each case.

Figure 3.21: Kidney function test of microparticles (MP), surface-modified microparticles (MP-Apt), SFB-loaded microparticles (MPS) and surface-modified SFB-loaded microparticles (MPS-Apt). Statistical differences are denoted as "∗∗" $p < 0.01$ and "∗∗∗" $p < 0.001$ and were calculated using controls in each case.

3.1.4.3 RBC Aggregation Test

RBC aggregation test was performed to monitor the effect of formulations on RBC. The presence of aptamer and SB showed minor structural and morphological changes in RBCs (Figure 3.22). These results were in accordance with the ROS assay. ROS dependent RBCs damage is one of the well-known mechanisms. Therefore, the potentiated effect was observed in the presence of both SFB and Apt. However, the damage was not too much extent to damage complete RBC morphology and results were comparable with the CBC profile. CBC profile showed a small decrease in RBC count but it was in normal profile range. On the other hand, hematocrit values were in the normal range of 39.70-71.80 % [147-148]. Therefore, this functionalized advance colloidal system can be used for targeted chemotherapy.

3.1.4.4 Histopathology

The histopathological investigation was done for heart, liver, kidney and lung. It was obvious from the results that mild to moderate toxicity was seen in case of heart muscles. Necrosis, infiltration of leukocyte, mild granulative tissue and collagen accumulation were observed in the case of aptamer and formulations containing either both SFB and Apt or alone. These results were in accordance with the body visceral index and plasma profile as heart weight increased in these cases as compared to the control group. Liver showed signs of fibrosis, pyknosis (condensation of nuclei due to apoptosis) and micro and macrovesicular fatty changes. The anisokaryosis (larger nuclei) and binucleated hepatocytes suggested regenerative responses as well as the fatty degeneration mostly in case of MP-Apt and MPS-Apt [149]. Some brown necrotic bodies were also visible. Kidneys did not show any major changes in any of the treatment groups. These findings demonstrated the presence of mild nephritis. On the other hand, no major change in lung histology was also obvious. Normal alveolar structures were observed and arterioles were also normal. These investigations reported the safety of this surface functionalized system.
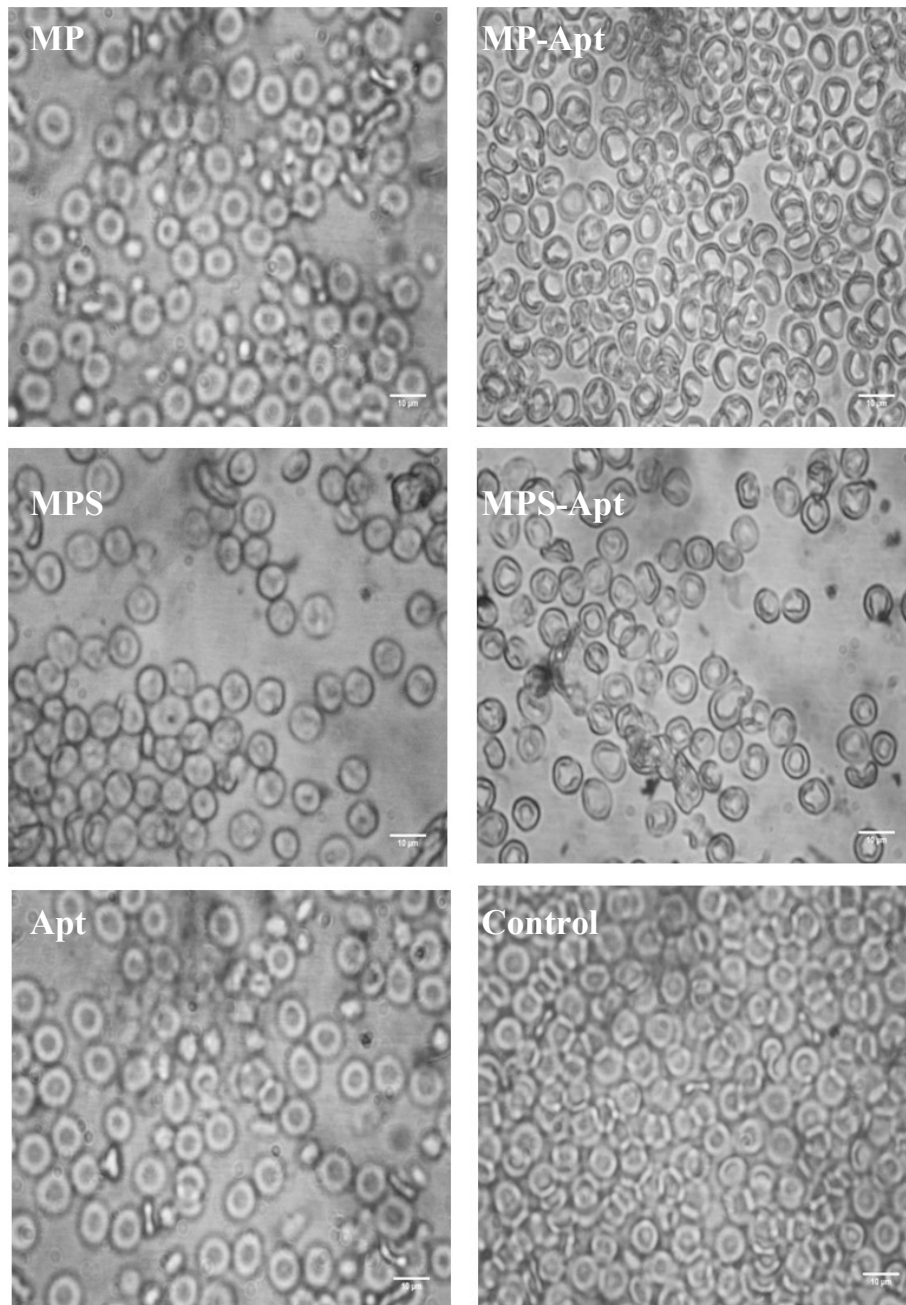
Figure 3.22: RBC aggregation test of microparticles (MP), surface-modified microparticles (MP-Apt), SFB-loaded microparticles (MPS), surface-modified SFB-loaded microparticles (MPS-Apt) and aptamer (Apt).
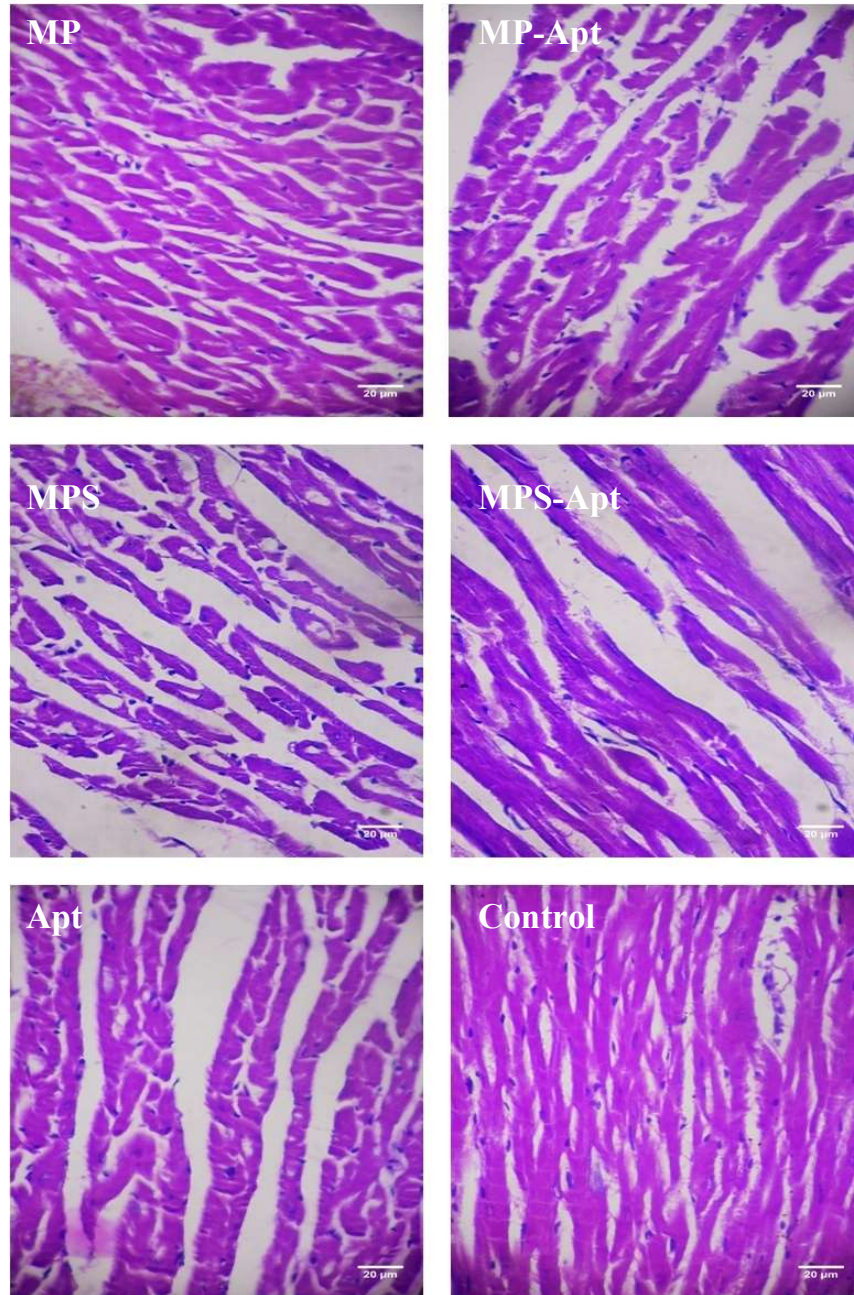
Figure 3.23: Effect of different formulations on histology of heart tissues; H & E staining of microparticles (MP), surface-modified microparticles (MP-Apt), SFB-loaded microparticles (MPS), surface-modified SFB-loaded microparticles (MPS-Apt) and aptamer (Apt).
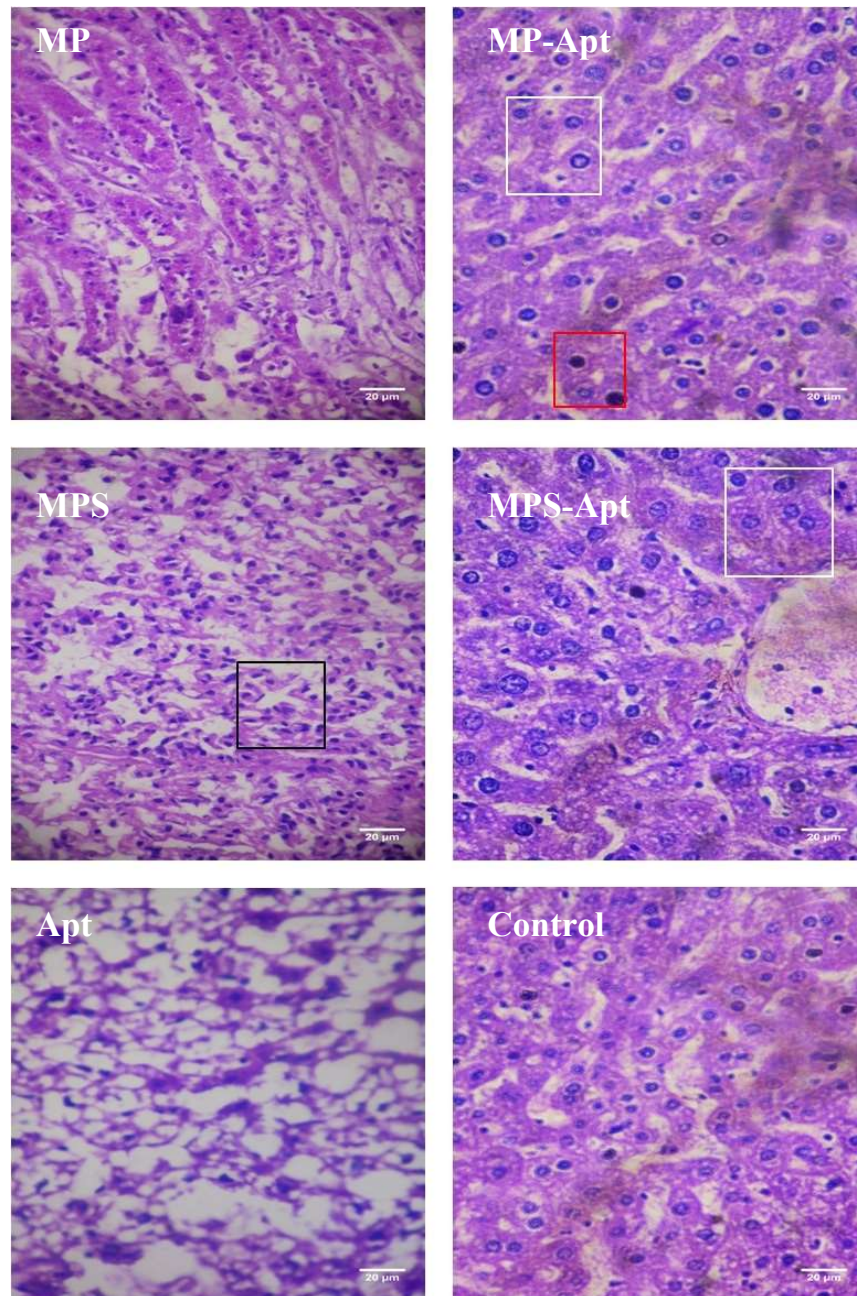
Figure 3.24: Effect of different formulations on histology of liver tissues; H & E staining of microparticles (MP), surface-modified microparticles (MP-Apt), SFB-loaded microparticles (MPS), surface-modified SFB-loaded microparticles (MPS-Apt) and aptamer (Apt). White boxes show anisokaryosis, Red box shows necrotic bodies and the black box shows pyknosis.
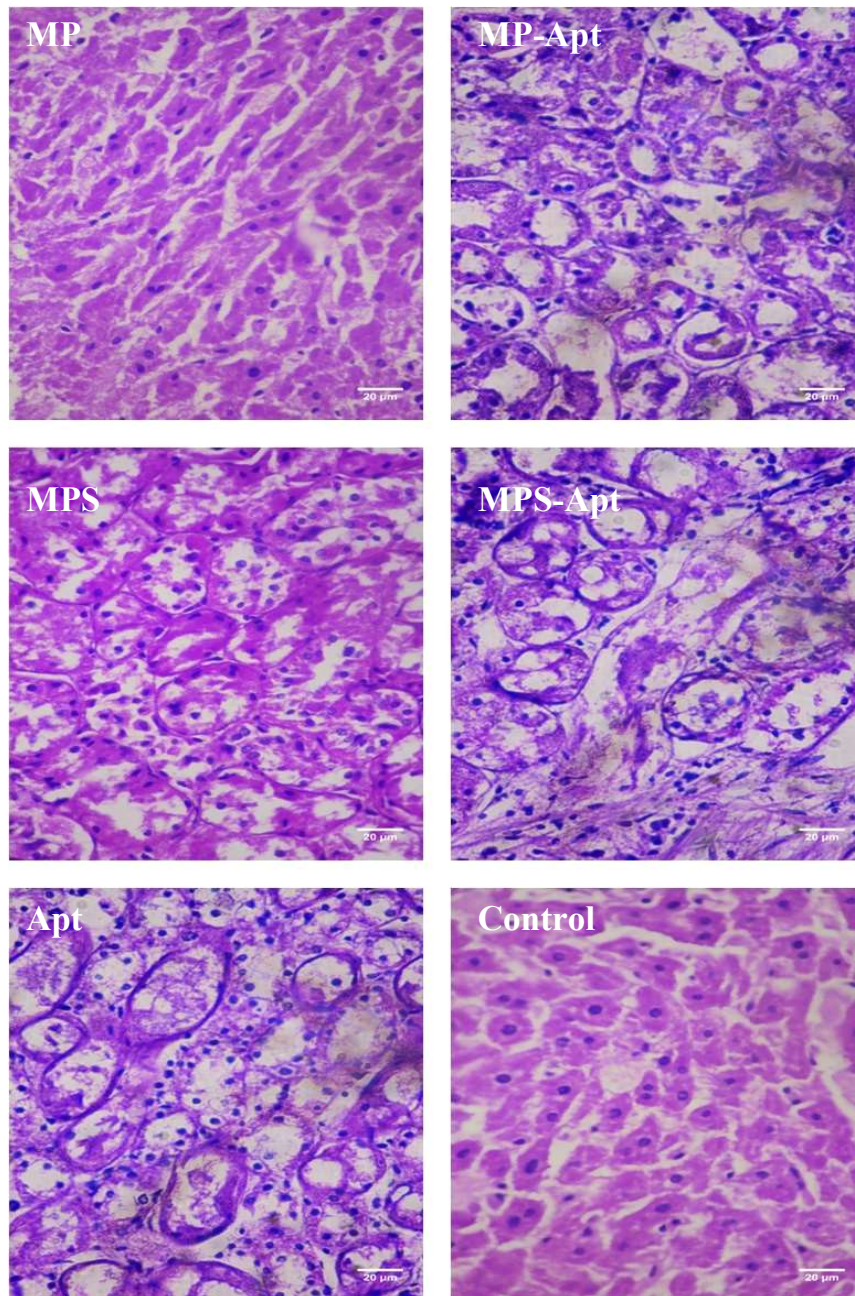
Figure 3.25: Effect of different formulations on histology of kidney tissues; H & E staining of microparticles (MP), surface-modified microparticles (MP-Apt), SFB-loaded microparticles (MPS), surface-modified SFB-loaded microparticles (MPS-Apt) and aptamer (Apt).

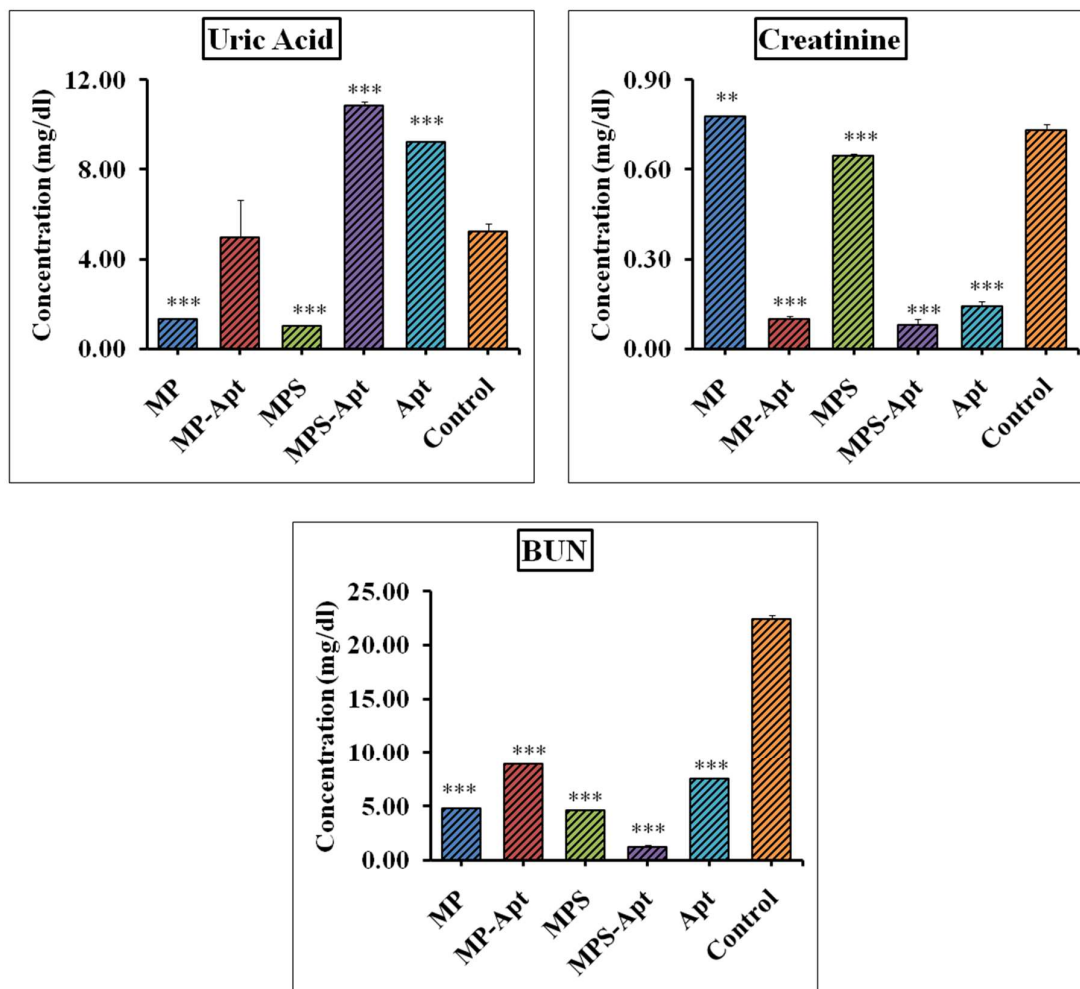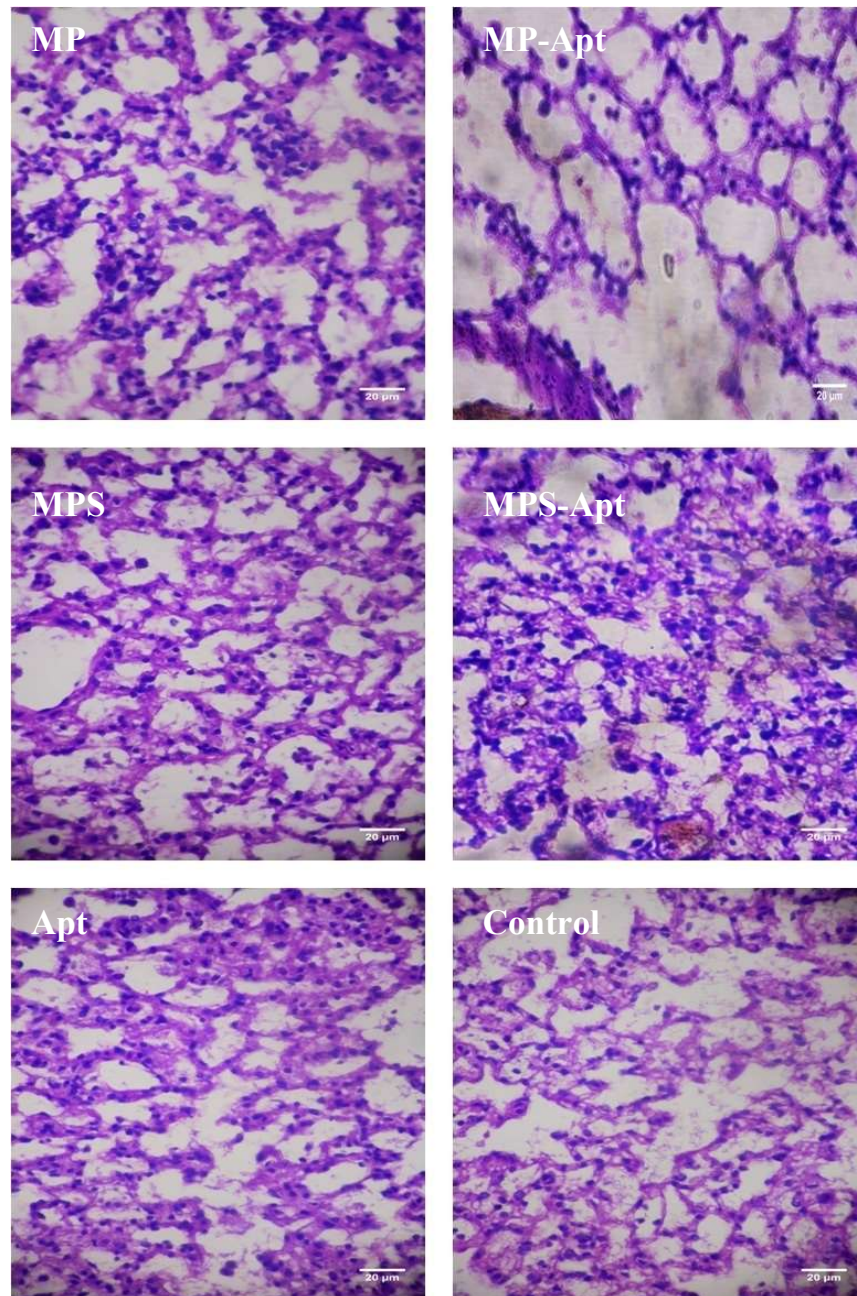**Figure 3.26:** Effect of different formulations on histology of lung tissues; H & E staining of microparticles (MP), surface-modified microparticles (MP-Apt), SFB-loaded microparticles (MPS), surface-modified SFB-loaded microparticles (MPS-Apt) and aptamer (Apt).

3.2 LIPOSOMES

3.2.1 Preparation of Liposomes

The size of liposomes plays an important role in cellular internalization [103]. Therefore, the concentrations of DPPC, cholesterol and DSPE-PEG (2000) cyanur used for the preparation of empty and SFB-loaded liposomes (LP, LPS respectively) were adjusted to 80:10:10, respectively. Sonication of dry lipid film after hydration is thought to be the most effective method of MLVs formation. However, sonicated liposomes are not stable to much extent as well as their size distribution is high, hence, extrusion was used as post process step [150]. Thus colloidal system was extruded 25 times through 200 nm polycarbonate membrane filters (Whatman, Buckinghamshire, UK) using an extruder (Avanti Mini, Avanti Polar Lipids Inc., Alabaster, USA).

3.2.2 Characterization

3.2.2.1 Encapsulation Efficiency and Aptamer Coupling

A challenging issue regarding the preparation of liposomes is encapsulation of chemotherapeutic agent. Therefore, encapsulation efficiency was calculated. Encapsulation efficiency of SFB was 64.1 ± 3.3 %. Binding of Apt on the surface of liposomes was evaluated by fluorescence analysis of Cyn 5. Fluorescence quantification at λ_{ex} 630 nm and λ_{em} 670 nm confirmed the attachment of Cyn 5 labeled Apt to the liposome surface. The results showed that 61.79 ± 2.45 and 60.41 ± 3.35 percent of Apt was bound on the surface of LP and LPS, respectively.

3.2.2.2 Physico-chemical Characterization of Liposomes

3.2.2.2.1 Particle size and zeta potential

Film hydration method used to prepare liposomes was optimized in preliminary testing for the concentration of all ingredients. Hence, results were highly reproducible. Optimized formulations were then assessed for hydrodynamic diameter and zeta potential measurements. The size distribution (Polydispersity Index; PdI) was found to be under 0.21 ± 0.02 in case of LP showing nearly monomodel distribution of size. It was obvious that hydrodynamic diameter was increased by incorporating the SFB into liposomes with a slight increase in PDI to 0.26 ± 0.01. On the other hand, the presence of Apt also changed the size

of the liposomes. Similar increase in diameter, after attachment of Apt on the surfaces, was also reported earlier [29, 91]. The incorporation of SFB as well as the presence of Apt also influenced the zeta potential. The zeta potential measurements were negative in all cases ranging from -21.8 ± 2.5 (LPS-Apt) to -14.0 ± 1.7 for LP (Table 3.3). Therefore, the incorporation of SFB as well as the presence of aptamer changed zeta potential also.

Table 3.3: Size and zeta potential of liposomes.

Formulations	Size ± SD (nm)	Zeta Potential ± SD (mV)	PDI ± SD
LP	120.71 ± 5.91	-14.01 ± 1.74	0.21 ± 0.02
LP-Apt	142.97 ± 12.56	-18.42 ± 1.17	0.25 ± 0.01
LPS	131.34 ± 9.14	-18.84 ± 1.26	0.26 ± 0.03
LPS-Apt	155.01 ± 11.92	-21.38± 2.53	0.28 ± 0.02

3.2.2.2.2 Atomic Force Microscopy (AFM)

Morphological characterization was done using an atomic force microscope (AFM). AFM analysis revealed diverse sizes of liposomes (Figure 3.27). The coupling of Apt resulted in an increase in the size and size distribution of the modified particles. Surface roughness (by RMS; Rq) of the liposomes was also calculated with 2.2 ± 1.2 nm and 5.4 ± 1.1 nm in case of LPS and LPS-Apt. This increase in Rq value represented surface modification in case of LPS-Apt. More the surface roughness more will be the wettability of the nanoparticles and thus will affect nanoparticle-cell interaction [97-98, 114-115].
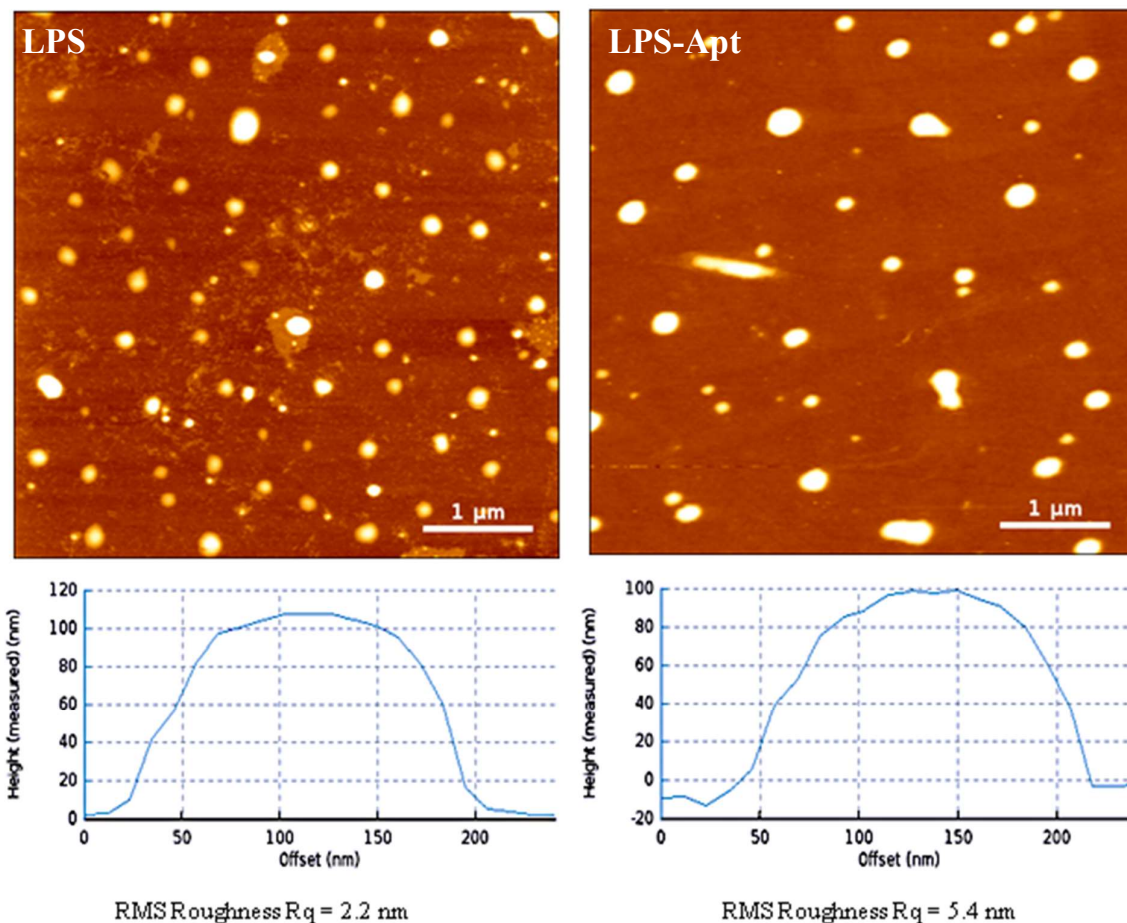
Figure 3.27: AFM images (height) of liposomes with surface roughness Rq; SFB-loaded liposomes (LPS) and surface-modified SFB-loaded liposomes (LPS-Apt).

3.2.2.3 Cell Culture Studies

3.2.2.3.1 2D Cell Viability and IC_{50}

The assessment of cell viability in the presence of formulations was done by MTT assay. The presence of both SFB and Apt resulted in a decrease in cell viability, with maximum effect at highest concentrations (4 µM SFB or equivalent). This response was dose-dependent i.e. increasing with decreasing the dose of the liposome and vice versa. Therefore, the lowest dose of the formulations (0.25 µM SFB or equivalent) showed a viability of 92.17 ± 3.25 % for LPS-Apt and to 94.27 ± 5.91 % in the case of LPS. Inhibitory response was strongest at heights concentrations when compared with LP with $p < 0.001$. IC_{50} value was 0.75 µM and 1.25 µM for LPS-Apt and LPS, respectively. Moreover, LP showed nearly more than 80 % cell viability even at the highest concentration (Figure 3.28).   This suggested that

formulations are relatively safe in the absence of SFB or Apt. The presence of aptamer in formulations showed an increase in the effect of chemotherapeutic agent due to the presence of drug on one hand and due to targeted delivery of the formulations in the presence of aptamer [116-117]. The combination of SFB and Apt exhibited targeted SFB liposomes delivery towards ErbB3 rich cells there by addressing the problem of generalized toxicity due to non-specific drug delivery.

Figure 3.28: *2D* Cell viability assay of liposomes (LP), surface-modified liposomes (LP-Apt), SFB-loaded liposomes (LPS) and surface-modified SFB-loaded liposomes (LPS-Apt). Statistical differences were denoted as "*" $p < 0.05$ and "***" $p < 0.001$.

3.2.2.3.2 3D Cell Viability

Effect of different formulations on the size of *3D* culture was also investigated. In the case of formulations without SFB an equivalent liposome amount was considered. It was evident that presence of SFB and/Apt decreased the culture size. After 24 h, culture size was 32.05 ± 75.97 % of that of original in case of LPS-Apt and 73.71 ± 8.82 % in case of LP [153]. This depicted the safety of formulations, in the absence of Apt or SFB. The presence of SFB along with Apt decreased cell viability significantly (Figure 3.29). This decrease indicated the interaction between anti-ErbB3-Apt modified liposomes and cells on one hand and anti-proliferative effect of SFB itself on the other hand. Therefore, this combination of anti-ErbB3-Apt and drug exhibited a synergistic effect thereby addressing the problem of resistance towards SFB [118].

3.2.2.3.3 Internalization Pathway

Clathrin and caveolae-mediated endocytosis pathways were evaluated to examine the mechanism of liposome internalization into MDA-MD-231 cell. Chlorpromazine and Filipin III were used to suppress the clathrin and the caveolae-mediated endocytosis, respectively. It was evident from the results that cells, pre-treated with chlorpromazine/Filipin III, showed increased cell viability as compared to control group (Figure 3.30). The presence of chlorpromazine and Filipin III resulted in the blockade of liposomal internalization. This was evident from the increased cell viability in chlorpromazine or Filipin III treated cells, suggesting both clathrin and caveolae-mediated internalization pathways. An increased cell viability in their presence endorsed that the dual clathrin and caveolae-mediated dependent pathways as possible mechanisms of liposomal internalization [154].
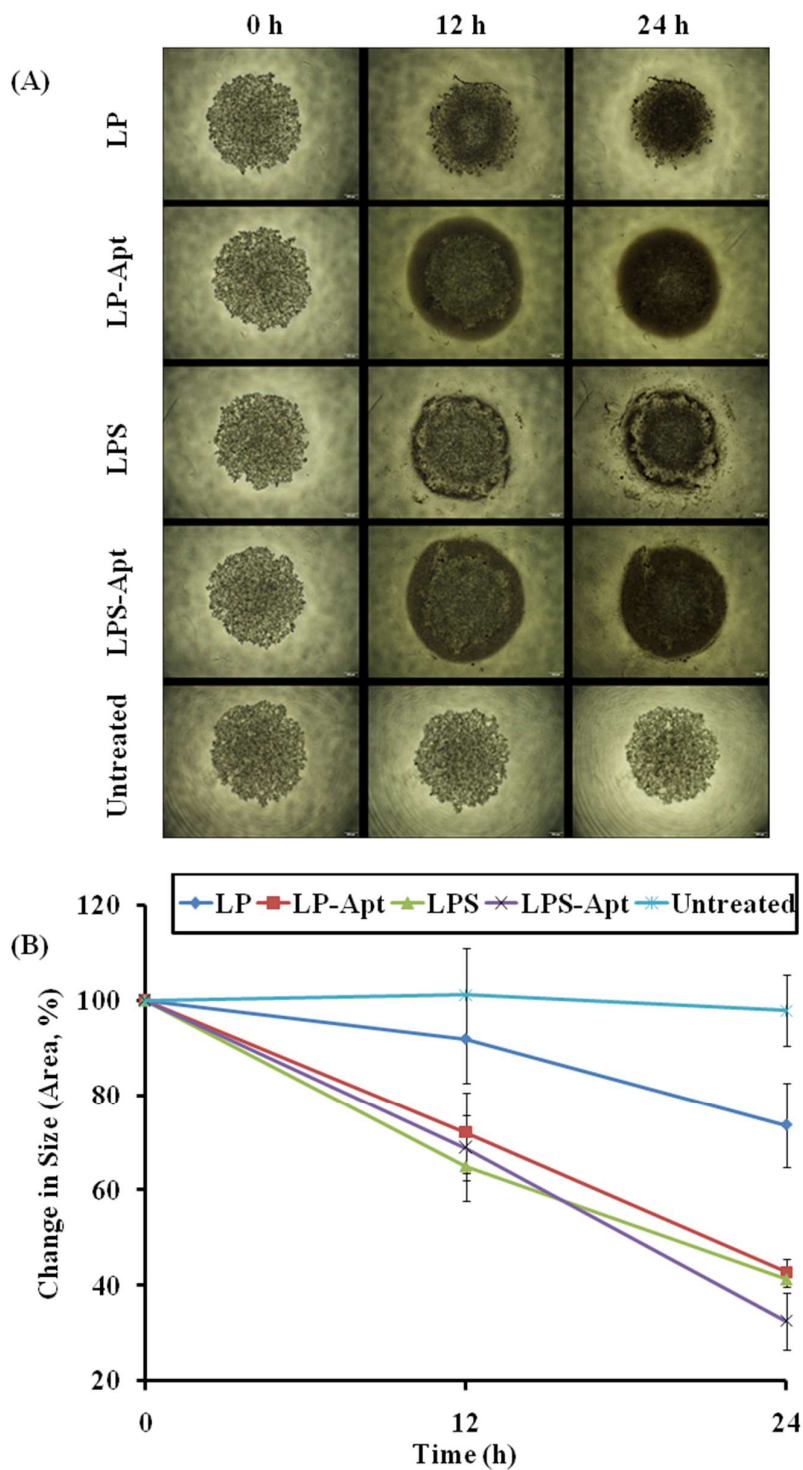
Figure 3.39: A) *3D* cell culture viability assay of liposomes; B) Change in percentage area of *3D* culture of liposomes (LP), surface-modified liposomes (LP-Apt), SFB-loaded liposomes (LPS) and surface-modified SFB-loaded liposomes (LPS-Apt).
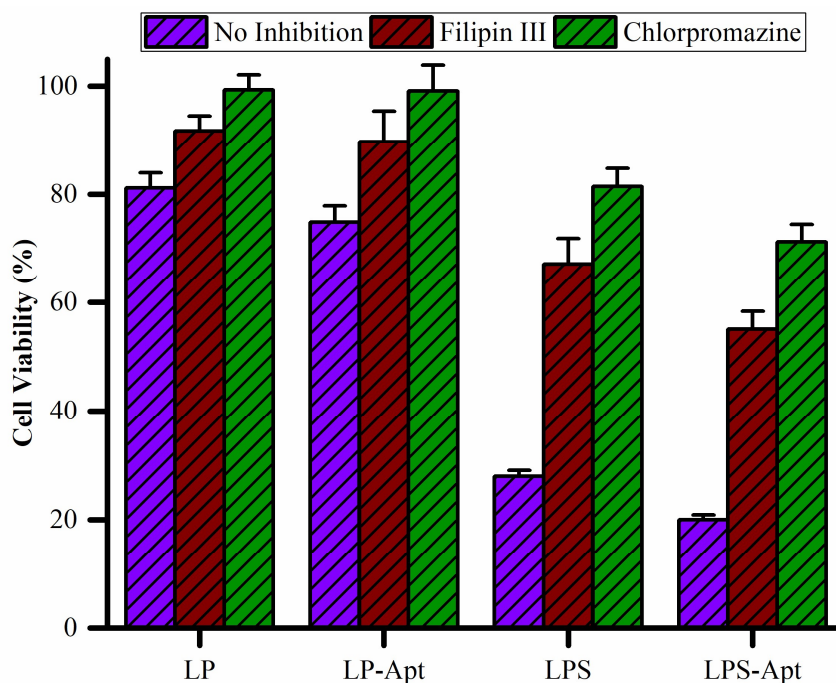
Figure 3.30: Pathway analysis of liposomes (LP), surface-modified liposomes (LP-Apt), SFB-loaded liposomes (LPS) and surface-modified SFB-loaded liposomes (LPS-Apt). Each formulation was equivalent to 2 µM SFB concentration in liposomes.

3.2.2.3.4 Apoptosis Assay

The mechanism of cells death was evaluated by DAPI staining. DAPI is a nuclear stain, which binds to double-stranded DNA. It can be used for the detection of chromatin or nuclear condensation and degradation. It can be used to detect the formation of apoptotic bodies which result ultimately in the death of cells. When cells were treated with different formulations, significant damage and apoptotic bodies formation was observed [125-127]. Chromatin fragmentation as well as nuclear condensation was observed in case of cells treated with SFB and Apt (Figure 3.31). On the other hand, un-treated cells show no clear evidence of apoptotic bodies formation. Therefore, the presence of SFB and Apt were thus responsible for the apoptosis leading to cell death. These results were also in good coordination with cell viability assay, showing more apoptotic bodies in the presence of both SFB and Apt as compared to other formulations.

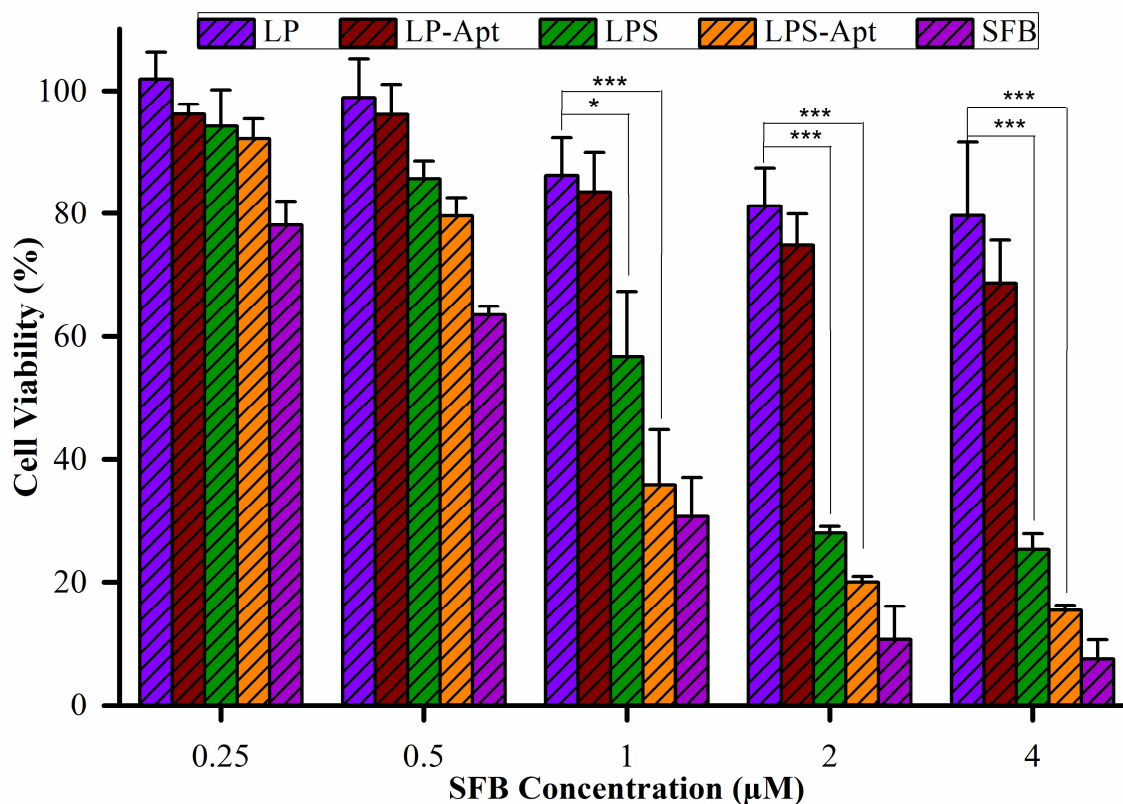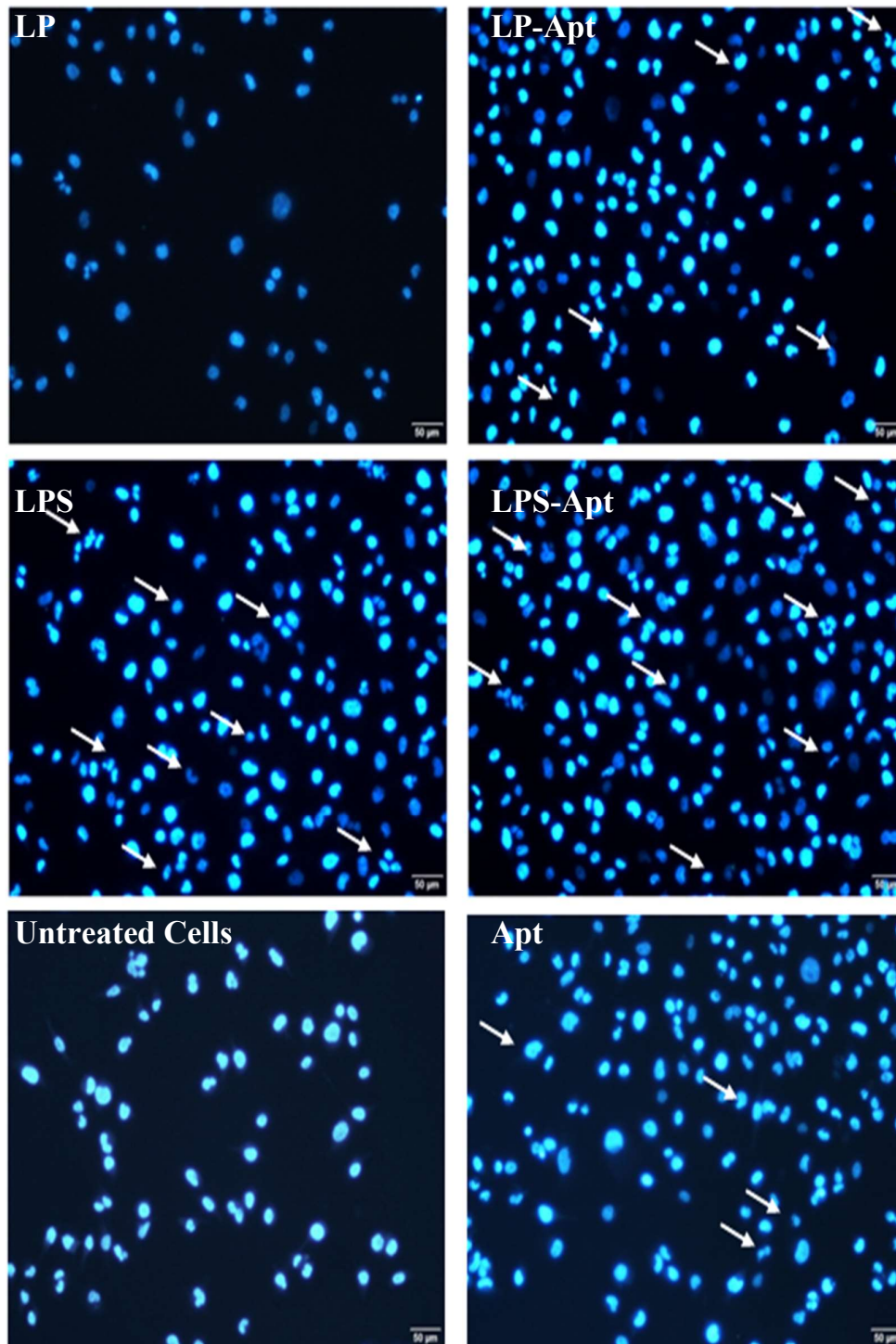**Figure 3.31:** Apoptosis assay showing nuclear condensation and chromatin fragmentation of liposomes (LP), surface-modified liposomes (LP-Apt), SFB-loaded liposomes (LPS) and surface-modified SFB-loaded liposomes (LPS-Apt).

3.2.2.3.5 Cellular Uptake

Cellular uptake was visualized by confocal laser scanning microscopy (CLSM). Cyn 5 was attached to 5' end of the aptamer, which was bound to surface of liposomes. The nucleus of the cell incubated with the formulations was stained with DAPI. CLSM images showed the presence of surface-modified liposomes within the cells. The red fluorescence of aptamer can be seen throughout the cytoplasm, particularly near the nucleus.

Clathrin-dependent as well as caveolae-mediated internalization (Figure 3.30) was found to be responsible for the transfer of liposomes from cell membrane to different cytoplasmic regions [154-155]. This might be the possible mechanism for the toxicity of SFB [139-141]. These pathways were then responsible for the movement of liposomes through cytoplasm and then to nuclear region. The z-stack images also showed the presence of Cyn 5 labeled aptamer near the nuclear region (Figure 3.32A). The intensity plot for co-localization shows DAPI on the x-axis and Cyn 5 on the y-axis. Co-localization coefficient was measured by ZEN software (Carl Zeiss, Jena, Germany). This ranges from 0 to 1, where 0 shows no co-localization and 1 shows 100 percent co-localization. Co-localization coefficients were between 0.4 and 0.7. This explains partial co-localized liposomes in nuclear region. The intensity plot depicted the more intense fluorescence of Cyn 5 channel in case of LP-Apt and aptamer treated cells. However, in the LPS-Apt treated cells, these channels were almost equally co-localized (Figure 3.32B). Aptamer delivered LPS to the nucleus, therefore DAPI and Cyn 5 fluorescence was nearly equally co-localized in case of LPS-Apt. Hence, the presence of anti-ErbB3 aptamer enhanced the internalization of liposomes by clathrin-mediated pathway. Therefore, this combination of SFB and anti-ErbB3-aptamer can be used to increase the chemotherapeutic effects. This combination, therefore, will not only increase the internalization of liposome but also decrease the toxicity due to non-specific drug delivery.
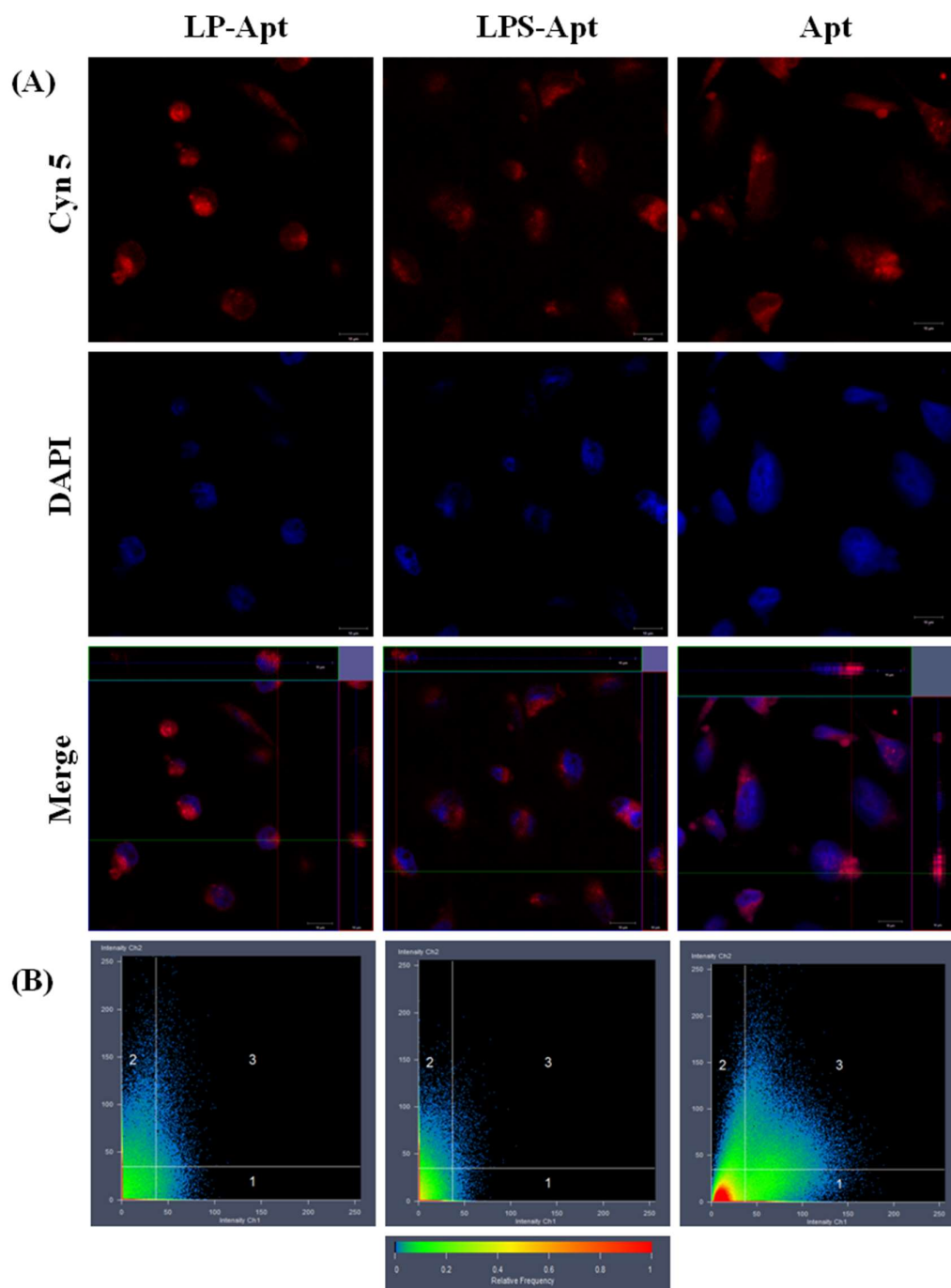
Figure 3.32: Cellular uptake of Cyn 5 labeled liposomes after 2 h in MDA-MB-231 cells; A) cellular uptake; merge images are represented in the form of z-stack to visualize the presence of aptamer functionalized microparticles near nucleus. B) co-localization of surface-modified liposomes (LP-Apt), surface-modified SFB-loaded liposomes (LPS-Apt) and aptamer (Apt) treated cells.

3.2.2.4 Chorioallantoic Membrane Assay

The chorioallantoic membrane (CAM) model offers an excellent ethical and cost effective alternative to *in vivo*. Therefore, CAM model was used to mimic the *in vivo* safety and evaluation of liposomal preparations. There are different sort of studies available for CAM model including angiogenesis, transfection and tumor growth. Transfecting ability of surface-modified liposomes was investigated during current study.

On the EDD 11, 50 µl of different formulations were injected into the mesoderm of CAM. No sign of major toxicity or retardation in the embryogenesis was observed for 24 h. CAM microvasculature was also intact and showed no injury. Furthermore, after 24 h 1 cm of the mesoderm of CAM was dissected and placed on clear glass slide after washing with 0.9 % NaCl. Uptake analysis performed using a confocal laser scanning microscope (LSM700, Carl Zeiss, Jena, Germany) showed the presence of Cyn 5 labeled liposomes in CAM (Figure 3.33). Similar results were reported previously [156], showing minimum toxicities of formulations and localization of formulations in mesoderm of CAM.
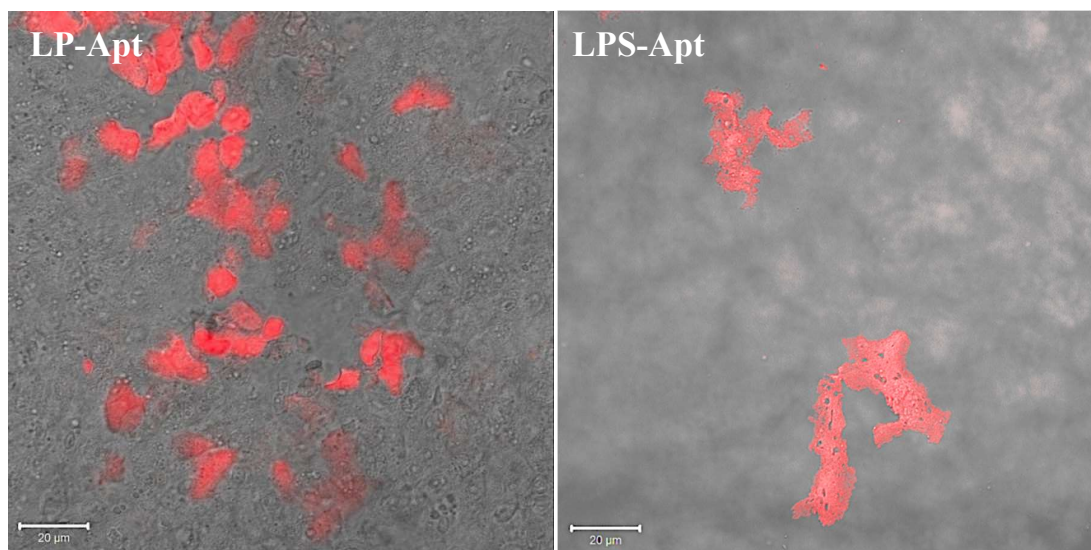
Figure 3.33: CLSM micrograph of CAM section showing presence of surface-modified liposomes (LP-Apt) and surface-modified SFB-loaded liposomes (LPS-Apt).

3.2.2.5 Hemocompatibility Studies

3.2.2.5.1 Ex vivo Hemolysis Assay

Compatibility of formulations with erythrocytes was evaluated by hemolysis assay. This assay determines the release of hemoglobin from erythrocytes after exposure to liposomes. Percentage of oxyhemoglobin formed after the reaction of released hemoglobin with atmospheric oxygen can be determined spectroscopically. Hemolytic potential among all formulations was less than 15 % indicating a good hemocompatibility profile (Figure 3.34). Maximum hemolysis of 12.59 ± 1.91 % was observed in case of pure drug. From the results, it can be concluded that the presence of SFB and Apt did not affect the normal physiology of erythrocytes, thereby rendering the formulations suitable for i.v. administration.
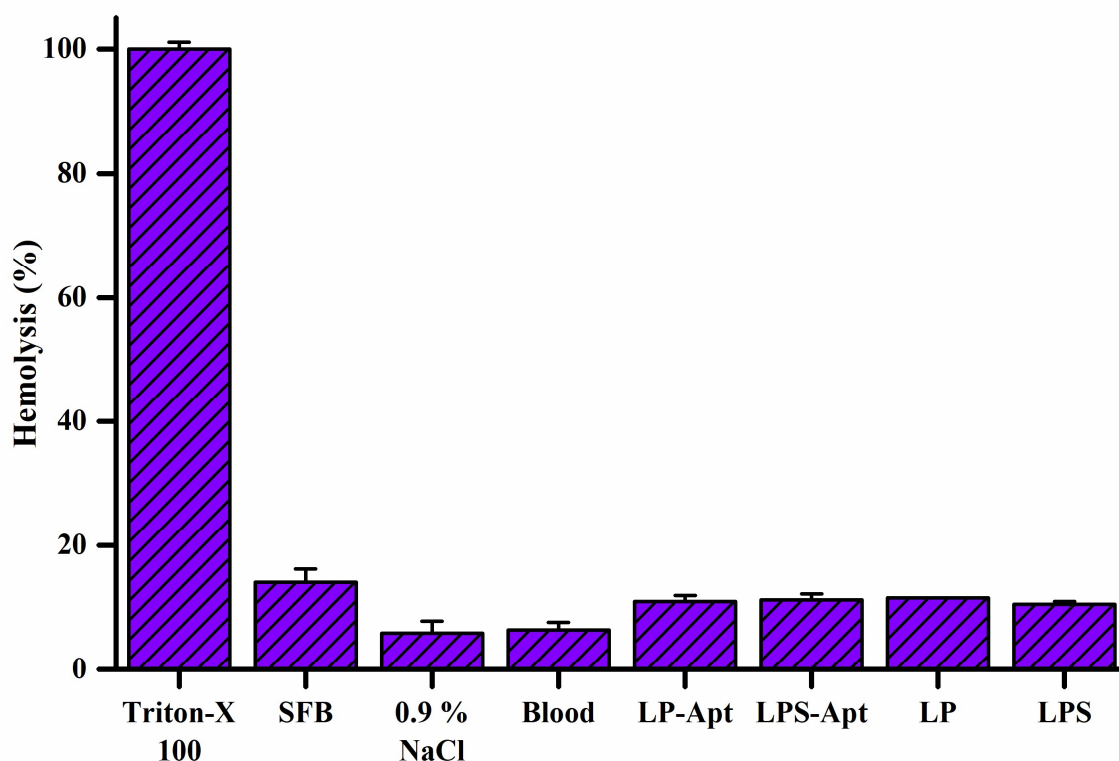
Figure 3.34: Hemolysis assay of liposomes (LP), surface-modified nanoparticles (LP-Apt), SFB-loaded nanoparticles (LPS) and surface-modified SFB-loaded nanoparticles (LPS-Apt). 1% Triton-X 100, 0.9 % NaCl and blood were used as controls.

Summary and Outlook

4.1 SUMMARY AND OUTLOOK

The current project gave a detailed insight of surface modification of different advance colloidal systems along with their *in vitro* and *in vivo* targeting capabilities. Three different colloidal systems (nanoparticles, microparticles and liposomes) were evaluated for their efficacies and consistencies in results.

The introduction contains an overview for the passive and active targeting of chemotherapeutic agents with different colloidal systems. Different methods of preparation and characterization of these colloidal systems were reviewed. This formed the root level for the use of these formulations in the current project. Furthermore, a brief introduction about aptamers and different examples of targeting molecules was also given to elaborate on aptamers' specific nature. This provided the basis of surface modification of colloidal formulations with aptamer of interest.

Sorafenib tosylate (SFB) was selected as a chemotherapeutic agent because it has low solubility and low bioavailability. Its LogP value is 4.54 with biopharmaceutical classification systems class IV. Systemic toxicity due to non-specific drug delivery is also issues with the use of SFB. Another problem associated with the use of this chemotherapeutic agent is the development of drug resistance after consecutive administrations. Therefore, the current study was designed to improve the efficiency of cancer therapy using sorafenib-loaded colloidal systems coupled with anti-ErbB3-aptamer (Apt). There first part of result and discussion included characterization of SFB-loaded PLGA matrix systems i.e. nanoparticles and microparticles. The encapsulation efficiencies revealed the loading of the drug inside these carrier systems. The physicochemical investigation by Fourier transform infrared spectroscopy, elemental analysis and fluorescence analysis elaborated the success of surface modification of these systems with Apt. Furthermore, morphological analysis by atomic force and scanning electron microscopy supported these results and showed an optimal surface roughness profile for cell surface interactions.

Cell culture studies showed a positive impact of the combination of SFB and Apt. The presence of SFB and Apt together showed maximum cytotoxicities compared to other formulations. Dose-dependent toxicities were demonstrated using the cell viability assay. Moreover, time-dependent formulation delivery, to the cytoplasm and subsequently to the nuclear membrane, was observed by CLSM visualization. Higher reactive oxygen species

production was observed in the presence of both SFB and Apt as compared to blank formulations. However, the aptamer alone did not significantly induce ROS production. Upon treatment of the cells with different concentration of particles, a significant dose-dependent ROS production was noticed. The metastatic inhibition by the particles, especially those with SFB and Apt was evident from the scratch test. The absence of both SFB and Apt resulted in complete healing of wound within 24 h.

Ex vivo hemolysis studies demonstrated the hemocompatibility of the PLGA matrices, thus mimicking *in vivo* safety of these formulations. The presence of SFB as well Apt did not change the hemolytic potential of formulations to much extent. All the formulations were more hemocampatible as compared to pure drug. Moreover, RBC aggregation test showed no profound change in the morphology of RBCs. In vivo assessment by the blood profiles along with serum biochemistry stamped the safety of the formulation. Nevertheless, heart and liver-specific toxicities were evident in the presence of SFB and Apt but the overall body visceral index was normal.

Results and discussion also included characterization of SFB-loaded liposomes. The physicochemical investigation of the liposomes using dynamic light scattering and laser Doppler velocimetry revealed nearly monomodel size range from 121 nm to 155 nm suitable for cellular internalization. However, the presence of SFB and Apt influenced the hydrodynamic diameters and zeta potentials of formulations. Furthermore, morphological characteristics were described by atomic force microscopy and showed optimal sizes and surface roughness profile for cell surface interactions.

Synergistic dose-dependent cytotoxicities were demonstrated using SFB and Apt in liposomes in *2D* cell culture techniques. The evaluation of toxicity was also visualized in *3D* cell cultures and revealed a decrease in *3D* culture sizes. This effect was also evident in apoptosis assay showing nuclear condensation as a possible mechanism of cell death. The presence of surface-modified liposomes, inside cells was visualized using CLSM. These investigations showed the presence of liposomes inside the cell, especially near the nuclear region (co-localization coefficient; 0.4-0.7).

In order to analyze the in vivo safety as well as the transfection potential of surface modified liposomes the chorioallantoic membrane model (CAM) was used. The presence of these formulations in the mesoderm of the CAM was visualized by CLSM. No evidence of clear toxicity was observed on the development of the embryo. Furthermore, the

hemocompatibility studies of liposomes also demonstrated the safety of these formulations when compared to pure drug.

Therefore, the combination of chemotherapeutic agent and aptamer together with colloidal drug delivery systems will pave the way to a powerful tool in anticancer therapies. Moreover, the presence of aptamer will also solve the problems of side effects of chemotherapeutic agents by specifically delivering the drug to resistant tumors.

4.2 Zusammenfassung und Ausblick

Die aktuelle Projektarbeit gibt einen detaillierten Einblick in die Oberflächenmodifikation verschiedener fortgeschrittener kolloidaler Systeme sowie in deren In-vitro- und In-vivo-Targeting-Fähigkeiten. Drei verschiedene kolloidale Systeme (Nanopartikel, Mikropartikel und Liposomen) wurden auf ihre Wirksamkeit und Konsistenz der Ergebnisse untersucht.

In der Einleitung wird ein Überblick zum passiven und aktiven Targeting von Chemotherapeutika mit unterschiedlichen Kolloidsystemen gegeben. Verschiedene Methoden zur Herstellung und Charakterisierung dieser kolloidalen Systeme werden besprochen. Dies bildete denAusgangspunkt für die Verwendung dieser Formulierungen im Promotionsprojekt. Darüber hinaus wurde eine kurze Einführung über Aptamere und verschiedene Beispiele für Targeting-Moleküle gegeben, um die selektiven Bindungseigenschaften der Aptamere zu erläutern. Dies lieferte die Grundlage für die Oberflächenmodifizierung kolloidaler Formulierungen mit dem interessierenden Aptamer.

Sorafenib-Tosylat (SFB) wurde als Chemotherapeutikum ausgewählt. Der Grund hierfür war die niedrige Löslichkeit und Bioverfügbarkeit mit einem LogP Wert von 4,54 und der Biopharmazeutischen Klassifikation von IV. Des Weiteren zeigt SFB aufgrund nicht-spezifischer Wechselwirkungen eine systemische Toxizität. Ein weiteres Problem, das bei Verwendung dieses Chemotherapeutikums entsteht, ist die Entwicklung einer Wirkstoffresistenznach mehrmaliger Applikation. Daher sollte die aktuelle Studie die Wirksamkeit der Krebstherapie unter Verwendung von mit SFB-beladenen kolloidalen Systemen in Kombination mit Anti-ErbB3-Aptamer (Apt) verbessern. Der erste Teil des Ergebnisses und der Diskussion umfasste die Charakterisierung von SFB-beladenen PLGA-Matrixsystemen, d. h. Nanopartikeln und Mikropartikeln. Die Daten zu Einkapselungseffizienzen zeigten eine erfolgreiche Beladung der Trägersysteme mit SFB. Die physikalisch-chemische Untersuchung mittels Fourier-Transformations-Infrarotspektroskopie, Elementaranalyse und Fluoreszenzanalyse bestätigte die Oberflächenmodifikation dieser Systeme mit Apt. Darüber hinaus stützten morphologische Analysen mittels Atomkraft- und Rasterelektronenmikroskopie diese Ergebnisse und zeigten ein optimales Oberflächenrauheitsprofil für Zelloberflächenwechselwirkungen.

Zellkulturstudien verdeutlichten einen positiven Einfluss der Kombination von SFB und Apt. Das Vorhandensein von SFB und Apt zusammen zeigte maximale Zytotoxizitäten im

Vergleich zu anderen Formulierungen. Dosisabhängige Toxizitäten wurden unter Verwendung des Zelllebensfähigkeitstests nachgewiesen. Darüber hinaus ist die zeitabhängige Abgabe der Formulierung an das Zytoplasma und anschließend an die Kernmembran mit Hilfe der CLSM-Visualisierung beobachtet worden. In Gegenwart von SFB und Apt konnte im Vergleich zu Kontrollpräparaten eine höhere Produktion reaktiver Sauerstoffspezies beobachtet werden. Das Aptamer allein induzierte jedoch keine signifikante ROS-Produktion. Bei Behandlung der Zellen mit unterschiedlicher Partikelkonzentration wurde eine signifikante dosisabhängige ROS-Produktion festgestellt. Die metastatische Hemmung durch die Partikel, insbesondere die mit SFB und Apt, wurde aus dem Kratztest ersichtlich. Das Fehlen von SFB und Apt führte zu einer vollständigen Wundheilung innerhalb von 24 Std.

Ex-vivo-Hämolysestudien zeigten die Hämokompatibilität der PLGA-Matrices und verdeutlichten die In-vivo-Sicherheit dieser Formulierungen. Das Vorhandensein von SFB sowie Apt änderte das hämolytische Potential der Formulierungen nicht wesentlich. Alle Formulierungen weisen eine höhere Hämokompatibiltät im Vergleich zu SFB auf. Der RBC-Aggregationstest wies keinemorphologische Veränderung von RBCs auf. Die In-vivo-Auswertung der Blutprofile sowie die Serumbiochemie bestätigten die Sicherheit der Formulierung. Trotzdem kam es in Gegenwart von SFB und Apt zu herz- und leberspezifischen Toxizitäten, jedoch war der viszerale Index des gesamten Körpers normal.

Ergebnisse und Diskussion umfassten die Charakterisierung von SFB-beladenen Liposomen. Die physikalisch-chemische Untersuchung der Liposomen mittels dynamischer Lichtstreuung und Laser-Doppler-Velocimetrie ergab eine nahezu monomodalen Größenverteilung von 121 nm bis 155 nm, der für die Internalisierung von Zellen geeignet ist. Das Vorhandensein von SFB und Apt beeinflusste jedoch die hydrodynamischen Durchmesser und Zeta-Potentiale der Formulierungen. Darüber hinaus wurden morphologische Eigenschaften durch Rasterkraftmikroskopie untersucht und zeigten optimale Größen und Oberflächenrauheitsprofile für Zelloberflächenwechselwirkungen.

Synergistische dosisabhängige Zytotoxizitäten wurden unter Verwendung von SFB und Apt in Liposomen in 2D-Zellkulturtechniken gezeigt. Die Bewertung der Toxizität wurde auch in 3D-Zellkulturen durchgeführt und resultierte in einer Flächenverkleinerung der 3D Kulturen. Dieser Effekt wurde auch im Apoptose-Assay deutlich, der die Kernkondensation als möglichen Mechanismus für den Zelltod zeigte. Das Vorhandensein von

oberflächenmodifizierten Liposomen in Zellen ist unter Verwendung von CLSM sichtbar gemacht worden. Diese Untersuchungen zeigten das Vorhandensein von Liposomen in der Zelle, insbesondere in der Nähe der Kernregion (Co-Lokalisierungskoeffizient; 0,4-0,7).

Zur Bestimmung der In-vivo-Sicherheit sowie des Transfektionspotentials von oberflächenmodifizierten Liposomen wurde das Chorioallantoismembranmodell (CAM) herangezogen. CLSM Studien zeigten das Vorhandensein der Formulierungen im Mesoderm des CAM und esgab keine Hinweise auf eine Toxizität während der Embryonalentwicklung. Studien bezüglich der Hämokompatibilität der Formulierungen bestätigten die Sicherheit im Vergleich zuSFB.

Zusammenfassend lässt sich sagen, dass eine kolloidale Formulierung bestehend aus einer Kombination von Chemotherapeutikum und Aptamerein leistungsstarkes Medikament in der Krebstherapie darstellt. Durch die Anwesenheit von Aptamer wird ebenso das Nebenwirkungspotential erheblich reduziert, da sich die Formulierungen spezifisch bei resistenten Tumoren akkumulieren und die Wirkstoffe freigeben.

Appendices

5.1 REFRENCES

[1]. Chabner, B. A., & Roberts Jr, T. G. (2005). Chemotherapy and the war on cancer. *Nature Reviews Cancer*, *5*(1), 1-8.

[2]. Schirrmacher, V. (2019). From chemotherapy to biological therapy: A review of novel concepts to reduce the side effects of systemic cancer treatment. *International Journal of Oncology*, *54*(2), 407-419.

[3]. Eder, J. P., Antman, K., Peters, W., Henner, W. D., Elias, A., Shea, T., ... & Schnipper, L. (1986). High-dose combination alkylating agent chemotherapy with autologous bone marrow support for metastatic breast cancer. *Journal of Clinical Oncology*, *4*(11), 1592-1597.

[4]. Smart, E., Lopes, F., Rice, S., Nagy, B., Anderson, R. A., Mitchell, R. T., & Spears, N. (2018). Chemotherapy drugs cyclophosphamide, cisplatin and doxorubicin induce germ cell loss in an in vitro model of the prepubertal testis. *Scientific reports*, *8*(1), 1-15.

[5]. Yoo, T. K., Moon, H. G., Han, W., & Noh, D. Y. (2017). Time interval of neoadjuvant chemotherapy to surgery in breast cancer: how long is acceptable?. *Gland Surgery*, *6*(1), 1-3.

[6]. Passot, G., Soubrane, O., Giuliante, F., Zimmitti, G., Goéré, D., Yamashita, S., & Vauthey, J. N. (2017). Recent advances in chemotherapy and surgery for colorectal liver metastases. *Liver Cancer*, *6*(1), 72-79.

[7]. Kang, K. M., Hong, K. S., Noh, G. T., Oh, B. Y., Chung, S. S., Lee, R. A., & Kim, K. H. (2013). Optimal time of initiating adjuvant chemotherapy after curative surgery in colorectal cancer patients. *Annals of Coloproctology*, *29*(4), 150-154.

[8]. Tohme, S., Simmons, R. L., & Tsung, A. (2017). Surgery for cancer: a trigger for metastases. *Cancer Research*, *77*(7), 1548-1552.

[9]. Baskar, R., Lee, KA, Yeo, R., & Yeoh, KW (2012). Cancer and radiation therapy: current advances and future directions. *International Journal of Medical Sciences*, *9* (3), 193-199.

[10]. Jackson, S. P., & Bartek, J. (2009). The DNA-damage response in human biology and disease. *Nature*, *461*(7267), 1071-1078.

[11]. Chen, HH, & Kuo, MT (2017). Improving radiotherapy in cancer treatment: promises and challenges. *Oncotarget*, *8* (37), 62742-62758.

[12]. Barton, M. B., Jacob, S., Shafiq, J., Wong, K., Thompson, S. R., Hanna, T. P., & Delaney, G. P. (2014). Estimating the demand for radiotherapy from the evidence: a review of changes from 2003 to 2012. *Radiotherapy and Oncology*, *112*(1), 140-144.

[13]. Vasir, J. K., & Labhasetwar, V. (2005). Targeted drug delivery in cancer therapy. *Technology in Cancer Research & Treatment*, *4*(4), 363-374.

[14]. Jang, S. H., Wientjes, M. G., Lu, D., & Au, J. L. S. (2003). Drug delivery and transport to solid tumors. *Pharmaceutical Research*, *20*(9), 1337-1350.

[15]. Dadwal, A., Baldi, A., & Kumar Narang, R. (2018). Nanoparticles as carriers for drug delivery in cancer. *Artificial Cells, Nanomedicine, and Biotechnology*, *46*(2), 295-305.

[16]. Cho, K., Wang, X. U., Nie, S., & Shin, D. M. (2008). Therapeutic nanoparticles for drug delivery in cancer. *Clinical Cancer Research*, *14*(5), 1310-1316.

[17]. Farkona, S., Diamandis, E. P., & Blasutig, I. M. (2016). Cancer immunotherapy: the beginning of the end of cancer?. *BMC Medicine*, *14*(1), 1-5.

[18]. Wraith, D. C. (2017). The future of immunotherapy: a 20-year perspective. *Frontiers in Immunology*, *8*, 1-6.

[19]. Arruebo, M., Vilaboa, N., Sáez-Gutierrez, B., Lambea, J., Tres, A., Valladares, M., & González-Fernández, Á. (2011). Assessment of the evolution of cancer treatment therapies. *Cancers*, *3*(3), 3279-3330.

[20]. Chakraborty, S., & Rahman, T. (2012). The difficulties in cancer treatment. *Ecancermedicalscience*, *6*. 1-6.

[21]. Taghavi, S., Ramezani, M., Alibolandi, M., Abnous, K., & Taghdisi, S. M. (2017). Chitosan-modified PLGA nanoparticles tagged with 5TR1 aptamer for in vivo tumor-targeted drug delivery. *Cancer Letters*, *400*, 1-8.

[22]. Savla, R., Taratula, O., Garbuzenko, O., & Minko, T. (2011). Tumor targeted quantum dot-mucin 1 aptamer-doxorubicin conjugate for imaging and treatment of cancer. *Journal of Controlled Release*, *153*(1), 16-22.

[23]. Krishna, R., & Mayer, L. D. (1997). Liposomal doxorubicin circumvents PSC 833-free drug interactions, resulting in effective therapy of multidrug-resistant solid tumors. *Cancer Research*, *57*(23), 5246-5253.

[24]. Wu, W., Luo, L., Wang, Y., Wu, Q., Dai, H. B., Li, J. S., ... & Wang, G. X. (2018). Endogenous pH-responsive nanoparticles with programmable size changes for targeted tumor therapy and imaging applications. *Theranostics*, *8*(11), 3038-3058.

[25]. Prabhakar, U., Maeda, H., Jain, R. K., Sevick-Muraca, E. M., Zamboni, W., Farokhzad, O. C., … Blakey, D. C. (2013). Challenges and key considerations of the enhanced permeability and retention effect for nanomedicine drug delivery in oncology. *Cancer Research*, *73*(8), 2412–2417.

[26]. McDonald, DM, & Baluk, P. (2002). Significance of blood vessel leakiness in cancer. *Cancer Research 62*. 5381-5385.

[27]. Mickan, A., Sarko, D., Haberkorn, U., & Mier, W. (2014). Rational design of CPP-based drug delivery systems: considerations from pharmacokinetics. *Current Pharmaceutical Biotechnology*, *15*(3), 200-209.

[28]. Alshehri, A., Grabowska, A., & Stolnik, S. (2018). Pathways of cellular internalisation of liposomes delivered siRNA and effects on siRNA engagement with target mRNA and silencing in cancer cells. *Scientific Reports*, *8*(1), 1-9.

[29]. Farokhzad, O. C., Cheng, J., Teply, B. A., Sherifi, I., Jon, S., Kantoff, P. W., ... & Langer, R. (2006). Targeted nanoparticle-aptamer bioconjugates for cancer chemotherapy in vivo. *Proceedings of the National Academy of Sciences*, *103*(16), 6315-6320.

[30]. Aravind, A., Varghese, SH, Veeranarayanan, S., Mathew, A., Nagaoka, Y., Iwai, S., ... & Kumar, DS (2012). Aptamer-labeled PLGA nanoparticles for targeting cancer cells. *Cancer Nanotechnology*, *3* (1), 1-12.

[31]. Sriraman, S. K., Aryasomayajula, B., & Torchilin, V. P. (2014). Barriers to drug delivery in solid tumors. *Tissue Barriers*, *2*(3), 1-8.

[32]. Petros, R. A., & DeSimone, J. M. (2010). Strategies in the design of nanoparticles for therapeutic applications. *Nature reviews Drug discovery*, *9*(8), 615-627.

[33]. Huang, M., Shen, A., Ding, J., & Geng, M. (2014). Molecularly targeted cancer therapy: some lessons from the past decade. *Trends in Pharmacological Sciences*, *35*(1), 41-50.

[34]. Tang, L., Yang, X., Yin, Q., Cai, K., Wang, H., Chaudhury, I., ... & Dobrucki, I. T. (2014). Investigating the optimal size of anticancer nanomedicine. *Proceedings of the National Academy of Sciences*, *111*(43), 15344-15349.

[35]. Vauthier, C., & Bouchemal, K. (2009). Methods for the preparation and manufacture of polymeric nanoparticles. *Pharmaceutical Research*, *26* (5), 1025-1058.

[36]. Muthu, MS, & Singh, S. (2009). Targeted nanomedicines: effective treatment modalities for cancer, AIDS and brain disorders.

[37]. Dinarvand, R., Sepehri, N., Manoochehri, S., Rouhani, H., & Atyabi, F. (2011). Polylactide-co-glycolide nanoparticles for controlled delivery of anticancer agents. *International Journal of Nanomedicine*, *6* , 877-895.

[38]. Tran, S., DeGiovanni, P. J., Piel, B., & Rai, P. (2017). Cancer nanomedicine: a review of recent success in drug delivery. *Clinical and Translational Medicine*, *6*(1), 1-22.

[39]. Paques, JP, van der Linden, E., van Rijn, CJ, & Sagis, LM (2014). Preparation methods of alginate nanoparticles. *Advances in Colloid and Interface Science*, *209* , 163-171.

[40]. Lin, TT, Gao, DY, Liu, YC, Sung, YC, Wan, D., Liu, JY, ... & Chen, Y. (2016). Development and characterization of sorafenib-loaded PLGA nanoparticles for the systemic treatment of liver fibrosis. *Journal of Controlled Release*, *221* , 62-70.

[41]. Wasiak, I., Kulikowska, A., Janczewska, M., Michalak, M., Cymerman, I. A., Nagalski, A., ... & Ciach, T. (2016). Dextran nanoparticle synthesis and properties. *PLoS One*, *11*(1), 1-17.

[42]. Lee, S. H., Heng, D., Ng, W. K., Chan, H. K., & Tan, R. B. (2011). Nano spray drying: a novel method for preparing protein nanoparticles for protein therapy. *International Journal of Pharmaceutics*, *403*(1-2), 192-200.

[43]. Kumar, MR, Bakowsky, U., & Lehr, CM (2004). Preparation and characterization of cationic PLGA nanospheres as DNA carriers. *Biomaterials*, *25* (10), 1771-1777.

[44]. Wang, Y., Li, P., Truong-Dinh Tran, T., Zhang, J., & Kong, L. (2016). Manufacturing techniques and surface engineering of polymer based nanoparticles for targeted drug delivery to cancer. *Nanomaterials*, *6*(2), 1-18.

[45]. Pal, SL, Jana, U., Manna, PK, Mohanta, GP, & Manavalan, R. (2011). Nanoparticle: An overview of preparation and characterization. *Journal of Applied Pharmaceutical Science*, *1*(6), 228-234.

[46]. Barreras-Urbina, CG, Ramírez-Wong, B., López-Ahumada, GA, Burruel-Ibarra, SE, Martínez-Cruz, O., Tapia-Hernández, JA, & Rodriguez Felix, F. (2016). Nano-and micro-particles by nanoprecipitation: Possible application in the food and agricultural industries. *International Journal of Food Properties*, *19* (9), 1912-1923.

[47]. Bharali, D. J., Khalil, M., Gurbuz, M., Simone, T. M., & Mousa, S. A. (2009). Nanoparticles and cancer therapy: a concise review with emphasis on dendrimers. *International Journal of Nanomedicine*, *4*, 1-7.

[48]. Deshpande, P. P., Biswas, S., & Torchilin, V. P. (2013). Current trends in the use of liposomes for tumor targeting. *Nanomedicine*, *8*(9), 1509-1528.

[49]. Alavi, M., Karimi, N., & Safaei, M. (2017). Application of Various Types of Liposomes in Drug Delivery Systems. *Advanced Pharmaceutical Bulletin*, *7*(1), 3–9.

[50]. Akbarzadeh, A., Rezaei-Sadabady, R., Davaran, S., Joo, S. W., Zarghami, N., Hanifehpour, Y., ... & Nejati-Koshki, K. (2013). Liposome: classification, preparation, and applications. *Nanoscale Research Letters*, *8*(1), 1-9.

[51]. Cortesi, R. (1999). Preparation of liposomes by reverse-phase evaporation using alternative organic solvents. *Journal of Microencapsulation* , *16* (2), 251-256.

[52]. Jaafar-Maalej, C., Diab, R., Andrieu, V., Elaissari, A., & Fessi, H. (2010). Ethanol injection method for hydrophilic and lipophilic drug-loaded liposomes preparation. *Journal of Liposomal Research* , *20* (3), 228-243.

[53]. Dua, JS, Rana, AC, & Bhandari, AK (2012). Liposomes: methods of preparation and applications. *International Journal of Pharmaceutical Sciences and Research*, *3* (2), 14-20.

[54]. Gmoshinski, I. V., Khotimchenko, S. A. E., Popov, V. O., Dzantiev, B. B., Zherdev, A. V., Demin, V. F., & Buzulukov, Y. P. (2013). Nanomaterials and nanotechnologies: methods of analysis and control. *Russian Chemical Reviews*, *82*(1), 48-76.

[55]. Mourdikoudis, S., Pallares, R. M., & Thanh, N. T. (2018). Characterization techniques for nanoparticles: Comparison and complementarity upon studying nanoparticle properties. *Nanoscale*, *10*(27), 12871-12934.

[56]. Manaia, E. B., Abuçafy, M. P., Chiari-Andréo, B. G., Silva, B. L., Junior, J. A. O., & Chiavacci, L. A. (2017). Physicochemical characterization of drug nanocarriers. *International Journal of Nanomedicine*, *12*, 4991-5011.

[57]. Brar, S. K., & Verma, M. (2011). Measurement of nanoparticles by light-scattering techniques. *TrAC Trends in Analytical Chemistry*, *30*(1), 4-17.

[58]. Lin, P. C., Lin, S., Wang, P. C., & Sridhar, R. (2014). Techniques for physicochemical characterization of nanomaterials. *Biotechnology Advances*, *32*(4), 711-726.

[59]. Bothun, G. D. (2008). Hydrophobic silver nanoparticles trapped in lipid bilayers: Size distribution, bilayer phase behavior, and optical properties. *Journal of Nanobiotechnology*, *6*(1), 1-10.

[60]. Huang, HC, Chang, PY, Chang, K., Chen, CY, Lin, CW, Chen, JH, ... & Chang, FH (2009). Formulation of novel lipid-coated magnetic nanoparticles as the sample for in vivo imaging. *Journal of Biomedical Science*, *16* (1), 1-10.

[61]. Cuche, A., Masenelli, B., Ledoux, G., Amans, D., Dujardin, C., Sonnefraud, Y., & Huant, S. (2008). Fluorescent oxide nanoparticles adapted to active tips for near-field optics. *Nanotechnology*, *20* (1), 1-6.

[62]. Sublemontier, O., Nicolas, C., Aureau, D., Patanen, M., Kintz, H., Liu, X., ... & Etcheberry, A. (2014). X-ray photoelectron spectroscopy of isolated nanoparticles. *The Journal of Physical Chemistry Letters*, *5*(19), 3399-3403.

[63]. Chen, C., Zhou, S., Cai, Y., & Tang, F. (2017). Nucleic acid aptamer application in diagnosis and therapy of colorectal cancer based on cell SELEX technology. *NPJ Precision Oncology*, *1* (1), 1-7.

[64]. Zhuo, Z., Yu, Y., Wang, M., Li, J., Zhang, Z., Liu, J., ... & Zhang, B. (2017). Recent advances in SELEX technology and aptamer applications in biomedicine. *International Journal of Molecular Sciences*, *18*(10), 1-19.

[65]. Zhou, J., & Rossi, J. (2017). Aptamers as targeted therapeutics: current potential and challenges. *Nature Reviews Drug Discovery*, *16*(3), 181-202.

[66]. Ng, EW, Shima, DT, Calias, P., Cunningham Jr, ET, Guyer, DR, & Adamis, AP (2006). Pegaptanib, a targeted anti-VEGF aptamer for ocular vascular disease. *Nature Reviews Drug Discovery*, *5*(2), 1-18.

[67]. Morita, Y., Leslie, M., Kameyama, H., Volk, D., & Tanaka, T. (2018). Aptamer therapeutics in cancer: Current and future. *Cancers*, *10* (3), 1-22.

[68]. Chi-hong, BC, Chernis, GA, Hoang, VQ, & Landgraf, R. (2003). Inhibition of heregulin signaling by aptamer that preferentially binds to the oligomeric form of human epidermal growth factor receptor-3. *Proceedings of the National Academy of Sciences*, *100* (16), 9226-9231.

[69]. Cerchia, L., Hamm, J., Libri, D., Tavitian, B., & De Franciscis, V. (2002). Nucleic acid aptamers in cancer medicine. *FEBS letters*, *528* (1-3), 12-16.

[70]. Mosafer, J., & Mokhtarzadeh, A. (2018). Cell surface nucleolin as a promising receptor for cancer cells AS1411 aptamer-mediated targeted drug delivery into cancer cells. *Current Drug Delivery* , *15* (9), 1323-1329.

[71]. Lupold, S. E. (2018). Aptamers and apple pies: a mini-review of PSMA aptamers and lessons from Donald S. Coffey. *American Journal of Clinical and Experimental Urology*, *6*(2), 1-9.

[72]. McKeague, M., & DeRosa, M. C. (2012). Challenges and opportunities for small molecule aptamer development. *Journal of Nucleic Acids, 1-20.*

[73]. Ozalp, V. C., Eyidogan, F., & Oktem, H. A. (2011). Aptamer-gated nanoparticles for smart drug delivery. *Pharmaceuticals*, *4*(8), 1137-1157.

[74]. Dembowski, S. K., & Bowser, M. T. (2018). Microfluidic methods for aptamer selection and characterization. *Analyst*, *143* (1), 21-32.

[75]. King, D., Yeomanson, D., & Bryant, H. E. (2015). PI3King the lock: targeting the PI3K/Akt/mTOR pathway as a novel therapeutic strategy in neuroblastoma. *Journal of Pediatric Hematology/Oncology*, *37*(4), 245-251.

[76]. Rexer, B. N., & Arteaga, C. L. (2012). Intrinsic and acquired resistance to HER2-targeted therapies in HER2 gene-amplified breast cancer: mechanisms and clinical implications. *Critical Reviews™ in Oncogenesis*, *17*(1). 1-16.

[77]. Hynes, N. E., & Lane, H. A. (2005). ERBB receptors and cancer: the complexity of targeted inhibitors. *Nature Reviews Cancer*, *5*(5), 341-354.

[78]. Wong, R. W. C., & Guillaud, L. (2004). The role of epidermal growth factor and its receptors in mammalian CNS. *Cytokine & Growth Factor Reviews*, *15*(2-3), 147-156.

[79]. Lynch, T. J., Bell, D. W., Sordella, R., Gurubhagavatula, S., Okimoto, R. A., Brannigan, B. W., ... & Louis, D. N. (2004). Activating mutations in the epidermal growth factor receptor underlying responsiveness of non–small-cell lung cancer to gefitinib. *New England Journal of Medicine*, *350*(21), 2129-2139.

[80]. Hashimoto, R., Straub, R. E., Weickert, C. S., Hyde, T. M., Kleinman, J. E., & Weinberger, D. R. (2004). Expression analysis of neuregulin-1 in the dorsolateral prefrontal cortex in schizophrenia. *Molecular Psychiatry*, *9*(3), 299.

[81]. Liu, X., Gu, X., Li, Z., Li, X., Li, H., Chang, J., ... & Lai, D. (2006). Neuregulin-1/erbB-activation improves cardiac function and survival in models of ischemic, dilated, and viral cardiomyopathy. *Journal of the American College of Cardiology*, *48*(7), 1438-1447.

[82]. Hynes, N. E., & MacDonald, G. (2009). ErbB receptors and signaling pathways in cancer. *Current Opinion in Cell Biology*, *21*(2), 177-184.

[83]. Olayioye, M. A., Neve, R. M., Lane, H. A., & Hynes, N. E. (2000). The ErbB signaling network: receptor heterodimerization in development and cancer. *The EMBO Journal*, *19*(13), 3159-3167.

[84]. Rowe, R. C., Sheskey, P., & Quinn, M. (2009). Handbook of pharmaceutical excipients. Libros Digitales-Pharmaceutical Press. 6th edition, *RPS Publishing,* 178, 500.

[85]. Bertram, J. P., Jay, S. M., Hynes, S. R., Robinson, R., Criscione, J. M., & Lavik, E. B. (2009). Functionalized poly (lactic-co-glycolic acid) enhances drug delivery and provides chemical moieties for surface engineering while preserving biocompatibility. *Acta Biomaterialia*, *5*(8), 2860-2871.

[86]. Brough, C., Miller, D. A., Keen, J. M., Kucera, S. A., Lubda, D., & Williams, R. O. (2016). Use of polyvinyl alcohol as a solubility-enhancing polymer for poorly water soluble drug delivery (part 1). *AAPS PharmSciTech*, *17*(1), 167-179.

[87]. Li, J., Wang, X., Zhang, T., Wang, C., Huang, Z., Luo, X., & Deng, Y. (2015). A review on phospholipids and their main applications in drug delivery systems. *Asian Journal of Pharmaceutical Sciences*, *10*(2), 81-98.

[88]. Bakowsky, H., Richter, T., Kneuer, C., Hoekstra, D., Rothe, U., Bendas, G., ... & Bakowsky, U. (2008). Adhesion characteristics and stability assessment of lectin-modified liposomes for site-specific drug delivery. *Biochimica et Biophysica Acta (BBA)-Biomembranes*, *1778*(1), 242-249.

[89]. Briuglia, M. L., Rotella, C., McFarlane, A., & Lamprou, D. A. (2015). Influence of cholesterol on liposome stability and on in vitro drug release. *Drug Delivery and Translational Research*, *5*(3), 231-242.

[90]. Magarkar, A., Dhawan, V., Kallinteri, P., Viitala, T., Elmowafy, M., Róg, T., & Bunker, A. (2014). Cholesterol level affects surface charge of lipid membranes in saline solution. *Scientific Reports*, *4*, 1-5.

[91]. Jain, L., Woo, S., Gardner, E. R., Dahut, W. L., Kohn, E. C., Kummar, S., … Figg, W. D. (2011). Population pharmacokinetic analysis of sorafenib in patients with solid tumours. *British Journal of Clinical Pharmacology*, *72*(2), 294–305.

[92]. Broecker-Preuss, M., Müller, S., Britten, M., Worm, K., Schmid, K. W., Mann, K., & Fuhrer, D. (2015). Sorafenib inhibits intracellular signaling pathways and induces cell cycle arrest and cell death in thyroid carcinoma cells irrespective of histological origin or BRAF mutational status. BMC Cancer, 15(1), 184.

[93]. Zhai, B. *et al.* Inhibition of Akt reverses the acquired resistance to sorafenib by switching protective autophagy to autophagic cell death in hepatocellular carcinoma. *Molecular Cancer Therapeutics* (2014).

[94]. Schoenberg, D. R. (2011). Mechanisms of endonuclease-mediated mRNA decay. *Wiley Interdisciplinary Reviews: RNA*, *2*(4), 582-600.

[95]. Ni, S., Yao, H., Wang, L., Lu, J., Jiang, F., Lu, A., & Zhang, G. (2017). Chemical modifications of nucleic acid aptamers for therapeutic purposes. *International Journal of Molecular Sciences*, *18*(8), 1683-1703.

[96]. Mohebi, S., Shafiee, H. A., & Ameli, N. (2017). Evaluation of enamel surface roughness after orthodontic bracket debonding with atomic force microscopy. *American Journal of Orthodontics and Dentofacial Orthopedics*, *151*(3), 521-527.

[97]. Nanda, K. K., Sarangi, S. N., & Sahu, S. N. (1998). Measurement of surface roughness by atomic force microscopy and Rutherford backscattering spectrometry of CdS nanocrystalline films. *Applied Surface Science*, *133*(4), 293-297.

[98]. Sitterberg, J., Özcetin, A., Ehrhardt, C., & Bakowsky, U. (2010). Utilising atomic force microscopy for the characterisation of nanoscale drug delivery systems. *European Journal of Pharmaceutics and Biopharmaceutics*, *74*(1), 2-13.

[99]. Pinnapireddy, S. R., Duse, L., Strehlow, B., Schäfer, J., & Bakowsky, U. (2017). Composite liposome-PEI/nucleic acid lipopolyplexes for safe and efficient gene delivery and gene knockdown. *Colloids and Surfaces B: Biointerfaces*, *158*, 93-101.

[100]. Duse, L., Baghdan, E., Pinnapireddy, S. R., Engelhardt, K. H., Jedelská, J., Schaefer, J., ... & Bakowsky, U. (2018). Preparation and characterization of curcumin loaded chitosan nanoparticles for photodynamic therapy. *Physica Status Solidi (a)*, *215*(15), 1-5.

[101]. Duse, L., Pinnapireddy, S. R., Strehlow, B., Jedelská, J., & Bakowsky, U. (2018). Low level LED photodynamic therapy using curcumin loaded tetraether liposomes. *European Journal of Pharmaceutics and Biopharmaceutics*, *126*, 233-241.

[102]. Möhwald, M., Pinnapireddy, S. R., Wonnenberg, B., Pourasghar, M., Jurisic, M., Jung, A., ... & Schneider, M. (2017). Aspherical, nanostructured microparticles for targeted gene delivery to alveolar macrophages. *Advanced Healthcare Materials*, *6*(20), 1700478.

[103]. Prabha, S., Zhou, W. Z., Panyam, J., & Labhasetwar, V. (2002). Size-dependency of nanoparticle-mediated gene transfection: studies with fractionated nanoparticles. *International Journal of Pharmaceutics*, *244*(1-2), 105-115.

[104]. Jonderian, A., & Maalouf, R. (2016). Formulation and in vitro interaction of rhodamine-B loaded PLGA nanoparticles with cardiac myocytes. *Frontiers in Pharmacology*, *7*, 458.

[105]. Prakapenka, A. V., Bimonte-Nelson, H. A., & Sirianni, R. W. (2017). Engineering poly (lactic-co-glycolic acid)(PLGA) micro-and nano-carriers for Controlled Delivery of 17β-Estradiol. *Annals of Biomedical Engineering*, *45*(7), 1697-1709.

[106]. Jain, G. K., Pathan, S. A., Akhter, S., Ahmad, N., Jain, N., Talegaonkar, S., ... & Ahmad, F. J. (2010). Mechanistic study of hydrolytic erosion and drug release behaviour of PLGA nanoparticles: Influence of chitosan. *Polymer Degradation and Stability*, *95*(12), 2360-2366.

[107]. Zhu, X., & Braatz, R. D. (2015). A mechanistic model for drug release in PLGA biodegradable stent coatings coupled with polymer degradation and erosion. *Journal of Biomedical Materials Research Part A*, *103*(7), 2269-2279.

[108]. Han, F. Y., Thurecht, K. J., Whittaker, A. K., & Smith, M. T. (2016). Bioerodable PLGA-based microparticles for producing sustained-release drug formulations and strategies for improving drug loading. *Frontiers in Pharmacology*, *7*, 185.

[109]. Muthu, M. S., & Singh, S. (2009). Targeted nanomedicines: effective treatment modalities for cancer, AIDS and brain disorders. *Nanomedicine,* 4(1), 105-118.

[110]. Dinarvand, R., Sepehri, N., Manoochehri, S., Rouhani, H., & Atyabi, F. (2011). Polylactide-co-glycolide nanoparticles for controlled delivery of anticancer agents. *International Journal of Nanomedicine*, *6*, 877-895.

[111]. Sah, H., Thoma, L. A., Desu, H. R., Sah, E., & Wood, G. C. (2013). Concepts and practices used to develop functional PLGA-based nanoparticulate systems. *International Journal of Nanomedicine*, *8*, 747-765.

[112]. Cao, J., Choi, J. S., Oshi, M. A., Lee, J., Hasan, N., Kim, J., & Yoo, J. W. (2019). Development of PLGA micro-and nanorods with high capacity of surface ligand conjugation for enhanced targeted delivery. *Asian Journal of Pharmaceutical Sciences*, *14*(1), 86-94.

[113]. Honary, S., & Zahir, F. (2013). Effect of zeta potential on the properties of nano-drug delivery systems-a review (Part 2). *Tropical Journal of Pharmaceutical Research*, *12*(2), 265-273.

[114]. Marrese, M., Guarino, V., & Ambrosio, L. (2017). Atomic force microscopy: a powerful tool to address scaffold design in tissue engineering. *Journal of Functional Biomaterials*, *8*(1), 7-27.

[115]. Miller, J. D., Veeramasuneni, S., Drelich, J., Yalamanchili, M. R., & Yamauchi, G. (1996). Effect of roughness as determined by atomic force microscopy on the wetting properties of PTFE thin films. *Polymer Engineering & Science*, *36*(14), 1849-1855.

[116]. Zhu, Y. J., Zheng, B., Wang, H. Y., & Chen, L. (2017). New knowledge of the mechanisms of sorafenib resistance in liver cancer. *Acta pharmacologica Sinica*, *38*(5), 614-622.

[117]. Zhai, B., & Sun, X. Y. (2013). Mechanisms of resistance to sorafenib and the corresponding strategies in hepatocellular carcinoma. *World Journal of Hepatology*, *5*(7), 345-352.

[118]. Bijman, M. N., van Berkel, M. P., Kok, M., Janmaat, M. L., & Boven, E. (2009). Inhibition of functional HER family members increases the sensitivity to docetaxel in human ovarian cancer cell lines. *Anti-Cancer Drugs*, *20*(6), 450-460.

[119]. Xu, F., Yu, Y., Le, X. F., Boyer, C., Mills, G. B., & Bast, R. C. (1999). The outcome of heregulin-induced activation of ovarian cancer cells depends on the relative levels of HER-2 and HER-3 expression. *Clinical Cancer Research*, *5*(11), 3653-3660.

[120]. Göstring, L., Malm, M., Höidén-Guthenberg, I., Frejd, F. Y., Ståhl, S., Löfblom, J., & Gedda, L. (2012). Cellular effects of HER3-specific affibody molecules. *PloS One*, *7*(6), 1-9.

[121]. Xiao, S., Liu, Z., Deng, R., Li, C., Fu, S., Chen, G., ... & Wang, S. (2017). Aptamer-mediated gene therapy enhanced antitumor activity against human hepatocellular carcinoma in vitro and in vivo. *Journal of Controlled Release*, *258*, 130-145.

[122]. Deng, H., Dutta, P., & Liu, J. (2018). Stochastic simulations of nanoparticle internalization through transferrin receptor dependent clathrin-mediated endocytosis. *Biochimica et Biophysica Acta (BBA)-General Subjects*, *1862*(9), 2104-2111.

[123]. Tang, H., Chen, H., Jia, Y., Liu, X., Han, Z., Wang, A., ... & Feng, X. (2017). Effect of inhibitors of endocytosis and NF-kB signal pathway on folate-conjugated nanoparticle endocytosis by rat Kupffer cells. *International Journal of Nanomedicine*, *12*, 6937-6947.

[124]. Dos Santos, T., Varela, J., Lynch, I., Salvati, A., & Dawson, K. A. (2011). Effects of transport inhibitors on the cellular uptake of carboxylated polystyrene nanoparticles in different cell lines. *PloS One*, *6*(9), 1-10.

[125]. Mani, KS, Kaminsky, W., & Rajendran, SP (2018). A facile atomic one-pot multicomponent synthesis of bioactive spiro-indenoquinoxaline pyrrolizines as potent antioxidants and anti-cancer agents. *New Journal of Chemistry* , *42* (1), 301-310.

[126]. Nicolete, R., dos Santos, D. F., & Faccioli, L. H. (2011). The uptake of PLGA micro or nanoparticles by macrophages provokes distinct in vitro inflammatory response. *International Immunopharmacology*, *11*(10), 1557-1563.

[127]. Wu, T., Duan, X., Hu, C., Wu, C., Chen, X., Huang, J., ... & Cui, S. (2019). Synthesis and characterization of gold nanoparticles from Abies spectabilis extract and its anticancer activity on bladder cancer T24 cells. *Artificial Cells, Nanomedicine, and Biotechnology*, *47*(1), 512-523.

[128]. He, Y., Mo, Q., Luo, B., Qiao, Y., Xu, R., Zuo, Z., ... & Wei, Y. (2016). Induction of apoptosis and autophagy via mitochondria-and PI3K/Akt/mTOR-mediated pathways by E. adenophorum in hepatocytes of saanen goat. *Oncotarget*, *7*(34), 54537-54548.

[129]. Will, M., Qin, A. C. R., Toy, W., Yao, Z., Rodrik-Outmezguine, V., Schneider, C., ... & Baselga, J. (2014). Rapid induction of apoptosis by PI3K inhibitors is dependent upon their transient inhibition of RAS–ERK signaling. *Cancer Discovery*, *4*(3), 334-347.

[130]. Coriat, R., Nicco, C., Chereau, C., Mir, O., Alexandre, J., Ropert, S., ... & Batteux, F. (2012). Sorafenib-induced hepatocellular carcinoma cell death depends on reactive oxygen species production in vitro and in vivo. *Molecular Cancer Therapeutics*, *11*(10), 2284-2293.

[131]. Gordon, LI, Burke, MA, Singh, AT, Prachand, S., Lieberman, Ed, Sun, L., & Ardehali, H. (2009). Blockade of the erbB2 receptor induces cardiomyocyte death through mitochondrial and reactive oxygen species-dependent pathways. *Journal of Biological Chemistry* , *284* (4), 2080-2087.

[132]. Son, Y., Cheong, Y. K., Kim, N. H., Chung, H. T., Kang, D. G., & Pae, H. O. (2011). Mitogen-activated protein kinases and reactive oxygen species: how can ROS activate MAPK pathways?. *Journal of Signal Transduction*, *2011*, 1-7.

[133]. Sauer, H., Wartenberg, M., & Hescheler, J. (2001). Reactive oxygen species as intracellular messengers during cell growth and differentiation. *Cellular Physiology and Biochemistry*, *11*(4), 173-186.

[134]. Belleudi, F., Marra, E., Mazzetta, F., Fattore, L., Giovagnoli, M. R., Mancini, R., ... & Ciliberto, G. (2012). Monoclonal antibody-induced ErbB3 receptor internalization

and degradation inhibits growth and migration of human melanoma cells. *Cell Cycle*, *11*(7), 1455-1467.

[135]. Roepstorff, K., Grøvdal, L., Grandal, M., Lerdrup, M., & van Deurs, B. (2008). Endocytic downregulation of ErbB receptors: mechanisms and relevance in cancer. *Histochemistry and Cell Biology*, *129*(5), 563-578.

[136]. Sasaki, T., Hiroki, K., & Yamashita, Y. (2013). The role of epidermal growth factor receptor in cancer metastasis and microenvironment. *BioMed Research International*, *2013*, 1-9.

[137]. Jiang, C., Xu, R., Li, X. X., Zhou, Y. F., Xu, X. Y., Yang, Y., ... & Zheng, X. S. (2018). Sorafenib and Carfilzomib Synergistically Inhibit the Proliferation, Survival, and Metastasis of Hepatocellular Carcinoma. *Molecular Cancer Therapeutics*, *17*(12), 2610-2621.

[138]. Yoshida, M., Yamashita, T., Okada, H., Oishi, N., Nio, K., Hayashi, T., ... & Sunagozaka, H. (2017). Sorafenib suppresses extrahepatic metastasis de novo in hepatocellular carcinoma through inhibition of mesenchymal cancer stem cells characterized by the expression of CD90. *Scientific Reports*, *7*(1), 1-10.

[139]. Adilakshmi, T., Ness-Myers, J., Madrid-Aliste, C., Fiser, A., & Tapinos, N. (2011). A nuclear variant of ErbB3 receptor tyrosine kinase regulates ezrin distribution and Schwann cell myelination. *Journal of Neuroscience*, *31*(13), 5106-5119.

[140]. Wang, YN, Yamaguchi, H., Hsu, JM, & Hung, MC (2010). Nuclear trafficking of the epidermal growth factor receptor family membrane proteins. *Oncogene*, *29* (28), 1-10.

[141]. Linggi, B., & Carpenter, G. (2006). ErbB receptors: new insights on mechanisms and biology. *Trends in Cell Biology*, *16*(12), 649-656.

[142]. Mahmoud, G., Jedelská, J., Omar, S. M., Strehlow, B., Schneider, M., & Bakowsky, U. (2018). Stabilized tetraether lipids based particles guided prophyrins photodynamic therapy. *Drug Delivery*, *25*(1), 1526-1536.

[143]. Hawkins, P. T., & Stephens, L. R. (2015). PI3K signalling in inflammation. *Biochimica et Biophysica Acta (BBA)-Molecular and Cell Biology of Lipids*, *1851*(6), 882-897.

[144]. Osada, T., Morse, M. A., Hobeika, A., Diniz, M. A., Gwin, W. R., Hartman, Z., ... & Kaneko, K. (2017). Vaccination targeting human HER3 alters the phenotype of infiltrating T cells and responses to immune checkpoint inhibition. *Oncoimmunology*, *6*(6), 1-12.

[145]. Adeyemi, OS, & Adewumi, I. (2014). Biochemical evaluation of silver nanoparticles in Wistar rats. *International Scholarly Research Notices*, *2014*, 1-8.

[146]. Shi, HB, Kong, M., Chen, G., Zhao, J., Shi, HL, Chen, Y., & Rowan, FG (2010). Compound pollen protein nutrient increases serum albumin in cirrhotic rats. *Gastroenterology Research* , *3*(6), 253-261.

[147]. Babu, E. P., Subastri, A., Suyavaran, A., Premkumar, K., Sujatha, V., Aristatile, B., ... & Thirunavukkarasu, C. (2017). Size Dependent Uptake and Hemolytic Effect of Zinc Oxide Nanoparticles on Erythrocytes and Biomedical Potential of ZnO-Ferulic acid Conjugates. *Scientific Reports*, *7*(1), 1-12.

[148]. Cardoso, A. V., Pereira, M. H., Marcondes, G. D. A., Ferreira, A. R., & Araújo, P. R. D. (2007). Microplate reader analysis of triatomine saliva effect on erythrocyte aggregation. *Materials Research*, *10*(1), 31-36.

[149]. Inomata, K., Tajima, K., Yagi, H., Higashi, H., Shimoda, H., Matsubara, K., ... & Shinoda, M. (2018). A Pre-Clinical Large Animal Model of Sustained Liver Injury and Regeneration Stimulus. *Scientific Reports*, *8*(1), 1-12.

[150]. Cho, N. J., Hwang, L., Solandt, J., & Frank, C. (2013). Comparison of extruded and sonicated vesicles for planar bilayer self-assembly. *Materials*, *6*(8), 3294-3308.

[151]. Nag, O. K., Yadav, V. R., Hedrick, A., & Awasthi, V. (2013). Post-modification of preformed liposomes with novel non-phospholipid poly (ethylene glycol)-conjugated hexadecylcarbamoylmethyl hexadecanoic acid for enhanced circulation persistence in vivo. *International Journal of Pharmaceutics*, *446*(1-2), 119-129.

[152]. Sawant, R. R., & Torchilin, V. P. (2012). Challenges in development of targeted liposomal therapeutics. *The AAPS Journal*, *14*(2), 303-315.

[153]. Amaral, R. L., Miranda, M., Marcato, P. D., & Swiech, K. (2017). Comparative analysis of 3D bladder tumor spheroids obtained by forced floating and hanging drop methods for drug screening. *Frontiers in Physiology*, *8*, 1-15.

[154]. Gao, H., Yang, Z., Zhang, S., Cao, S., Shen, S., Pang, Z., & Jiang, X. (2013). Ligand modified nanoparticles increases cell uptake, alters endocytosis and elevates glioma distribution and internalization. *Scientific Reports*, *3*, 1-8.

[155]. Kou, L., Bhutia, Y. D., Yao, Q., He, Z., Sun, J., & Ganapathy, V. (2018). Transporter-guided delivery of nanoparticles to improve drug permeation across cellular barriers and drug exposure to selective cell types. *Frontiers in Pharmacology*, *9*, 1-16.

[156]. Plenagl, N., Duse, L., Seitz, B. S., Goergen, N., Pinnapireddy, S. R., Jedelska, J., ... & Bakowsky, U. (2019). Photodynamic therapy–hypericin tetraether liposome conjugates and their antitumor and antiangiogenic activity. *Drug Delivery*, *26*(1), 23-33.

5.2 Research Output

[1]. **Muhammad Yasir Ali**, Imran Tariq, Sajid Ali, Muhammad Umair Amin, Konrad Engelhardt, Shashank Reddy Pinnapireddy, Lili Duse, Jens Schäfer and Udo Bakowsky; Targeted ErbB3 cancer therapy: A synergistic approach to effectively combat cancer, submitted to International Journal of Pharmaceutics.

[2]. **Muhammad Yasir Ali**, Imran Tariq, Muhammad Farhan Sohail, Muhammad Umair Amin, Sajid Ali, Shashank Reddy Pinnapireddy, Asad Ali, Jens Schäfer and Udo Bakowsky; Selective anti-erbb3 aptamer modified sorafenib microparticles: *in vitro* and *in vivo* toxicity assessment. Submitted to European Journal of Pharmaceutics and Biopharmaceutics.

[3]. **Muhammad Yasir Ali**, Imran Tariq, Sajid Ali, Muhammad Umair Amin, Shashank Reddy Pinnapireddy, Lili Duse, Jens Schäfer and Udo Bakowsky; Selective sorafenib-loaded liposomal chemotherapy: An extensive cytotoxicity assessment; Manuscript in preparation.

[4]. Imran Tariq, Shashank Reddy Pinnapireddy, Lili Duse, **Muhammad Yasir Ali**, Sajid Ali, Muhammad Umair Amin, Nathalie Goergen, Jarmila Jedelská, Jens Schäfer and Udo Bakowsky; Lipodendriplexes: A promising nanocarrier for enhanced gene delivery with minimal cytotoxicity, European Journal of Pharmaceutics and Biopharmaceutics, 135 (2019), 72-82.

[5]. Imran Tariq, **Muhammad Yasir Ali**, Muhammad Farhan Sohail, Muhammad Umair Amin, Sajid Ali, Nadeem Irfan Bukhari, Abida Raza, Shashank Reddy Pinnapireddy, Jens Schäfer and Udo Bakowsky; A comprehensive biodistribution and toxicity profile of PAMAM based lipid triblock nano carriers after system delivery; Manuscript in preparation.

[6]. Imran Tariq, **Muhammad Yasir Ali**, Harshavardhan Janga, Sajid Ali, Muhammad Umair Amin, Uzma Ali, Shashank Reddy Pinnapireddy, Jens Schäfer and Udo Bakowsky; Downregulation of MDR 1 gene contributes to caspase dependant apoptosis in colon carcinoma: A gravity to space investigation; Manuscript in preparation.

[7]. Sajid Ali, Muhammad Umair Amin, **Muhammad Yasir Ali**, Imran Tariq,Shashank Reddy Pinnapreddy, Lili Duse, Nathalie Goergen, Christian Wölk, Gerd Hause, Jarmila Jedelská, Jens Schäfer and Udo Bakowsky; Wavelength-dependent photo-cytotoxicity

to ovarian carcinoma cells using temoporfin loaded tetraether liposomes as an efficient drug delivery system; Manuscript in preparation.

[8]. Muhammad Umair Amin, Sajid Ali, Imran Tariq, **Muhammad Yasir Ali**, Shashank Reddy Pinnapreddy, Christian Wölk, Gerd Hause, Jana Brüßler and Udo Bakowsky; Development of a smart drug delivery system based on Ultrasoundresponsive lipid coated mesoporous silica nanoparticles; Manuscript in preparation.

5.3 Presentations and Workshops

[1]. Aptamer guided sorafenib microspheres: *in vitro* and *in vivo* assessment; Oral Presentation; **Muhammad Yasir Ali**; Emerging trends of nanomedicine and drug delivery research (Nano Delivery 2019); March 18-20, 2019; London, UK.

[2]. Aptamer modified PLGA nanoparticles for the sight specific tumor targeting of sorafenib; Oral Presentation; **Muhammad Yasir Ali**; International conference and exhibition on pharmaceutical nanotechnology and nanomedicine; April 18-19, 2018; Las Vegas USA.

[3]. Toxicity assessment of functionalized sorafenib microspheres: *in vitro* and *in vivo* assessment; Poster Presentation; **Muhammad Yasir Ali**, Imran Tariq, Muhammad Farhan Sohail, Asad Ali, Muhammad Umair Amin, Sajid Ali, Shashank Reddy Pinnapireddy, Jens Schaefer and Udo Bakowsky; Functional biomaterials and release of nucleic acid drugs; 23rd Annual meeting at Leipzig University; 7-8 March, 2019; Leipzig, Germany.

[4]. In vivo biodistribution and toxicity profile of liposome conjugated polyamidoamine dendrimeric system; Poster Presentation; Imran Tariq, **Muhammad Yasir Ali**, Muhammad Farhan Sohail, Sajid Ali, Muhammad Umair Amin, Nadeem Irfan Bukhari, Abida Raza, Jens Schäfer and Udo Bakowsky; Functional biomaterials and release of nucleic acid drugs; 23rd Annual meeting at Leipzig University; 7-8 March, 2019; Leipzig, Germany.

[5]. Doxorubicin loaded lipid coated mesoporous silica nanoparticles as advance drug delivery system; Poster Presentation; Muhammad Umair Amin, Sajid, Ali, **Muhammad Yasir Ali**, Imran Tariq, Jana Brüßler and Udo Bakowsky; Functional biomaterials and release of nucleic acid drugs; 23rd Annual meeting at Leipzig University; 7-8 March, 2019; Leipzig, Germany

[6]. Low dose photo-activation of liposomes containing Temoporfin as potent dye; Poster Presentation. Sajid Ali, Umair Amin, Imran Tariq, **Muhammad Yasir Ali**, Jarmila Jedelská, Jens Schaefer and Udo Bakowsky; Functional biomaterials and release of nucleic acid drugs; 23rd Annual meeting at Leipzig University; 7-8 March, 2019; Leipzig, Germany.

[7]. Particle characterization in medicine and biology; Workshop;Malvern Panalytical;September 20-2018, Frankfurt, Germany.

[8]. Laboratory Animal Handling Course; MARA, Philipps University Marburg; August, 2018.

[9]. Aptamer based nanoparticles and liposomes as carrier for targeted anti cancerous drug; Poster Presentation; **Muhammad Yasir Ali**, Jens Schäfer and Udo Bakowsky; 21st Annual meeting at Philipps University Marburg (CRS Local Chapter); March 2-3, 2017; Marburg, Germany.

5.4 CURRICULUM VITAE

PERSONAL INFORMATION

Name	**MUHAMMAD YASIR ALI**
Address	FRIEDRICH EBERT STR. 119, 35039 MARBURG, GERMANY
Place of Birth	BAHAWALPUR, PAKISTAN
Telephone	+4915905109266
E-mail	m.yasirali14@gmail.com
	aliy@staff.uni-marburg.de
Nationality	Pakistani
Date of birth	01-01-1985

EDUCATION AND PROFESSIONAL TRAINING

Matriculation *(BISE, Bahawalpur, Pakistan)*	*1998*
F.Sc. *(BISE, Bahawalpur, Pakistan)*	*2001*
B. Pharmacy *(Islamia University, Bahawalpur, Pakistan)*	*2002-06*
M. Phil (Pharmaceutics) *(Islamia University, Bahawalpur, Pakistan)*	*2007-09*
Two months Professional Training	Roche Pakistan Limited
Ph.D. (Philipps University, Marburg, Germany)	**2016 to date**
Laboratory Animal Handling Course *(MARA, Philipps University Marburg)*	Department of Biology, Philipps University Marburg

RESEARCH EXPERIENCES

Yasir ALI, Nisar-ur-RAHMAN, Muneeb A. IDREES, Sabeeh MOHSIN, Saeed AHMED & Irshad AHMED "Sustained Release of Captopril From Matrix Tablet Using Methylcellulose in a New Derivative Form" *Lat. Am. J. Pharm.* 30 (9): 1696-1701 (2011).

Idrees MA., Rahman NU., Ahmad S., **Ali MY**., Ahmad "Enhance transdermal delivery of flurbiprofen via microemulsions: Effects of different types of surfactants and cosurfactants" *DARU* 19 (6): 1-6(2011).

Shahid Rasool, Uzma Saleem, Saeed Mahmood, **M. Yasir Ali**, Ghulam Abbas and Bashir Ahmad "Prevention and treatment of dengue with

natural drugs" *Pak. J. Pharm.* 24(1 & 2): 51-53, (2011).

Zartasha ASLAM, Khalid P. AKHTER, Mahmood AHMAD, Muhammad N. AAMIR, Muhammad NAEEM &**Muhammad Y. ALI** "Preparation of Modified-Release Tramadol Tablets and Drug Release Evaluation using Dependent and Independent Modeling Approaches" *Lat. Am. J. Pharm.* 31 (10): 1417-21 (2012).

Saeed ul Hassan, Shahid Rasool, Uzma Niaz, Muhammad Khalil Rehman, **Muhammad Yasir Ali**, Ghulam Abbas, Nasir Rasool, Muhammad Riaz and Khizar Abbas "Dermatological potential of crude extracts and different fractions of *Achyranthes aspera* Linn." *AJPP* 6(44):3096-3101 (2012).

Imran TARIQ, Ahmad M. MUMTAZ, Tariq SAEED, Pervaiz A. SHAH, Syed A. RAZA, Najam ul Hassan JAWA, **Muhammad Yasir ALI**& Ghulam ABBAS "*In Vitro* Release Studies of Diclofenac Potassium Tablet from Pure and Blended Mixture of Hydrophilic and Hydrophobic Polymers" *Lat. Am. J. Pharm.* 31 (3): 380-7 (2012)

Muhammad Yasir Ali, M. Imran Qadir, Shahid Rasool , Ghulam Abbas, Saeed Ahmed, Zartasha Aslam, Daulat Haleem, Shahid Masood, Bashir Ahmad, Effectiveness of *Viola odorata* Flower Decoction for Tonsillitis and Peritonsillar Abscess, *JRLMC* 2: 51-53 (2013).

Muhammad Zaman, Shahid Rasool, **Muhammad Yasir Ali**, Junaid Qureshi, Sherjeel Adnan, Muhammad Hanif, Rai Muhammad Sarfraz, Hira Ijaz, Asif Mahmood, "Fabrication and Analysis of Hydroxypropylmethyl Cellulose and Pectin-Based Controlled Release Matrix Tablets Loaded with Loxoprofen Sodium" *Adv. Poly. Tech.* 1(1): 1-7(2014).

Muhammad Zaman, ShahidRasool, **Muhammad Yasir Ali**, Muhammad Shafeeq ur Rahman, Rai Muhammad Sarfraz, Abdullah Akram, "In-Vitro Release Kinetics Study of Loxoprofen Sodium From Natural Polymers Based Sustained Release Matrix System" *Am. J. PharmTech Res.* 4(2): 115-125 (2014).

Imran Tariq, Shashank Reddy Pinnapireddy, Lili Duse, **Muhammad Yasir Ali**, Sajid Ali, Muhammad Umair Amin, Nathalie Goergen, Jarmila Jedelská, Jens Schäfer and Udo Bakowsky; Lipodendriplexes: A promising nanocarrier for enhanced gene delivery with minimal cytotoxicity, *European Journal of Pharmaceutics and Biopharmaceutics*, 135, 72-82 (2019).